General Disclaimer
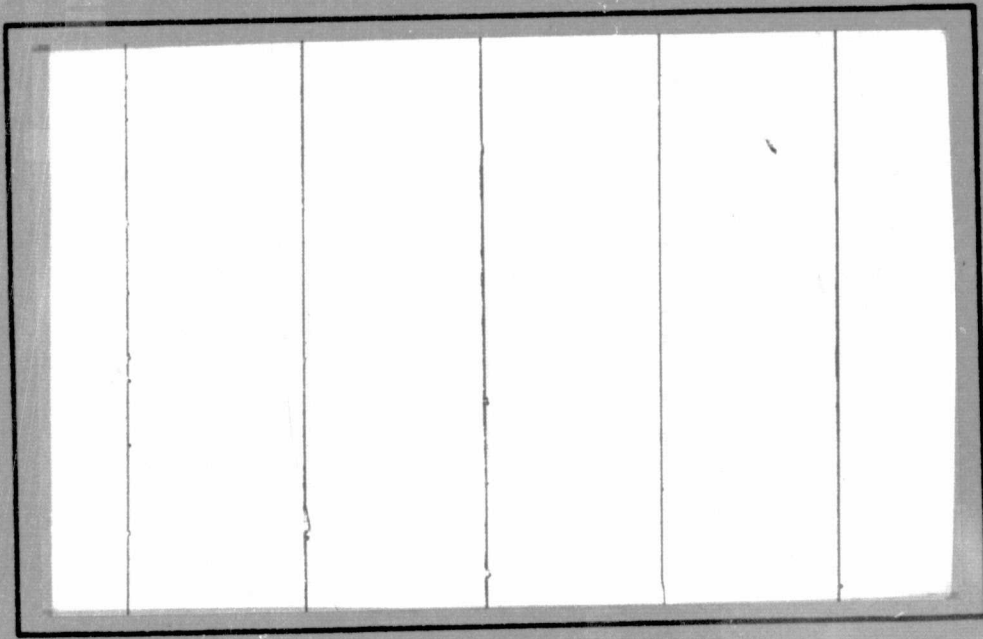
One or more of the Following Statements may affect this Document

- This document has been reproduced from the best copy furnished by the organizational source. It is being released in the interest of making available as much information as possible.

- This document may contain data, which exceeds the sheet parameters. It was furnished in this condition by the organizational source and is the best copy available.

- This document may contain tone-on-tone or color graphs, charts and/or pictures, which have been reproduced in black and white.

- This document is paginated as submitted by the original source.

- Portions of this document are not fully legible due to the historical nature of some of the material. However, it is the best reproduction available from the original submission.

NGR-47-004-129

COLLEGE
OF
ENGINEERING

VIRGINIA
POLYTECHNIC
INSTITUTE AND
STATE
UNIVERSITY

JUL 1976
RECEIVED
NASA STI FACILITY
INPUT BRANCH

BLACKSBURG,
VIRGINIA

College of Engineering
Virginia Polytechnic Institute and State University
Blacksburg, VA 24061

VPI-E-76-10   June, 1976

Nonlinear Analysis of Laminated

Fibrous Composites

Gary D. Renieri
Carl T. Herakovich

Department of Engineering Science and Mechanics

This work constituted Dr. Renieri's Ph.D. dissertation.

BIBLIOGRAPHIC DATA SHEET	1. Report No. VPI-E-76-10	2.	3. Recipient's Accession No.
4. Title and Subtitle NONLINEAR ANALYSIS OF LAMINATED FIBROUS COMPOSITES			5. Report Date June, 1976
			6.
7. Author(s) Gary D. Renieri, Carl T. Herakovich			8. Performing Organization Rept. No. VPI-E-76-10
9. Performing Organization Name and Address Virginia Polytechnic Institute and State University Engineering Science and Mechanics Blacksburg, Virginia 24061			10. Project/Task/Work Unit No.
			11. Contract/Grant No. NGR-47-004-090
12. Sponsoring Organization Name and Address National Aeronautics & Space Administration Langley Research Center Hampton, Virginia 23665			13. Type of Report & Period Covered
			14.

15. Supplementary Notes

16. Abstracts

see page i

17. Key Words and Document Analysis.   17a. Descriptors

composites, laminates, edge effects, interlaminar stresses, failure, tension, compression, thermal stresses, nonlinear behavior, Ramberg-Osgood, boron/epoxy, graphite/epoxy, boron/aluminum, finite elements

17b. Identifiers/Open-Ended Terms

17c. COSATI Field/Group

18. Availability Statement Distribution unlimited	19. Security Class (This Report) UNCLASSIFIED	21. No. of Pages
	20. Security Class (This Page) UNCLASSIFIED	22. Price

INSTRUCTIONS FOR COMPLETING FORM NTIS-35 (Bibliographic Data Sheet based on COSATI

Guidelines to Format Standards for Scientific and Technical Reports Prepared by or for the Federal Government, PB-180 600).

1. **Report Number.** Each individually bound report shall carry a unique alphanumeric designation selected by the performing organization or provided by the sponsoring organization. Use uppercase letters and Arabic numerals only. Examples FASEB-NS-73-87 and FAA-RD-73-09.

2. Leave blank.

3. **Recipient's Accession Number.** Reserved for use by each report recipient.

4. **Title and Subtitle.** Title should indicate clearly and briefly the subject coverage of the report, subordinate subtitle to the main title. When a report is prepared in more than one volume, repeat the primary title, add volume number and include subtitle for the specific volume.

5. **Report Date.** Each report shall carry a date indicating at least month and year. Indicate the basis on which it was selected (e.g., date of issue, date of approval, date of preparation, date published).

6. **Performing Organization Code.** Leave blank.

7. **Author(s).** Give name(s) in conventional order (e.g., John R. Doe, or J.Robert Doe). List author's affiliation if it differs from the performing organization.

8. **Performing Organization Report Number.** Insert if performing organization wishes to assign this number.

9. **Performing Organization Name and Mailing Address.** Give name, street, city, state, and zip code. List no more than two levels of an organizational hierarchy. Display the name of the organization exactly as it should appear in Government indexes such as Government Reports Index (GRI).

10. **Project/Task/Work Unit Number.** Use the project, task and work unit numbers under which the report was prepared.

11. **Contract/Grant Number.** Insert contract or grant number under which report was prepared.

12. **Sponsoring Agency Name and Mailing Address.** Include zip code. Cite main sponsors.

13. **Type of Report and Period Covered.** State interim, final, etc., and, if applicable, inclusive dates.

14. **Sponsoring Agency Code.** Leave blank.

15. **Supplementary Notes.** Enter information not included elsewhere but useful, such as: Prepared in cooperation with . . . Translation of . . . Presented at conference of . . . To be published in . . . Supersedes . . . Supplements . . . Cite availability of related parts, volumes, phases, etc. with report number.

16. **Abstract.** Include a brief (200 words or less) factual summary of the most significant information contained in the report. If the report contains a significant bibliography or literature survey, mention it here.

17. **Key Words and Document Analysis. (a). Descriptors.** Select from the Thesaurus of Engineering and Scientific Terms the proper authorized terms that identify the major concept of the research and are sufficiently specific and precise to be used as index entries for cataloging.
    (b). Identifiers and Open-Ended Terms. Use identifiers for project names, code names, equipment designators, etc. Use open-ended terms written in descriptor form for those subjects for which no descriptor exists.
    (c). COSATI Field/Group. Field and Group assignments are to be taken from the 1964 COSATI Subject Category List. Since the majority of documents are multidisciplinary in nature, the primary Field/Group assignment(s) will be the specific discipline, area of human endeavor, or type of physical object. The application(s) will be cross-referenced with secondary Field/Group assignments that will follow the primary posting(s).

18. **Distribution Statement.** Denote public releasability, for example "Release unlimited", or limitation for reasons other than security. Cite any availability to the public, other than NTIS, with address, order number and price, if known.

19 & 20. **Security Classification.** Do not submit classified reports to the National Technical Information Service.

21. **Number of Pages.** Insert the total number of pages, including introductory pages, but excluding distribution list, if any.

22. **NTIS Price.** Leave blank.

ABSTRACT

A computerized analysis of the nonlinear behavior of fibrous composite laminates including axial loading, thermal loading, temterature dependent properties, and edge effects is presented. Ramberg-Osgood approximations are used to represent lamina stress-strain behavior and percent retention curves are employed to model the variation of properties with temperature. Balanced, symmetric laminates comprised of either boron/epoxy, graphite/epoxy, or borsic-aluminum are analyzed using a quasi-three-dimensional finite element analysis. An incremental loading procedure is developed where the mechanical properties of each finite element may be adjusted depending on the temperature and/or the strain level.

Results are presented for the interlaminar stress distributions in cross-ply, angle-ply, and more complex laminates. Elastic results for the boundary layer effect are shown to compare favorably with existing numerical solutions. It is shown that for angle-ply laminates the fiber orientation for maximum stress due to mechanical loading is matrix material dependent whereas the fiber orientation for maximum thermal stress is not matrix material dependent. It is also shown that the combined nonlinear thermal and mechanical analysis exhibits signficant differences from the linear elastic results.

Nonlinear stress-sstrain curves for a variety of composite laminates in tension and compression are obtained and compared to other existing theories and experimental results. It is shown that excellent agreement between theory and experiment is exhibited

for many, but not all, laminates. The inclusion of thermal effects is shown to give improved predictions.

It is also shown that the mode of failure is laminate dependent. Whereas angle-ply laminates fail as the result of in-plane strains exceeding maximum values, other laminates fail according to either a first ply failure theory, a progressive failure theory, or they fail as a result of edge effects.

ACKNOWLEDGEMENT

TABLE OF CONTENTS

LIST OF FIGURES

LIST OF TABLES

LIST OF SYMBOLS

A	area
C_1, C_2, C_3, C_4, C_5, C_6	constants of integration
C_{ij}	lamina stiffness matrix
$\overline{C}_{ij}$	transformed lamina stiffness matrix
E	Young's modulus
E_e	elastic modulus (Young's or shear)
$\overline{E}$	current modulus (extensional or shear)
$\overline{E}_{11}$, $\overline{E}_{22}$, $\overline{E}_{33}$	current extensional moduli
F	average force
F_i, F_{ij}	1st and 2nd order tensors respectively
G	shear modulus
$\overline{G}_{23}$, $\overline{G}_{13}$, $\overline{G}_{12}$	current shear moduli
H	laminate half thickness
K	Ramberg-Osgood coefficient
$\mathcal{K}$, $\mathcal{K}'$	elemental stiffness matrices
S_{ij}	lamina compliance matrix
T	temperature
U, V, W	displacement functions of coordinates y and z
U_K	finite element strain energy
W_K	finite element potential energy

a_1, a_2, a_3, a_4,

  a_5, a_6, a_7,

  a_8, a_9 constants for each finite element

b   laminate half width

f_{ij} nodal forces

f_1, f_2, f_3,

  f_4, f_5, f_6 functions of coordinates y and z

n   Ramberg-Osgood coefficient

u, v, w   displacements

x, y, z   laminate coordinates

Δ delta function

α_1, α_2, α_3 coefficients of thermal expansion in the principal lamina directions

α_x, α_y, α_z,

  α_{xy} coefficients of thermal expansion in the laminate directions

γ_{23}, γ_{13}, γ_{12} shear strains with respect to the lamina directions

γ_{yz}, γ_{xz}, γ_{xy} shear strains with respect to the laminate directions

δ_{ij} displacement column matrix

$d\varepsilon_1$, $d\varepsilon_2$ increments of lamina principal strains

$d\bar{\varepsilon}_1$, $d\bar{\varepsilon}_2$ increments of equivalent strain

ε_1, ε_2, ε_3 normal strains with respect to the lamina directions

ε_x, ε_y, ε_z normal strains with respect to the laminate directions

ε^e elastic limit strain

ε^0 over strain

ε^P	current strain
ε^u	ultimate strain
ε_A	percent retention limit strain
ε_E	elastic strain component
ε_I	inelastic strain component
θ	orientation angle
ν	Poisson's ratio
ξ_x	uniform applied strain
$\overline{\xi}_x$	uniform determined strain
$d\sigma_1$, $d\sigma_2$	increments of lamina principal stresses
σ_1, σ_2, σ_3	normal stresses with respect to the lamina directions
σ_x, σ_y, σ_z	normal stresses with respect to the laminate directions
σ^e	elastic limit stress
σ^P	current stress
σ^u	ultimate stress
τ_{23}, τ_{13}, τ_{12}	shear stresses with respect to the lamina directions
τ_{yz}, τ_{xz}, τ_{xy}	shear stresses with respect to the laminate directions
ψ_K	finite element total potential energy

Chapter 1

INTRODUCTION

With the ever increasing demand for lighter-weight and higher
strength structural components, the design engineers of the aerospace
industry have turned to the use of composite materials. These materials
offer the engineer the means to meet structural requirements by varying
ply orientations and/or volume fraction of matrix and fiber. An area
of concern to the engineer designing with fiber composite materials
has been the ability to accurately predict the stiffness and strength
of these materials. The present study was undertaken to develop a
reliable computerized analysis of the nonlinear behavior of fibrous
composite laminates to include thermal loading, temperature dependent
properties and edge effects.

Many researchers have used the plane stress lamination theory in
their quest to predict laminate response. Other researchers have indi-
cated that a knowledge of interlaminar stresses, which are not con-
sidered for in-plane lamination theory, is needed to accurately predict
the ultimate strength of laminates. While various elastic and non-
linear approaches have been employed in previous research endeavors,
relatively little attention has been given to the influence of thermal
stresses and strains which may be present within a given laminate.

In an attempt to predict the nonlinear stress-strain behavior
including edge effects and thermal effects for balanced, symmetric
laminates, a quasi-three-dimensional nonlinear finite element analysis

was developed. Lamina properties were allowed to change with respect to both temperature and strain levels. Uniaxial loading of various laminates and materials at room temperature were considered. Initial thermal stresses and strains were determined through an incremental cooling analysis from an elevated stress-free temperature to room temperature. The laminates were then subjected to incremental strain loading. At each stage of the incremental procedure the mechanical properties of each finite element may be altered depending on the temperature and/or the strain level. Such a procedure allowed the pro- perties of finite elements within a given layer to change independently of other finite elements in the layer. This feature cannot be handled with lamination theory.

Three material systems were considered, boron/epoxy, borsic/ aluminum and graphite/epoxy.

Chapter 2

HISTORICAL SURVEY

One of the earliest endeavors to theoretically predict the elas-
tic properties of laminates consisting of arbitrarily oriented plies
of orthotropic materials was presented by Smith [1] in 1953. Smith's
objective was to determine the effective shear modulus for various
laminations of plywood while assuming a state of plane stress through
the thickness. In 1961 Reissner and Stavsky [2] extended the work of
Smith [1] to include the coupling phenomenon between in-plane stretch-
ing and transverse bending for laminates consisting of orthotropic
lamina. While many modern day researchers in the field of composites
refer to the more recent (1969) work of Ashton, et al., [3] when noting
the so-called "Lamination Theory," the basic formulation was presented
in the work of Reissner and Stavsky [2]. A more detailed description
of lamination theory and its assumptions was presented by Ashton and
Whitney [4] in 1970.

2.1 Laminate Analysis Studies

In 1964 Tsai [5] presented a theoretical method for predicting
the elastic constants of a lamina from the properties of the constitu-
ent materials. Tsai then used the lamination theory of Reissner and
Stavsky [2] to analytically predict the elastic constants for laminates.
Good agreement was shown between theory and experiment for a glass/
epoxy composite. Azzi and Tsai [6] extended the work of Tsai [5] to
develop viable experimental techniques for confirming the validity of

3

the analytical predictions. Subsequently, Azzi and Tsai [7] presented an analytical technique for predicting the strength of transversely isotropic laminates. The plane stress form of Hill's yield condition [8] for orthotropic materials was employed to predict laminate failure. Theoretical and experimental tensile strengths for unidirectional glass/epoxy laminates were shown to agree quite well. It was noted that the stress-strain curves for each of the test specimens were virtually linear and elastic up to failure. The method did not consider the possibility of differing tensile and compressive properties.

In 1965 Tsai [9] presented a method to model the load transfer from one lamina as it failed to the remaining unfailed laminae. Hill's plane stress yield condition [8] was used to determine lamina failure. After the failure of each lamina, the stiffness matrix was degraded by setting the appropriate elastic constants to a small fraction of their original values. All laminae were assumed to behave linear elastically up to failure. Tsai took into account both mechanical and thermal loading. Initial thermal stresses were calculated from room temperature thermal coefficients and the curing temperature. Good agreement between theory and experiment for the ultimate stress was exhibited for simple tensile loading of glass/epoxy composites. Again, the method did not allow for different properties in tension and compression.

A brittle fracture criteria which was similar to Hill's orthotropic yield condition [8] was proposed by Hoffman [10] in 1967. The fracture theory contained linear terms and could account for differing

tensile and compressive properties. Experimental verification was limited to uniaxial tensile and compressive tests on variously oriented composite specimens. Good agreement was shown between theory and experiment for the ultimate stress. Initial thermal stresses were not considered.

Prior to 1968 all investigations concerned with laminate strength were based on linear elastic behavior of the individual lamina. Of the literature previously cited only the work of Tsai [9] included initial thermal stresses. With the development of the advanced composites (such as boron/epoxy and graphite/epoxy) which exhibited nonlinear lamina behavior there came an increased need to theoretically predict the mechanical behavior of these materials using nonlinear techniques.

In 1969 Petit and Waddoups [11] developed an analytical method for determining the nonlinear stress-strain response to failure for laminates comprised of lamina with nonlinear stress-strain behavior. While previous investigators had determined failure based on the inter-action of stress values, Petit and Waddoups presented an independent failure theory based on lamina principal strains. The laminate response was established by a piecewise linear approach and incremental application of average laminate stresses. At each increment of load the increment of laminate strains was determined and added to the previous strains to give the total laminate strains. Individual lamina strains in the principal lamina directions were then calculated from the strain transformation equations. By referring these lamina strains to their respective stress-strain curves, which were represented by

linear segments, updated moduli and stiffnesses were determined for the next load increment. However, when a single lamina failed in a certain manner the respective modulus was set to a high negative value for unloading and then set to zero. This method allowed remaining un-failed laminae to continue to load. Failure was assumed to occur when a principal strain reached the ultimate value in each lamina or when the stiffness matrix became singular. Good agreement between theory and experiment for the prediction of stress-strain curves was shown for various boron/epoxy laminates subjected to both tensile and com-pressive loading. While the method did allow for differing tensile and compressive properties thermal stresses were not included.

While graphite/epoxy was considered in the work of Tsai and Wu [12] in 1971 a linear elastic analysis was employed. Tsai and Wu pro-posed a general strength criterion for anisotropic materials. The basic assumption of the criterion was that a failure surface in the stress-space had the following scalar form

$$f(\sigma_K) = F_i \sigma_i + F_{ij} \sigma_i \sigma_j = 1 \qquad (2.1)$$

where F_i and F_{ij} are first and second order tensors respectively. While the theory represented an improvement over existing theories, the applicability of it for orthotropic materials required the reliable determination of the F_{12} interaction term. Limited uniaxial tension and compression as well as pure shear tests were performed on a graphite/epoxy system and compared to the theory. Good agreement was exhibited for ultimate stress.

Chiu [13], using the orthotropic yield condition of Hill [8], proposed the concept of a stepwise reduction in load carrying capacity after a lamina reached initial yield. Chiu noted that failure in one direction of a certain layer implies neither total failure of the layer, nor of the whole laminate. Chiu assumed that the yield value and ultimate stress were identical for longitudinal tension and compression, respectively. For transverse tension and compression the yield values were set equal to 1/2 of their respective ultimate values and for shear the yield value was assumed to be 1/5 of the ultimate value. Chiu's theory proved favorable when compared with experimental results for two boron/epoxy laminates. However, Chiu did not consider thermal stresses.

In 1972 Kaminski, et al., [14] performed static tension and compression tests up to failure on various boron/epoxy laminates. Results were compared to theoretical predictions obtained from a nonlinear laminate analysis program referred to as RD5. Good agreement was exhibited for tension results. While good agreement was shown for some compression results, there were cases where the theory gave poor results with respect to the failure point. In an effort to achieve better agreement between theory and experiment two separate techniques were investigated. One method incorporated the use of pseudo lamina stress-strain curves while the other method considered a reduction of various terms of the stiffness matrix. In general, neither of the two techniques gave sufficiently better theoretical results. Initial thermal stresses were not included in the analysis.

Hashin, et al., [15] extended the work of Petit and Waddoups [11] by using Ramberg-Osgood [16] approximations to represent the lamina nonlinear stress-strain curves. While Hashin's analysis was more elaborate than that of Petit and Waddoups, no provisions were made for individual lamina failure or lamina unloading. Compression loading was not considered and comparison between theory and experiment did not show improvement over the previous work of Petit and Waddoups.

A more recent investigation was presented by Sandhu [17] for predicting the response to failure of composite laminates. Cubic spline interpolation functions were used to represent the lamina stress-strain curves. Incremental loading was used and updated material properties were determined as functions of equivalent strains. Sandhu proposed that it was erroneous to determine new material properties at each load increment as functions of the individual lamina strains. For plane stress Sandhu noted that

$$d\varepsilon_1 = S_{11}d\sigma_1 + S_{12}d\sigma_2$$
$$d\varepsilon_2 = S_{12}d\sigma_1 + S_{22}d\sigma_2$$

(2.2)

or

$$d\sigma_1 = (d\varepsilon_1 - S_{12}d\sigma_2)/S_{11}$$
$$d\sigma_2 = (d\varepsilon_2 - S_{12}d\sigma_1)/S_{22}$$

(2.3)

where $d\varepsilon$ and $d\sigma$ are incremental strains and stresses, respectively, and the S's are compliance coefficients. Then assuming that the incremental stresses could be related to incremental equivalent strains, $d\bar{\varepsilon}$,

$$d\sigma_1 = d\bar{\varepsilon}_1/S_{11}$$

$$d\sigma_2 = d\bar{\varepsilon}_2/S_{11}$$

(2.4)

Comparing Eqs. (2-3) and (2-4) the equivalent strains become

$$d\bar{\varepsilon}_1 = d\varepsilon_1 - S_{12}d\sigma_2$$

$$d\bar{\varepsilon}_2 = d\varepsilon_2 - S_{12}d\sigma_1$$

(2.5)

Updated properties were then assumed to be functions of the total equivalent strains. By noting Eqs. (2-4) it can be seen that Sandhu's assumption is identical to proposing that the updated properties are functions of the total lamina stresses.

The ultimate load carrying capacity of the laminates was determined by the plywise application a failure criterion which assumed that the strain energies under longitudinal, transverse, and shear loadings were independent parameters. Sandhu's analysis provided better agreement between theory and experiment for tensile loading of various boron/epoxy laminates than the method proposed by Petit and Waddoups [11]. Thermal stresses were not considered.

Hahn and Tsai [18] considered the uniaxial loading of a crossply graphite/epoxy composite. Using photo-micrographs taken during a uniaxial test, Hahn and Tsai noted that when the load was below the level at which 90° layers were predicted to fail, no cracks were observed in the 90° layers. However, after the specimen was subjected to a load above this level, cracks were observed in the 90° layer. Hahn and Tsai stated that "although the load is carried entirely by 0° layers in the failed regions, outside these regions 90° layers are

still effective in supporting the load." It was also noted that in the undamaged region the modulus (loading direction) was equal to the composite modulus whereas in the failed regions the 0° layers were the only load carrying members. To account for this phenomenon Hahn and Tsai developed an analytical model which was compatible with gradual, not complete, failure of 90° layers. They also noted that the gradual failure model could be applied to other lay-up configurations.

In 1974 Hahn and Pagano [19] proposed that since the fabrication of composite laminates invariably involves temperature differentials of several hundred degrees Fahrenheit, significant residual (curing) stresses develop in these laminates. They also noted that despite this fact, a disciplined analytical treatment of these stresses could not be found in the literature.

Hahn and Pagano developed an incremental thermal analysis to predict the residual thermal stresses and strains over a laminate. Good agreement was shown between theory and experiment for the residual curing strains of two boron/epoxy laminates. They suggested that a knowledge of these residual stresses and strains could play an important role in developing satisfactory failure criteria.

Recently, Foye [20] theoretically predicted the residual curing stresses in a boron/epoxy composite. A micromechanical analysis using a finite element representation of a fiber and matrix was employed. Foye noted instances where the residual stresses exceeded yield in the matrix resin material.

2.2 Interlaminar Stresses

For a thin laminate of finite width subjected to uniaxial loading there exist relatively high interlaminar concentrations at the free edge. Interlaminar normal and interlaminar shear stresses cannot be determined for in-plane loading of symmetric laminates from lamination theory. Researchers have proposed that interlaminar stresses are an important factor in determining the strength of a composite laminate. The finite difference and finite element methods of solution as well as analytical approximations have been used to determine the interlaminar stresses due to inplane loading of laminates but relatively little work has been done to determine the interlaminar stresses due to thermal loading and nonlinear effects.

Pipes and Pagano [21, 22] used an elastic quasi-three-dimensional finite difference technique to evaluate the interlaminar stresses and the influence of stacking sequence on laminate strength for uniform axial strain loading. Pipes, Kaminski, and Pagano [23] extended the work of Pipes and Pagano [21, 22] and noted the possibility of free-edge singularities in angle-ply laminates. Using the same finite difference analysis Pipes [24] presented interlaminar stress results for cross-ply and six-layered laminate configurations subjected to uniform axial strain loading. The investigations of References [21-24] were basically concerned with the behavior of graphite epoxy. The finite difference technique did include a thermal formulation but thermal results were not shown. In fact, only in Reference [21] was any mention made of possible thermal stresses and that was with respect

to stacking sequence.

Isakson and Levy [25] considered the plane stress solution involving the application of the finite-element method. However, the fibrous layers were considered to be orthotropic and separated by layers of finite isotropic thickness that developed only interlaminar shearing stresses. Thus, the method was not capable of determining interlaminar normal stresses. Isakson and Levy's work was similar to earlier work done by Puppo and Evensen [26] who modeled a laminate as orthotropic layers separated by isotropic shear supporting layers. Here, too, interlaminar normal stresses could not be handled due to the plane stress assumption. Levy, Armen and Whiteside [27] extended the work of Isakson and Levy [25] to include plastic deformation of the shear layer. Again, the formulations of References [25-27] did not include thermal loading.

Herakovich and Brooks [28] employing the finite element program of Foye and Baker [29] considered the stress distributions in composite reinforced metals subjected to uniform axial strain loading and thermal loading. Finite element subsections were taken at the free edge. Results showed relatively high interlaminar normal stresses at the intersection of the free-edge and material interfaces especially when the thermal mismatch was significant between layers. The analysis was completely elastic and limited to orthotropic materials oriented in either of the two principal in-plane directions.

Rybicki [30] was able to consider interlaminar stress distributions and noted the effects of stacking sequence by using a three-

dimensional finite-element scheme employing Maxwell stress functions. Thermal and nonlinear effects were not included.

Herakovich [31] has pointed out the significance of interlaminar thermal stresses with respect to loading stresses and stacking sequence for boron/epoxy reinforced metal laminates. Using the finite element program of Foye and Baker [29] Herakovich showed that the magnitude of the interlaminar stresses as a result of thermal mismatch between layers of a laminate could influence the strength of the laminate. Again, the analysis was elastic.

Pagano [32] recently provided a mathematical formulation to determine the interlaminar normal stress at the mid-plane for symmetric cross/ply laminates with thermal and nonlinear effects excluded. Another mathematical formulation for all the stress distributions in symmetric laminates has been presented by Tang and Levy [33]. Some stress distributions were shown to agree quite well with the results of previous investigators [21-24]. Again, their work did not include thermal or nonlinear effects.

Recently Hsu [34] presented a perturbation technique for determining interlaminar stress distributions at interfaces of cross-ply and angle-ply laminates. Graphite/epoxy laminates with stacking sequences of $[0/90]_s$, $[90/0]_s$, $[+45/-45]_s$ and $[-45/45]_s$ were considered. The analysis was limited to elastic strain loading.

Summary

Linear elastic techniques have been used to determine laminate strength using lamination theory. Failure was determined using various

forms of stress interaction failure criteria. However, with the development of nonlinear techniques came the independent failure theories based on lamina ultimate strains. Such was the case for the studies of References [11, 14, 15]. Another independent failure theory was presented by Sandhu [17] where strain energies were assumed to be independent parameters. Thermal effects were completely absent from the nonlinear analyses.

For studies which were concerned with interlaminar stresses and the free edge a nonlinear analysis has virtually been ignored.

Chapter 3

PROBLEM FORMULATION

The problem under investigation is the uniaxial loading of balanced, symmetric composite laminates. Nonlinear, thermal and edge effects on such laminates are considered. Typical laminate geometry is shown in Fig. 1 where $L > b \gg H$. For nonlinear analyses the loading, whether thermal or mechanical, will be an incremental procedure consisting of the solution of successive linear problems. Thus, the following derivation of equations is with respect to any given incremental load.

3.1 Generalized Plane Strain Problem

For a long prismatic bar under the influence of applied strain at the ends or uniform temperature change, the state of stress and strain removed from the ends is independent of position along the bar, i.e., generalized plane strain. Lekhnitskii [35] was the first to consider this problem. For strains independent of coordinate x, the strain-displacement relations can be written as functions of the y and z coordinates as

$$
\begin{aligned}
\varepsilon_x &= u,_x = f_1(y,z) \\
\varepsilon_y &= v,_y = f_2(y,z) \\
\varepsilon_z &= w,_z = f_2(y,z) \\
\gamma_{yz} &= v,_z + w,_y = f_4(y,z) \\
\gamma_{xz} &= w,_x + u,_z = f_5(y,z) \\
\gamma_{xy} &= u,_y + v,_x = f_6(y,z)
\end{aligned}
\tag{3.1}
$$

15
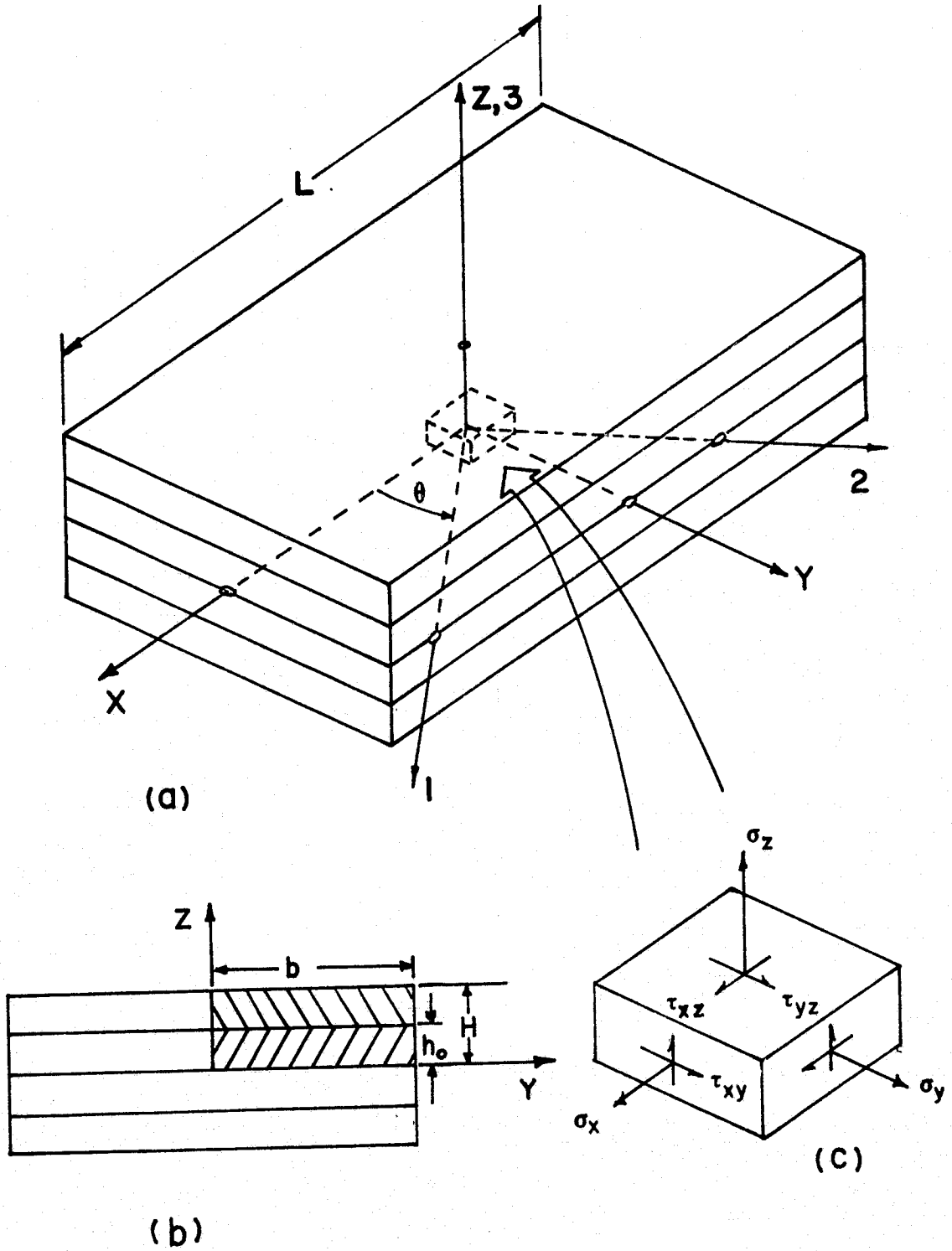
Figure 1. Typical Laminate Geometry

where a comma denotes partial differentiation. The equilibrium equations neglecting body forces reduce to at a point

$$\tau_{xy,y} + \tau_{xz,z} = 0$$
$$\sigma_{y,y} + \tau_{yz,z} = 0 \qquad (3.2)$$
$$\tau_{yz,y} + \sigma_{z,z} = 0$$

Mathematical manipulation of Eqs. (3.1) yields the displacement field

$$u(x,y,z) = x(C_1 y + C_2 z + C_3) + U(y,z)$$

$$v(x,y,z) = x(C_4 z + C_6) - C_1 \frac{x^2}{2} + V(y,z) \qquad (3.3)$$

$$w(x,y,z) = x(-C_4 y + C_5) - C_2 \frac{x^2}{2} + W(y,z)$$

where C_1 through C_6 are unknown constants and U, V and W are unknown functions of y and z.

3.1.1 Balanced Symmetric Laminates

For balanced, symmetric laminates the problem reduces to the analysis of a quarter-section shown cross-hatched in Fig. 1b. The following symmetry and antisymmetry conditions must then prevail with respect to the x-y and x-z planes:

<u>x-y Plane</u>
$$u(x,y,z) = u(x,y,-z)$$
$$v(x,y,z) = v(x,y,-z)$$
$$w(x,y,z) = -w(x,y,-z)$$

$$(3.4)$$

<u>x-z Plane</u>

$$v(x,y,z) = -v(x,-y,z)$$

$$w(x,y,z) = w(x,-y,z)$$

and the experimentally verified [36] condition that

$$u(\overline{x},y,z) = -u(\overline{x},-y,z) \tag{3.5}$$

where $\overline{x}$ is a relative position chosen as zero.

Substitution of Eqs. (3.4) and Eqs. (3.6) into Eqs. (3.3) results in

$$C_1 = C_2 = C_4 = C_5 = C_6 = 0 \tag{3.6}$$

and

$$U(y,z) = U(y,-z)$$

$$V(y,z) = V(y,-z)$$

$$W(y,z) = -W(y,-z)$$

$$U(y,z) = -U(-y,z) \tag{3.7}$$

$$V(y,z) = -V(-y,z)$$

$$W(y,z) = W(-y,z)$$

The reduced forms of Eqs. (3.3) are then

$$u = C_3 x + U(y,z)$$

$$v = V(y,z) \tag{3.8}$$

$$w = W(y,z)$$

The constant C_3 is the uniform applied axial strain, ε_x.

The appropriate traction free boundary conditions are, noting Fig. 1

$$\sigma_y(\pm b, z) = 0$$
$$\tau_{xy}(\pm b, z) = 0 \qquad\qquad (3.9)$$
$$\tau_{yz}(\pm b, z) = 0$$

along the free edges, and

$$\sigma_z(y, \pm H) = 0$$
$$\tau_{yz}(y, \pm H) = 0 \qquad\qquad (3.10)$$
$$\tau_{xz}(y, \pm H) = 0$$

on the top and bottom surfaces of the laminate.

The antisymmetry conditions of Eqs. (3.7) yield the following restrictions on the displacement fields

$$U(0, z) = 0$$
$$V(0, z) = 0 \qquad\qquad (3.11)$$
$$W(y, 0) = 0$$

The symmetry conditions of Eqs. (3.7) in turn yield the conditions

$$U_{,z}(y, 0) = 0$$
$$V_{,z}(y, 0) = 0 \qquad\qquad (3.12)$$
$$W_{,y}(0, z) = 0$$

The boundary value problem represented by Eqs. (3.8) through Eqs. (3.12) is independent of material behavior. For an orthotropic lamina oriented in the principal material directions the three-dimensional constitutive relationships are

$$\begin{Bmatrix} \sigma_1 \\ \sigma_2 \\ \sigma_3 \\ \tau_{23} \\ \tau_{13} \\ \tau_{12} \end{Bmatrix} = \begin{bmatrix} C_{11} & C_{12} & C_{13} & 0 & 0 & 0 \\ C_{12} & C_{22} & C_{23} & 0 & 0 & 0 \\ C_{13} & C_{23} & C_{33} & 0 & 0 & 0 \\ 0 & 0 & 0 & C_{44} & 0 & 0 \\ 0 & 0 & 0 & 0 & C_{55} & 0 \\ 0 & 0 & 0 & 0 & 0 & C_{66} \end{bmatrix} \begin{Bmatrix} \varepsilon_1 \\ \varepsilon_2 \\ \varepsilon_3 \\ \gamma_{23} \\ \gamma_{13} \\ \gamma_{12} \end{Bmatrix} \tag{3.13}$$

and with the 1 axis perpendicular to a plane of isotropy

$$C_{33} = C_{22}, \quad C_{13} = C_{12}, \quad C_{55} = C_{66}$$
$$C_{44} = \frac{1}{2}(C_{22} - C_{23}) \tag{3.14}$$

For a coordinate transformation in the 1-2 plane, that is, about the 3 axis (Fig. 1), the relations for the transformed stresses and strains are

$$\{\sigma\}_{xyz} = [T_1]\{\sigma\}_{123}$$
$$\{\varepsilon\}_{xyz} = [T_2]\{\varepsilon\}_{123} \tag{3.15}$$

and thus

$$\{\sigma\}_{xyz} = [\overline{C}]\{\varepsilon\}_{xyz} \tag{3.16}$$

where

$$[\overline{C}] = [T_1][C][T_2]^{-1} \tag{3.17}$$

and

$$
[T_1] = \begin{bmatrix}
m^2 & n^2 & 0 & 0 & 0 & 2mn \\
n^2 & m^2 & 0 & 0 & 0 & -2mn \\
0 & 0 & 1 & 0 & 0 & 0 \\
0 & 0 & 0 & m & -n & 0 \\
0 & 0 & 0 & n & m & 0 \\
-mn & mn & 0 & 0 & 0 & (m^2-n^2)
\end{bmatrix}
$$

$$
[T_2] = \begin{bmatrix}
m^2 & n^2 & 0 & 0 & 0 & mn \\
n^2 & m^2 & 0 & 0 & 0 & -mn \\
0 & 0 & 1 & 0 & 0 & 0 \\
0 & 0 & 0 & m & -n & 0 \\
0 & 0 & 0 & n & m & 0 \\
-2mn & 2mn & 0 & 0 & 0 & (m^2-n^2)
\end{bmatrix}
$$

(3.18)

$$
m = \cos\theta \quad , \quad n = \sin\theta
$$

and [C] is defined by Eq. (3.13).

Expanding Eq. (3.16)

$$
\begin{Bmatrix}
\sigma_x \\
\sigma_y \\
\sigma_z \\
\tau_{yz} \\
\tau_{xz} \\
\tau_{xy}
\end{Bmatrix}
=
\begin{bmatrix}
\overline{C}_{11} & \overline{C}_{12} & \overline{C}_{13} & 0 & 0 & \overline{C}_{16} \\
\overline{C}_{12} & \overline{C}_{22} & \overline{C}_{23} & 0 & 0 & \overline{C}_{26} \\
\overline{C}_{13} & \overline{C}_{23} & \overline{C}_{33} & 0 & 0 & \overline{C}_{36} \\
0 & 0 & 0 & \overline{C}_{44} & \overline{C}_{45} & 0 \\
0 & 0 & 0 & \overline{C}_{45} & \overline{C}_{55} & 0 \\
\overline{C}_{16} & \overline{C}_{26} & \overline{C}_{36} & 0 & 0 & \overline{C}_{66}
\end{bmatrix}
\begin{Bmatrix}
\varepsilon_x \\
\varepsilon_y \\
\varepsilon_z \\
\gamma_{yz} \\
\gamma_{xz} \\
\gamma_{xy}
\end{Bmatrix}
$$

(3.19)

For a uniform temperature distribution, ΔT, the lamina principal thermal strains, $\{\varepsilon^T\}_{123}$, are

$$\{\varepsilon^T\}_{123} = \begin{Bmatrix} \alpha_1 \Delta T \\ \alpha_2 \Delta T \\ \alpha_3 \Delta T \\ 0 \\ 0 \\ 0 \end{Bmatrix} \qquad (3.20)$$

and then transformed

$$\{\varepsilon^T\}_{xyz} = \begin{Bmatrix} \alpha_x \Delta T \\ \alpha_y \Delta T \\ \alpha_z \Delta T \\ 0 \\ 0 \\ \alpha_{xy} \Delta T \end{Bmatrix} \qquad (3.21)$$

where

$$\begin{aligned}
\alpha_x &= m^2 \alpha_1 + n^2 \alpha_2 \\
\alpha_y &= n^2 \alpha_1 + m^2 \alpha_2 \\
\alpha_z &= \alpha_3 \\
\alpha_{xy} &= 2mn(\alpha_2 - \alpha_1)
\end{aligned} \qquad (3.22)$$

and the α's are respective thermal coefficients. The strains in Eq. (3.19) become for the uniform temperature distribution, noting that $\{\varepsilon^0\}$ represents the total strain,

$$\{\varepsilon\}_{xyz} = \begin{Bmatrix} \varepsilon_x^o - \alpha_x \Delta T \\ \varepsilon_y^o - \alpha_y \Delta T \\ \varepsilon_z^o - \alpha_z \Delta T \\ \gamma_{yz}^o \\ \gamma_{xz}^o \\ \gamma_{xy}^o - \alpha_{xy} \Delta T \end{Bmatrix} \qquad (3.23)$$

The finite element method was employed to solve the complete boundary value problem given by Eqs. (3.8) through Eqs. (3.12), Eq. (3.19) and Eq. (3.23).

3.2 Finite Element Formulation

The basis of the finite element method is the representation of a body or structure by an assemblage of subdivisions called "finite elements." Figure 2a shows a typical triangular finite element discretization of the quarter-section shown cross-hatched in Fig. 1b. Simple functions are then chosen to approximate the distribution or variation of the actual displacements over each element. These functions are usually referred to as "displacement functions." A variational principle of mechanics, such as the principle of minimum potential energy, can then be employed to obtain the set of equilibrium equations for each element. The equilibrium equations for the entire body are then obtained by combining the equations for the individual elements in such a way that continuity of displacements is preserved at the interconnecting nodes. The equations are modified for the given force or displacement boundary conditions and then solved to obtain the unknown
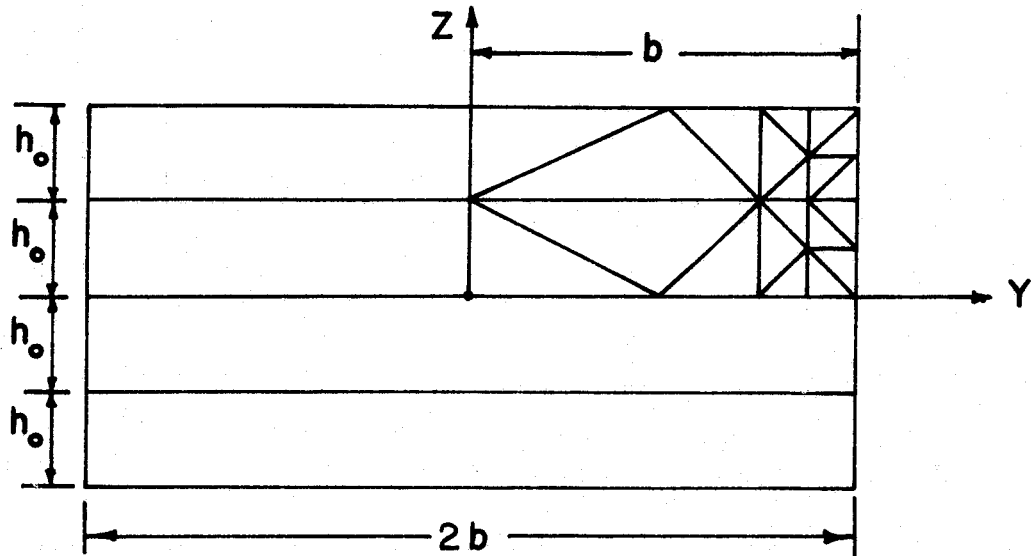
(a)
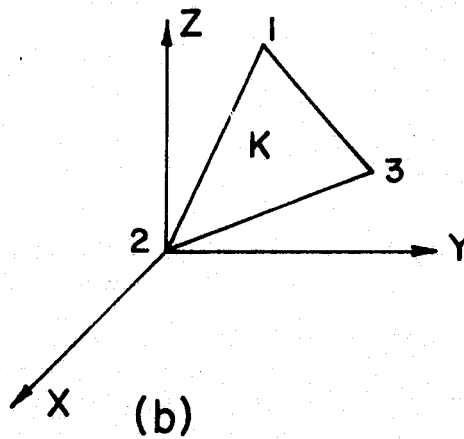
(b)

Figure 2. Finite Element Discretization and Element Geometry

displacements. Desired solutions in terms of strains and/or stresses can then be determined.

The constant stress-constant strain triangular element consisting of three nodes, Fig. 2b, was chosen for this investigation. The form of the displacement functions which satisfy Eqs. (3.8) and yield constant strains when substituted into Eqs. (3.1) are the linear relations

$$u = a_1 + a_2y + a_3z + \xi_x x$$
$$v = a_4 + a_5y + a_6z \qquad (3.24)$$
$$w = a_7 + a_8y + a_9z$$

3.2.1 Uniform Axial Strain Loading

Substituting Eqs. (3.24) into Eqs. (3.2) yields

$$\varepsilon_x = \xi_x$$
$$\varepsilon_y = a_5$$
$$\varepsilon_z = a_9$$
$$\gamma_{yz} = a_6 + a_8 \qquad (3.25)$$
$$\gamma_{xz} = a_3$$
$$\gamma_{xy} = a_2$$

The quarter-section shown cross-hatched in Fig. 1b is replaced by triangular elements as shown in Fig. 2a. The value of ξ_x is the prescribed uniform strain loading over all the elements and is normal to the finite element grid. The values of the a's in Eqs. (3.25) must be determined as functions of the displacements at the three nodes of each element. Considering, therefore, Eqs. (3.24) and the nodal

displacements of an arbitrary finite element K, Fig. 2b, the displacements become

$$
\begin{Bmatrix} u_1 \\ u_2 \\ u_3 \end{Bmatrix} = \begin{bmatrix} 1 & y_1 & z_1 \\ 1 & y_2 & z_2 \\ 1 & y_3 & z_3 \end{bmatrix} \begin{Bmatrix} a_1 \\ a_2 \\ a_3 \end{Bmatrix} + \begin{Bmatrix} \xi_x x_1 \\ \xi_x x_2 \\ \xi_x x_3 \end{Bmatrix}
$$

$$
\begin{Bmatrix} v_1 \\ v_2 \\ v_3 \end{Bmatrix} = \begin{bmatrix} 1 & y_1 & z_1 \\ 1 & y_2 & z_2 \\ 1 & y_3 & z_3 \end{bmatrix} \begin{Bmatrix} a_4 \\ a_5 \\ a_6 \end{Bmatrix} \tag{3.26}
$$

$$
\begin{Bmatrix} w_1 \\ w_2 \\ w_3 \end{Bmatrix} = \begin{bmatrix} 1 & y_1 & z_1 \\ 1 & y_2 & z_2 \\ 1 & y_3 & z_3 \end{bmatrix} \begin{Bmatrix} a_7 \\ a_8 \\ a_9 \end{Bmatrix}
$$

Using Cramer's Rule and letting

$$
\begin{aligned}
y_{ij} &= y_i - y_j \\
z_{ij} &= z_i - z_j
\end{aligned} \tag{3.27}
$$

and realizing that

$$
2A_K = 2 \times (\text{Area of Element K}) = \text{Det} \begin{vmatrix} 1 & y_1 & z_1 \\ 1 & y_2 & z_2 \\ 1 & y_3 & z_3 \end{vmatrix}
$$

the a's that are needed for Eqs. (3.25) are found to be

$$a_3 = \frac{1}{2A_K} [y_{32}u_1' + y_{13}u_2' + y_{21}u_3']$$

$$a_2 = \frac{1}{2A_K} [z_{23}u_1' + z_{31}u_2' + z_{12}u_3']$$

$$a_5 = \frac{1}{2A_K} [z_{23}v_1 + z_{31}v_2 + z_{12}v_3]$$

$$a_9 = \frac{1}{2A_K} [y_{32}w_1 + y_{13}w_2 + y_{21}w_3] \qquad (3.28)$$

$$a_6 = \frac{1}{2A_K} [y_{32}v_1 + y_{13}v_2 + y_{21}v_3]$$

$$a_8 = \frac{1}{2A_K} [z_{23}w_1 + z_{31}w_2 + z_{12}w_3]$$

where

$$u_i' = u_i - \xi_x x_i \qquad i = 1, 2, 3 \qquad (3.29)$$

Noting that $x_1 = x_2 = x_3$ (initial coordinates) the $\xi_x x_i$ term is then either multiplied by

$$y_{32} + y_{13} + y_{21} = 0 \qquad (3.30)$$

or

$$z_{23} + z_{31} + z_{12} = 0 \qquad (3.31)$$

The first two of Eqs. (3.28) then reduce to

$$a_3 = \frac{1}{2A_K} [y_{32}u_1 + y_{13}u_2 + y_{21}u_3]$$

$$a_2 = \frac{1}{2A_K} [z_{32}u_1 + z_{31}u_2 + z_{12}u_3] \qquad (3.32)$$

letting

$$a = z_{23}/2 \quad , \quad b = y_{32}/2 \quad , \quad c = z_{31}/2$$

$$d = y_{13}/2 \quad , \quad e = z_{12}/2 \quad , \quad g = y_{21}/2 \qquad (3.33)$$

and using the results obtained for the a's the strains become

$$
\left\{
\begin{array}{c}
\varepsilon_x \\
\varepsilon_y \\
\varepsilon_z \\
\gamma_{yz} \\
\gamma_{xz} \\
\gamma_{xy}
\end{array}
\right\}_K
= \frac{1}{A_K}
\left[
\begin{array}{l}
\xi_x A_K \\
av_1 + cv_2 + ev_3 \\
bw_1 + dw_2 + gw_3 \\
bv_1 + dv_2 + gv_3 + aw_1 + cw_2 + ew_3 \\
bu_1 + du_2 + gu_3 \\
au_1 + cu_2 + eu_3
\end{array}
\right]
\tag{3.34}
$$

Equation (3.34) represents the strain-displacement relations of a finite element for a prescribed uniform axial strain load. However, it may be advantageous to prescribe the average force over the cross-section and solve for the resulting uniform strain. The need to do this arises in thermal loading for which the resultant forces normal to the cross-section is prescribed as zero. Of course, thermal loading is not the only case where the resultant force is prescribed but the following analysis is developed with the thermal problem in mind.

3.2.2 Thermal Loading - Average Force

Consider $\bar{\xi}_x$ to be an unknown uniform strain value over the quarter-section of Fig. 2a and F to be the average force over the section. Letting $\{\varepsilon^o\}^K$ represent the total strain in an element, $\{\varepsilon^T\}^K$ the elemental thermal strains, and $\{\varepsilon\}^K$ the resulting mechanical strains, then

$$
\{\varepsilon\}^K_{123} = \{\varepsilon^o\}^K_{123} - \{\varepsilon^T\}^K_{123}
\tag{3.35}
$$

and transforming

$$\{\varepsilon\}_{xyz}^{K} = \{\varepsilon^\circ\}_{xyz}^{K} - [T_2]_K \{\varepsilon^T\}_{123}^{K} \qquad (3.36)$$

Letting $\{\varepsilon^\circ\}_{xyz}^{K}$ have the functional form of Eq. (3.34) and noting Eq. (3.20) then

$$
\left\{
\begin{array}{c}
\varepsilon_x \\
\varepsilon_y \\
\varepsilon_z \\
\gamma_{yz} \\
\gamma_{xz} \\
\gamma_{xy}
\end{array}
\right\}_K
=
\left[
\begin{array}{l}
\overline{\varepsilon}_x - (m^2 \alpha_1 \Delta T + n^2 \alpha_2 \Delta T) \\
(av_1 + cv_2 + ev_3)/A_K - (n^2 \alpha_1 \Delta T + m^2 \alpha_2 \Delta T) \\
(bw_1 + dw_2 + gw_3)/A_K - \alpha_3 \Delta T \\
(bv_1 + dv_2 + gv_3 + aw_1 + cw_2 + ew_3)/A_K \\
(bu_1 + du_2 + gu_3)/A_K \\
(au_1 + cu_2 + eu_3)/A_K + 2mn\Delta T(\alpha_1 - \alpha_2)
\end{array}
\right]
\qquad (3.37)
$$

Equation (3.37) represents the strain-displacement relations when the uniform strain must be determined.

3.2.3 Minimization of Total Potential Energy

The total potential energy, ψ, of a system is the sum of the strain energy, U, and the potential energy of the external loads, W.

$$\psi = U + W \qquad (3.38)$$

The strain energy over an arbitrary element K is given by

$$U_K = \frac{1}{2} \int \{\varepsilon\}_K^T [\mathcal{C}]_K \{\varepsilon\}_K \, dvol \qquad (3.39)$$

and for an element of unit thickness and constant strains the strain energy can be written as

$$U_K = \frac{A_K}{2} \{\varepsilon\}_K^T [\mathcal{C}]_K \{\varepsilon\}_K \qquad (3.40)$$

The external work over the element is given as

$$W_K = -(f_{ij}\delta_{ij})_K \tag{3.41}$$

where $i = 1, 2, 3$ -- Nodes

                $j = x, y, z$ -- Directions

Substituting Eqs. (3.40) and (3.41) into Eq. (3.38) yields the total potential energy for the element.

$$\psi_K = U_K + W_K = \frac{A_K}{2} \{\epsilon\}_K^T [C]\{\epsilon\}_K - (f_{ij}\delta_{ij})_K \tag{3.42}$$

For the prescribed strain loading, substitution of Eqs. (3.34) into Eq. (3.42) and minimizing ψ_K with respect to each displacement, noting that

$$\delta_{ij}\Big|_{\substack{i = 1 \\ j = x}} = \delta_{1x} = u_1 \quad \text{etc.} \tag{3.43}$$

the elemental stiffness matrix can be formed. Thus performing

$$\begin{Bmatrix} \partial\psi/u_i \\ \partial\psi/v_i \\ \partial\psi/w_i \end{Bmatrix} = 0 \qquad i = 1, 2, 3 \tag{3.44}$$

yields

$$
\begin{bmatrix} \mathcal{K} \\ 9\times 9 \end{bmatrix}
\begin{Bmatrix} u_1 \\ u_2 \\ u_3 \\ v_1 \\ v_2 \\ v_3 \\ w_1 \\ w_2 \\ w_3 \end{Bmatrix}
+ \xi_x
\begin{Bmatrix} C_{16}a \\ C_{16}c \\ C_{16}e \\ C_{12}a \\ C_{12}c \\ C_{12}e \\ C_{13}b \\ C_{13}d \\ C_{13}g \end{Bmatrix}_K
=
\begin{Bmatrix} f_{1x} \\ f_{2x} \\ f_{3x} \\ f_{1y} \\ f_{2y} \\ f_{3y} \\ f_{1z} \\ f_{2z} \\ f_{3z} \end{Bmatrix}_K
\qquad (3.45)
$$

where $\mathcal{K}$ is the elemental stiffness matrix given in Appendix A.

For the average force loading the strains in Eq. (3.42) are replaced by the strains of Eq. (3.37). Minimizing ψ_K with respect to each displacement and $\overline{\xi}_K$ the elemental stiffness equations take the form

$$
\begin{bmatrix} \mathcal{K}' \\ 10\times 10 \end{bmatrix}
\begin{Bmatrix} u_1 \\ u_2 \\ u_3 \\ v_1 \\ v_2 \\ v_3 \\ w_1 \\ w_2 \\ w_3 \\ \overline{\xi}_x \end{Bmatrix}
-
\begin{Bmatrix} T \\ H \\ E \\ R \\ M \\ A \\ L \\ \\ T \\ E \\ R \\ M \\ S \end{Bmatrix}_K
=
\begin{Bmatrix} f_{1x} \\ f_{2x} \\ f_{3x} \\ f_{1y} \\ f_{2y} \\ f_{3y} \\ f_{1z} \\ f_{2z} \\ f_{3z} \\ F_K \end{Bmatrix}_K
\qquad (3.46)
$$

where $\mathcal{K}'$ is the elemental stiffness matrix for average force loading. The forms of $\mathcal{K}'$ and the "thermal terms" can be found in Appendix A. The additional equation can be written as

$$\sum_{k=1}^{n} F_K = F \qquad (3.47)$$

where n is the number of elements. If there is no thermal loading then the problem reduces to an average force loading problem and the "thermal terms" vanish. For thermal analyses the value of F is set to zero.

Depending on the nature of the problem, the elemental stiffness matrices will be of the form given in Eq. (3.45) or Eq. (3.46). The total stiffness matrix for the cross-section is then formed by combining the elemental stiffness matrices for all the elements. The total stiffness matrix for N number of nodes will be 3N x 3N for the prescribed uniform strain-analysis and (3N + 2) x (3N + 1) for the average force analysis, the additional equation being Eq. (3.47). The displacement boundary conditions are those of Eqs. (3.11).

3.2.4 Program NONCOM

A finite element program using the analysis of the previous sections has been developed. Various subroutines were written which allow reduction in data input, one of which is a subdividing mesh generator (Appendix A). The others include a boundary condition generator for symmetric problems and a force dividing routine to approximate a constant stress loading condition in either of the two

or both in-plane directions.

Basically, the program involves the storing of the elemental stiffness matrices. Then the master stiffness matrix is formed, while accounting for force and displacement boundary conditions, and stored on disks in prescribed record lengths. Double precisioned Gaussian reduction is then performed to form an upper triangular matrix followed by backward substitution in a general equation solver. The word "general" here means that the equation solver is dependent only on the size of the matrix (to date it can handle a 3000 by 3000 matrix but computer time would be excessive) and not how the matrix was formed.

3.2.5 Boundary Requirements for Laminates

As previously mentioned the boundary conditions for balanced, symmetric laminate studies are given by Eqs. (3.9), (3.10), (3.11) and (3.12). However, only the displacement boundary conditions of Eqs. (3.11) can be prescribed in the present finite element formulation. It is important that the results of any analyses in this investigation satisfy the remaining boundary conditions. The most interesting conditions are those of Eqs. (3.12). While the conditions of Eqs. (3.12) are essentially slope requirements of the respective displacement functions a different view will shed more light on the conditions.

By considering Eqs. (3.8) and the equations for the shear strains γ_{xz} and γ_{yz} from Eqs. (3.1) the strain-displacement for γ_{xz} and γ_{yz} can be written as

$$\gamma_{xz} = U,_z(y,z) + W,_x(y,z)$$
$$\gamma_{yz} = V,_z(y,z) + W,_y(y,z)$$

(3.48)

At $z = 0$, Eqs. (3.48) become

$$\gamma_{xz}(y,0) = U,_z(y,0) + W,_x(y,0)$$
$$\gamma_{yz}(y,0) = V,_z(y,0) + W,_y(y,0)$$

(3.49)

and at $y = 0$

$$\gamma_{yz}(0,z) = V,_z(0,z) + W,_y(0,z)$$

(3.50)

Substitution of Eqs. (3.11) and Eqs. (3.12) into Eqs. (3.49) and Eq. (3.50) will give the additional conditions that

$$\gamma_{xz}(y,0) = 0$$
$$\gamma_{yz}(y,0) = 0$$
$$\gamma_{yz}(0,z) = 0$$

(3.51)

Chapter 4

NONLINEAR DEVELOPMENT

Modern composite materials such as boron/epoxy, graphite/epoxy and borsic/aluminum generally exhibit nonlinear transverse and shear behavior. In addition, many of the mechanical properties of these materials are highly temperature dependent. An incremental loading procedure was developed to theoretically predict the response to failure of various laminate configurations comprised of such materials. The lamina properties were allowed to change with respect to both temperature and strain levels.

4.1 Incremental Procedure of Analysis

Uniform axial strain and thermal loading of balanced, symmetric composite laminates were considered. Initial thermal stresses and strains due to a temperature change from an elevated stress-free temperature (the temperature at which bonding occurs) to room temperature were determined through an incremental thermal analysis. The laminates were then subjected to incremental uniaxial strain loading. The finite element formulation of Section 3.2 was employed for the analyses. At each stage of the incremental procedure the mechanical properties of each finite element could be altered depending on the temperature and/or the strain level. This procedure allowed the properties at a point (finite element) within a given layer to change independently of other regions in the layer.

4.1.1 Determination of Current Material Properties

Nonlinear lamina stress-strain curves were represented by Ramberg-Osgood [16] approximations (Appendix B). The form of the Ramberg-Osgood equation used in the present investigation was

$$\varepsilon = \frac{\sigma}{E_e} + K\sigma^n \tag{4.1}$$

where E_e is the constant elastic modulus, and K and n are the Ramberg-Osgood coefficients. The appropriate components of stress and strain and modulus are used in Eq. (4.1) for normal or shear behavior. Solving Eq. (4.1) for the slope $d\sigma/d\varepsilon$ yields

$$\frac{d\sigma}{d\varepsilon} = \bar{E} = \frac{E_e}{KE_e n\sigma^{n-1} + 1} \tag{4.2}$$

where $\bar{E}$ is the current modulus. A parallel research effort by M. Renieri [37] has also shown that Eq. (4.1) gives an adequate representation of the nonlinear stress-strain curves of structural adhesives. Ramberg-Osgood parameters determined in the investigation of M. Renieri can be applied directly to the present analysis for problems where an adhesive layer is considered.

Previous investigators [12, 14, 15] have considered the functional form of the current modulus to be dependent on the current principal material strain. This same assumption was made for the present analysis. Equation (4.2) is made strain dependent by determining the stress value which corresponds to the current principal lamina strain. Noting Fig. 3 the corresponding stress, σ^P, at the
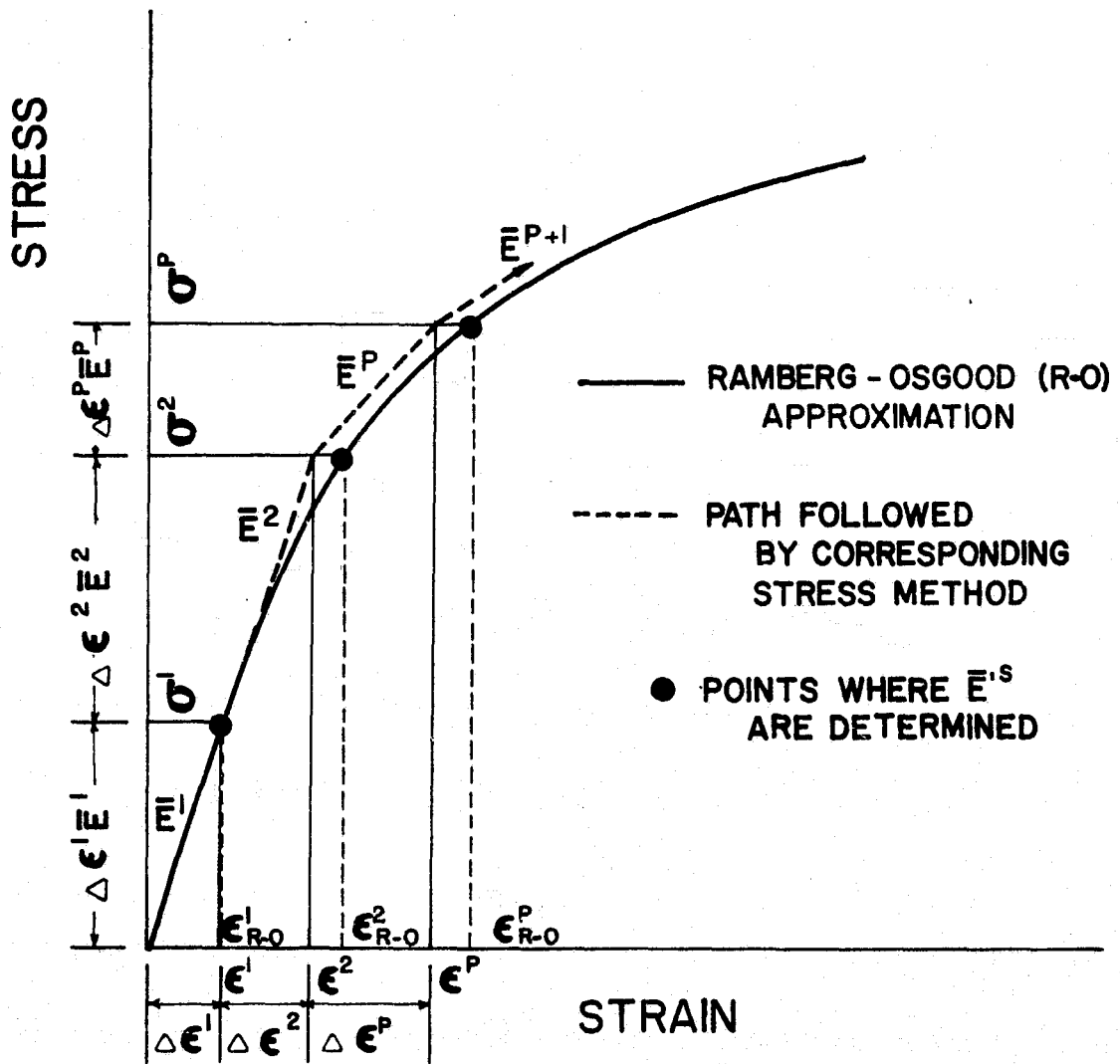
Figure 3. Graphical Representation of Method to Determine Current
Modulus

end of load increment P is

$$\sigma^P = \sum_{i=1}^{P} \Delta E^i \bar{E}^i \qquad (4.3)$$

where ΔE^i is the increment of principal strain during the ith loading increment. Substituting Eq. (4.3) into Eq. (4.2) yields for the $P + 1^{st}$ increment

$$\bar{E}^{P+1} = \frac{E_e}{KE_e n \left[\sum_{i=1}^{P} \Delta E^i \bar{E}^i \right]^{n-1} + 1} \qquad (4.4)$$

It can be seen from Fig. 3 that the value of $\bar{E}$ for the $P + 1^{st}$ increment of loading is based upon the slope of the Ramberg-Osgood curve at the stress σ^P. Thus, the value of the current modulus is actually being interpolated at a strain, ϵ_{R-0}^P, which is greater than ϵ^P. However, the smaller the load increment the smaller the difference between ϵ_{R-0}^P and ϵ^P. Equations of the form of Eq. (4.4) were used to determine the current values of the moduli $\bar{E}_{11}$, $\bar{E}_{22}$, $\bar{E}_{33}$, $\bar{G}_{23}$, $\bar{G}_{13}$ and $\bar{G}_{12}$ for each finite element at the end of each load increment.

Thermal loading consisted of applying increments of uniform temperature change to the laminate. The lamina moduli are temperature dependent as shown by the percent retention of room temperature property curves in Appendix B (Figures B-9 through B-11). A study of available experimental results [14, 41, 42] showed that the percent retention curves gave a good approximation up to some value of strain denoted by ϵ_A as shown in Fig. 4. The percent retention curves did
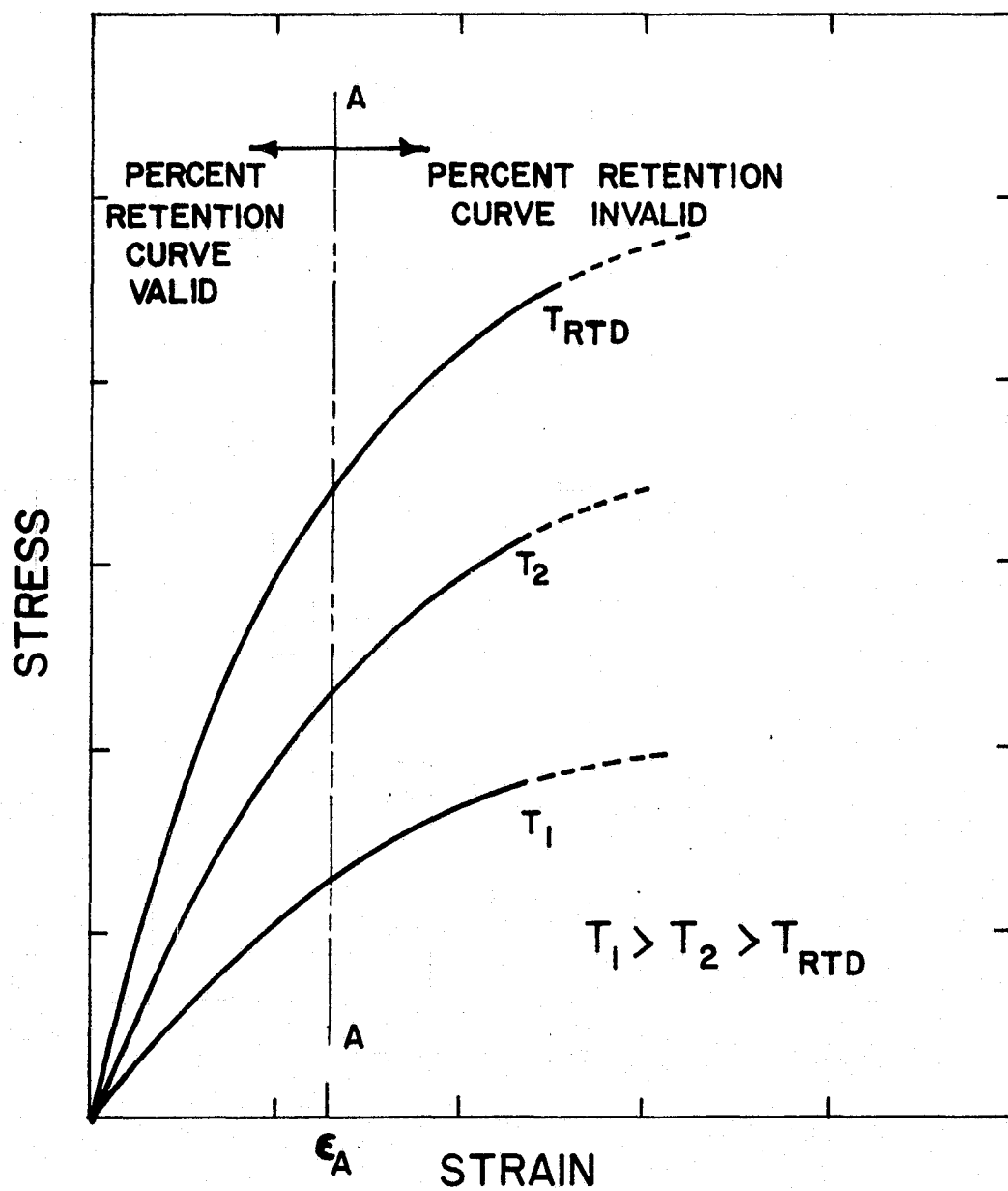
Figure 4. Typical Nonlinear Stress-Strain Curves as a Function of Temperature

not provide good approximations for large nonlinear strains and hence this thermal analysis is limited to strains below ε_A. Values of ε_A are given in Appendix B.

At the end of each thermal increment the lamina principal strains were determined for each finite element. Forms of Eq. (4.4) were then used to determine the current moduli with the values of $\overline{E}^i$ being room temperature values. Once an $\overline{E}^{P+1}$ was determined for room temperature it was reduced to the value associated with the current temperature (mid-point of increment). The percent retention curves were represented by linear segments and thus direct linear interpolation was used to reduce the value of any modulus $\overline{E}^{P+1}$.

Figure B-12 of Appendix B illustrates that the coefficients of expansion also vary with temperature. Again, linear interpolation was used to determine the current values of the coefficients of thermal expansion during the incremental loading. Values were calculated at the mid-point of each increment.

After thermal cooling the laminate was subjected to uniaxial strain loading. Such an analysis can result in the unloading of certain strain components. For the present analysis all strain unloading was assumed to follow the respective stress-strain curve. This assumption was made based on the fact that initial thermal strains were limited to cases where the individual strains remained below the value of ε_A shown in Fig. 4. This is an area where future research endeavors should be conducted.

4.1.2 Nonlinear Lamina Data

The present investigation, which allows for different proper-
ties in tension and compression, had the following limitations:

- σ_2 - ε_2 and σ_3 - ε_3 data are identical.

- Shear stress-strain data were the same for all three principal
  material shear directions.

- Poisson's ratios do not vary with strain.

Thus, for a given material system five stress-strain curves were re-
quired--σ_1 - ε_1 curves in tension and compression, σ_2 - ε_2 curves in
tension compression, and a τ_{12} - γ_{12} curve.

The present analysis also requires percent retention of room
temperature properties data for the above stress-strain curves. The
following assumptions with regard to temperature were postulated:

- Percent retention is identical for tensile and compressive
  behavior.

- Poisson's ratios are independent of temperature.

Coefficients of thermal expansion data were required for the
principal material directions 1, 2 and 3. The value of α_2 and α_3 were
assumed to be identical.

All thermal data were assumed to be identical for both coupon
and sandwich beam values. An adequate explanation of the differences
between coupon and sandwich beam tests can be found in Reference [14].

4.2 Progressive Failure Theory

The following is a proposed theory of individual lamina behavior
in a composite laminate after a respective principal material strain

has reached its ultimate value. The theory assumes that the failing lamina will continue to support the load at regions removed from the region of failure, even in the failing direction. Since the present analysis cannot handle localized failure along the x-direction (see Fig. 1) a progressive reduction of the current modulus of the failing component of strain was assumed.

Letting ε^u represent the ultimate strain value in the principal direction the over-strain, ε^0 (strain in excess of the ultimate strain ε^u), is calculated from

$$\varepsilon^0 = \varepsilon^P - \varepsilon^u \qquad (4.5)$$

where ε^P is the current strain. The progressive failure theory proposes that the current modulus above ε^u is

$$\bar{E}^{P+1} = \bar{E}^P(\varepsilon^u - \varepsilon^0)/\varepsilon^u \qquad (4.6)$$

where $\bar{E}^P$ is the previous modulus and $\bar{E}^{P+1}$ is the current modulus for the next load increment. Substituting Eq. (4.6) into Eq. (4.5) the current modulus becomes

$$\bar{E}^{P+1} = \bar{E}^P(2\varepsilon^u - \varepsilon^P)/\varepsilon^u \qquad (4.7)$$

Thus, as ε^P increases, the value of $\bar{E}^{P+1}$ decreases.

Using Eq. (4.7) in conjunction with the Ramberg-Osgood interpolation of Section 4.1.1 the value of the strain ε^P is associated with the corresponding stress, σ^P (Eq. 4.3). Thus, replacing ε^u with the ultimate stress, σ^u, Eq. 4.7 becomes

$$\bar{E}^{P+1} = \bar{E}^P(2\sigma^u - \sigma^P)/\sigma^u \qquad (4.8)$$

It should be noted that the value of σ^P is limited to (to avoid a negative modulus)

$$\sigma^P < 2\sigma^u \qquad (4.9)$$

In other words, considerable over-straining would be unrealistic.

4.2.1 Total Failure

The progressive failure theory was applied to finite elements which had reached individual component failure values. Cross-ply and angle-ply laminates were initially considered. The laminates were initially subjected to thermal cooling and then uniaxially strain loaded. Failure modes were noted and total failure was evident when at least one failure level had been reached in each element.

More complex laminates were then considered and the failure modes noted. For some cases all elements experienced at least one failure mechanism while other cases showed failure mechanisms occuring only at the free-edge. The results of these analyses will be discussed in Chapters 5 and 6.

Chapter 5

INTERLAMINAR STRESSES AND THE BOUNDARY LAYER

Previous investigations [22-28, 31, 34] have shown that interlaminar stress concentrations exist in a boundary layer region at the free-edge of composite laminates. These stress concentrations generally exist at material or laminae interfaces with the maximum value of the interlaminar stresses σ_z and τ_{xz} occurring at the free-edge. The maximum value of the interlaminar stress τ_{yz} occurs at a location slightly removed from the free-edge because of the stress-free boundary condition $\tau_{yz}(b,z) = 0$.

This chapter is concerned with the distribution of the interlaminar stresses along the laminate interfaces and through the laminate thickness resulting from both thermal and uniaxial strain loading. The material systems considered were graphite/epoxy, boron/epoxy and borsic/aluminum (material properties are given in Appendix B). The stress-free temperature for these materials must be known for the thermal loading.

5.1 Stress-Free Temperature

The maximum temperature of the curing cycle for composite laminates is referred to as the "cure temperature." The stress-free temperature is the temperature at which bonding occurs. If bonding initiates at the maximum temperature during curing then the stress-free temperature and the cure temperature are identical. However, Oken and June [38] noted that the stress-free temperature was

44

considerably lower than the cure temperature for boron/epoxy rein-
forced metals. Tsai and Hahn [39] noted that for some boron/epoxy
laminates the stress-free temperature was slightly below the cure
temperature. Viswanathan [40] calculated the stress-free tempera-
ture for unidirectional borsic/aluminum to be 430°F which is well
below the cure temperature of approximately 1000°F.

The cure temperature for boron/epoxy and graphite/epoxy is
350°F and in keeping with the findings of the previous mentioned in-
vestigations a stress-free temperature of 270°F was assumed for
these epoxy matrix materials. The stress-free temperature for
borsic/aluminum was assumed to be 430°F as determined by Viswanathan
[40]. It should be noted that the method of analysis is not depen-
dent on these temperatures. Results could be obtained for any arbi-
trary temperature.

5.2 Averaging of Finite Element Results

The present analysis provides results in the form of displace-
ments at the finite element nodes and constant strains and stresses
for each element. Realizing that interlaminar stresses must be con-
tinuous throughout a laminate, the magnitudes of these stresses at
interfaces were determined by averaging the values of the stresses
in the finite elements on both sides of the interface (elements can-
not contain the interface). For example, noting Fig. 5a, the mag-
nitude of an interlaminar stress component at point A was determined
by averaging the value of stress component from finite elements
1, 2, 3 and 4. A similar technique was employed to determine
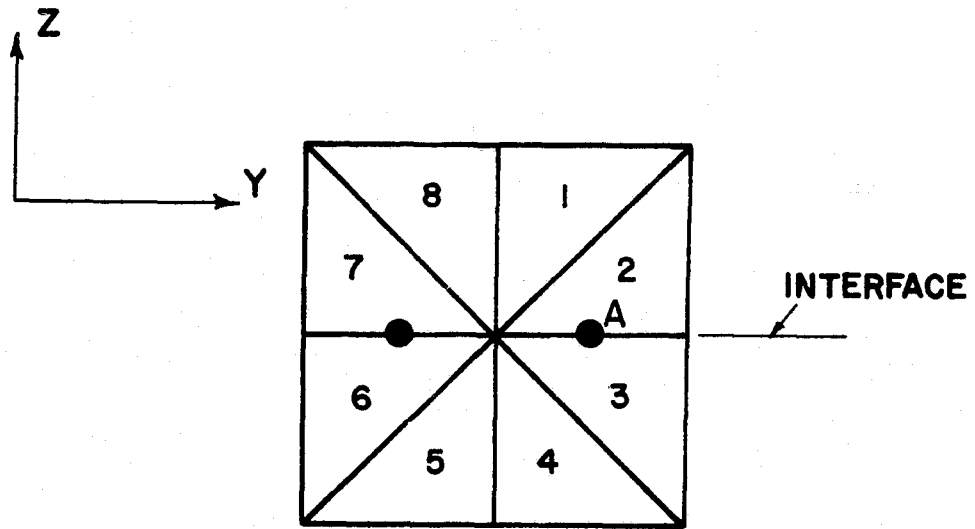
a. Interfacial Stress Distribution
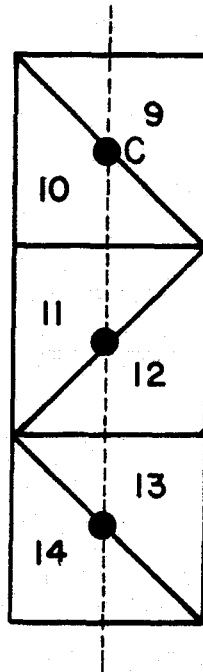
b. Through Thickness Distribution

Figure 5. Method for Computing Interlaminar Stresses

interlaminar stress distributions through the thickness. For example, noting Fig. 5b, the value of an interlaminar stress at point C is the average of the stresses on elements 9 and 10.

5.3 Linear Elastic Results

To determine the accuracy of the present method of analysis results were obtained for strain loading of three graphite/epoxy laminates for which numerical solutions were available. These laminates were the four layer cross-ply $[90/0]_s$ and $[0/90]_s$ laminates, the four layer $[+45/-45]_s$ laminate, and the six layer $[+45/-45/0]_s$, $[+45/0/-45]_s$ and $[0/+45/-45]_s$ laminates.

Figures 6 and 7 show the 80 and 320 finite element grids used for the laminates with two layers above the mid-plane and Figs. 8 and 9 show the 80 and 320 finite element grids used for laminates with three layers above the mid-plane. As indicated in the figures, smaller elements were used near the free-edge because of the expected stress concentrations in this region. (Figures 6 through 9 were drawn by the plotter in the VPI&SU Computer Center.)

The geometric parameters used in all elastic analyses were (Fig. 1)

$$h_0 = 0.02 \text{ inches}$$

$$b = 15 \, h_0$$

The magnitude of the applied strain, ξ_x, was 0.1%. Elastic results for a larger applied strain can be obtained by directly scaling the 0.1% strain results. However, the magnitude of the strain load can
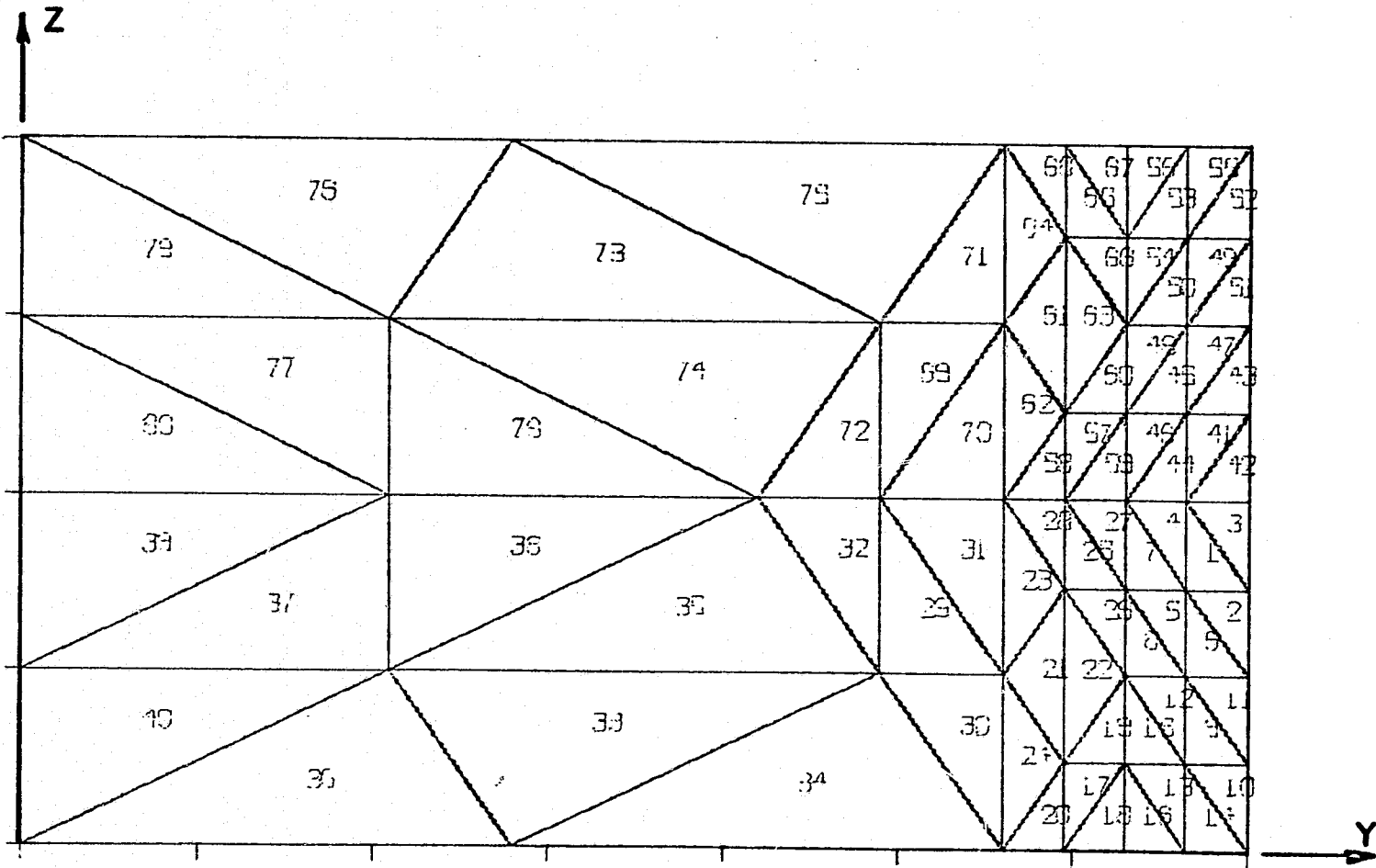
Figure 6. 80 Element Grid for Two Layers Above the Mid-Plane
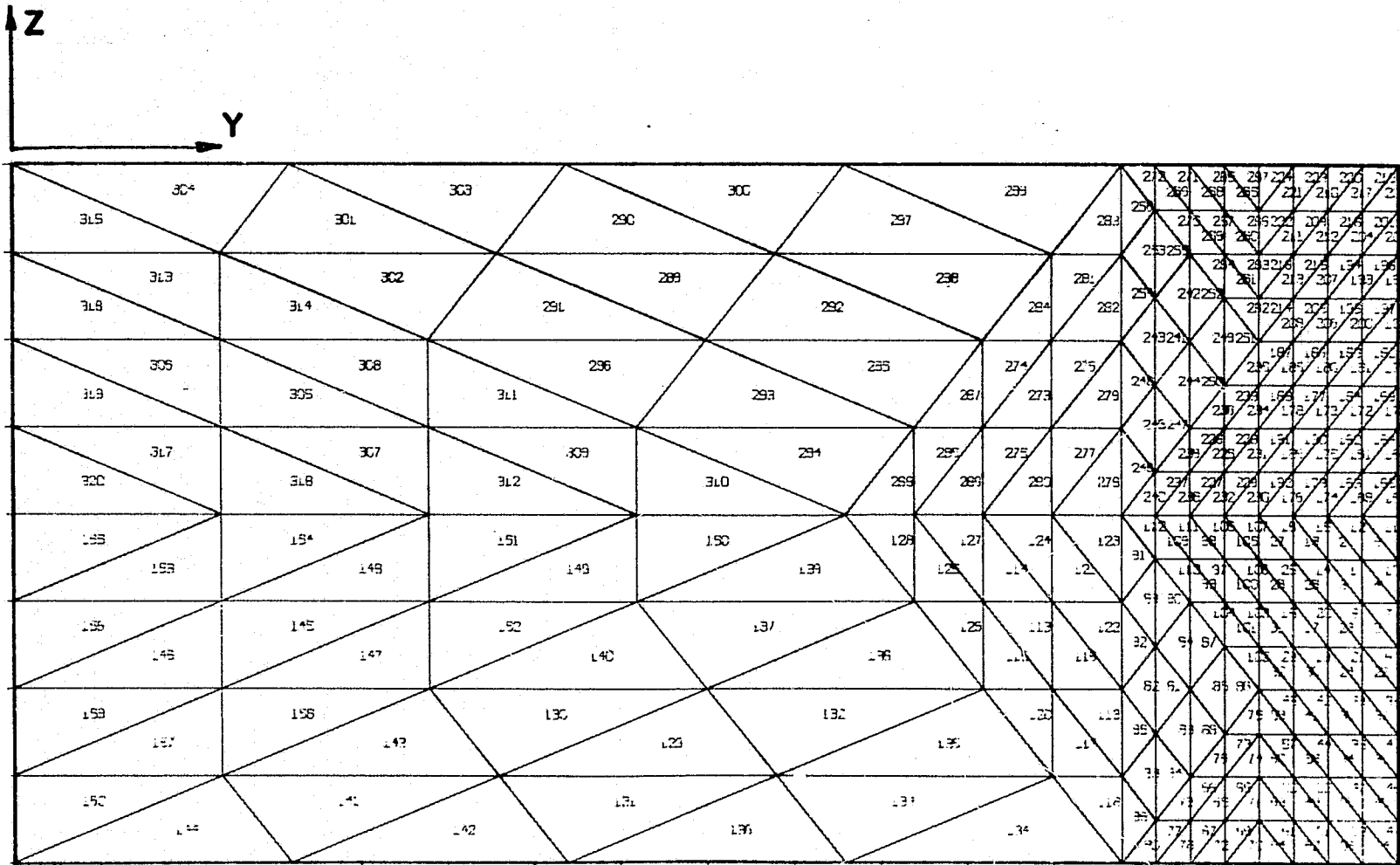
Figure 7. 320 Element Grid for Two Layers Above the Mid-Plane

49
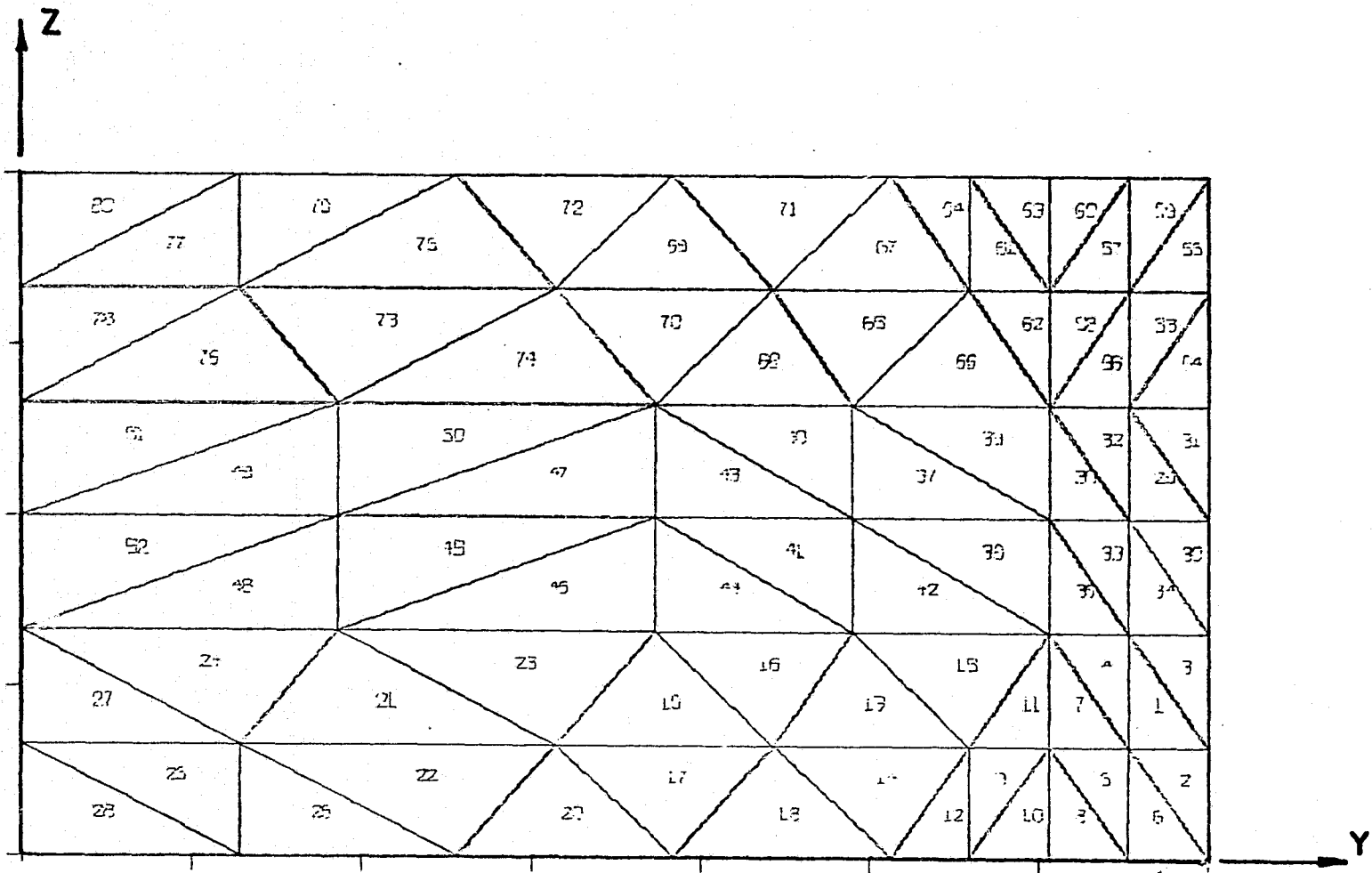
Figure 8. 80 Element Grid for Three Layers Above the Mid-Plane

50
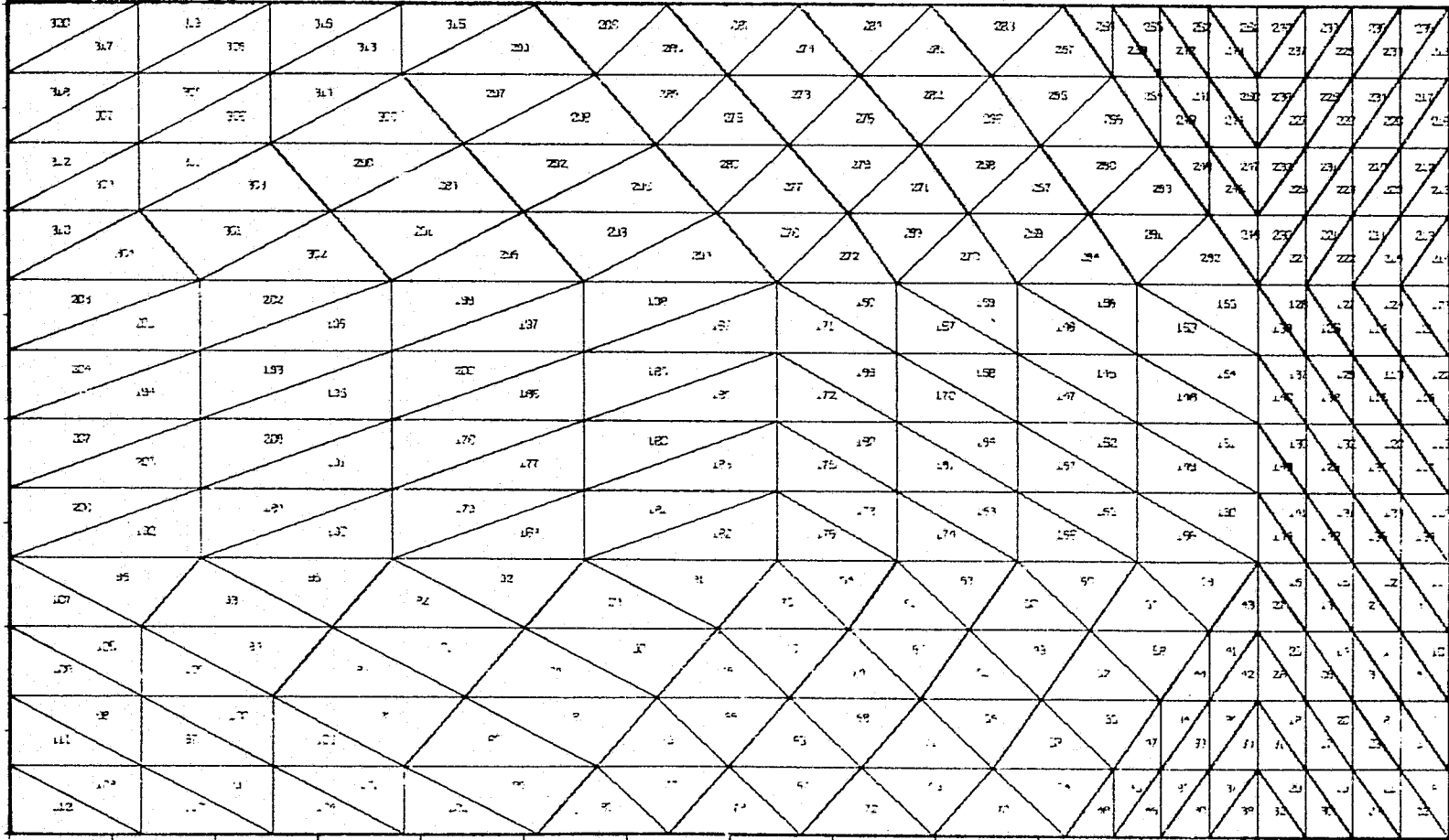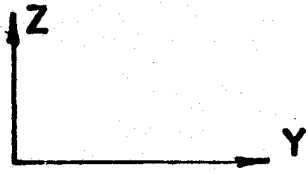
Figure 9. 320 Element Grid for Three Layers Above the Mid-Plane

be any applied value for the present method of analysis.

The results of the present analysis were compared where applicable to results obtained from the finite element program of Foye and Baker [29] and results of the finite difference program [FDP] of Pipes and Pagano [22] and Pipes [24]. Some of the finite difference results were taken from the references and others were obtained especially for this investigation. All results obtained in the present investigation were computed on the VPI&SU computer (IBM-370 Model 158). Unless shown otherwise on the following figures, the elastic results presented in this section are based upon the 80 element grids. The finite difference grids of References [22, 24] were, in a z by y fashion, 9 nodes by 31 nodes for two layers above the mid-plane and 13 nodes by 31 nodes for three layers above the mid-plane.

5.3.1 Satisfaction of Boundary Conditions

The results of the present analysis for the graphite/epoxy laminates under consideration indicated that the symmetry conditions along $y = 0$ and $z = 0$ (Eqs. (3.12)) were satisfied. While the finite element results did not satisfy the stress-free boundary conditions (Eqs. 3.9 and 3.10) exactly, it was observed that these conditions were more nearly satisfied as the size of the elements along the free-edges of the laminates decreased.

5.3.2 Cross-Ply Graphite/Epoxy Laminate

The distribution of τ_{yz} along the interface $z/h_0 = 1.0$ is shown for both stacking sequences in Fig. 10. As indicated in the figure, the results of the present analysis agreed quite well with the results of the finite difference solution of Pipes. Results obtained from the finite element solution of Foye and Baker using the same grid gave the same results as the present analysis. The results indicate that a boundary layer exists in the region extending from $y/b = 0.5$ to the free-edge. For $y/b < 0.5$ the laminate theory is recovered. The finite difference method of solution forces the stress-free boundary condition $\tau_{yz}(b,z) = 0$. It can be seen in Fig. 10 that the 320 element results satisfy this condition more clearly than the 80 element results.

The σ_z distribution along the interface $z/h_0 = 1.0$ is shown in Fig. 11. Again, the results were the same when compared to the finite element solution of Foye and Baker and good agreement was also exhibited between the present analysis and the finite difference solution of Pipes. As indicated in Fig. 11, the sign of the stress distribution changed when the stacking sequence was reversed. This phenomenon indicates that the $[0/90]_s$ lay-up could possibly experience delamination due to the relatively high tensile stress at the free-edge. The stress distributions in Fig. 11 also indicate that the present solution may more closely satisfy the self-equilibrating condition $\Sigma F_z = \int_0^b \sigma_z \, dy = 0$ than the finite difference solution. Again, the boundary layer region extended from $y/b = 0.5$ to the

Figure 10. Distribution of τ_{yz} Along Interface $z/h_o = 1.0$ of Cross-Ply Graphite/Epoxy Laminate
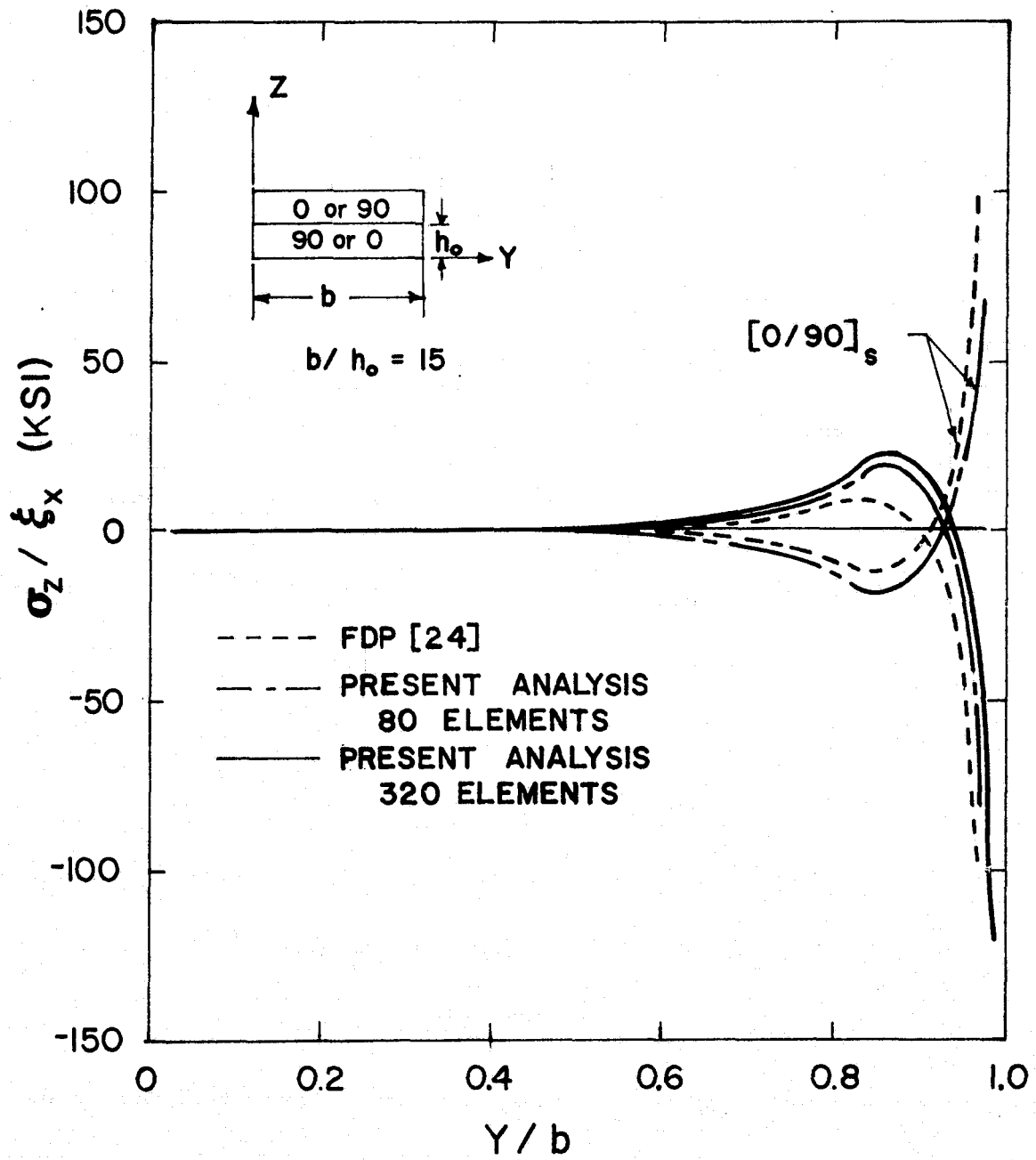
Figure 11. Distribution of σ_z Along Interface $z/h_o = 1.0$ of Cross-Ply Graphite/Epoxy Laminate

free-edge with laminate theory being recovered for y/b < 0.5.

5.3.3 Angle-Ply Graphite/Epoxy Laminate

The τ_{xz} distribution along the interface $z/h_0 = 1.0$ is shown in Fig. 12. As indicated in the figure, the magnitudes of τ_{xz} near the free-edge as obtained from the present analysis and the finite difference solution of Pipes agreed quite well. However, the present analysis exhibited a smaller boundary layer with both solutions recovering laminate theory removed from the free-edge. The results of the finite difference solution which were obtained using the VPI&SU computer exhibited some instability at the free-edge. Results published in Reference [22] did not indicate this instability.

Figure 13 shows the τ_{yz} distribution along the interface $z/h_0 = 1.0$. Results obtained for the finite difference solution of Pipes indicated a relatively high instability near the free-edge. The present finite element solution did not exhibit such instability. Both solutions exhibited a boundary layer region between $y/b = 0.4$ and the free-edge with the recovery of laminate theory occurring for $y/b < 0.4$. Both solutions indicated that σ_y vanishes at $y = 0$ for all z. Thus, equilibrium of the upper +45° layer (free body) requires that

$$\Sigma F_y = \int_0^b \tau_{yz} \, dy = 0 \qquad (5.1)$$

As shown in the figure, the finite difference solution of Pipes cannot possibly satisfy Eq. (5.1). The present analysis, however,
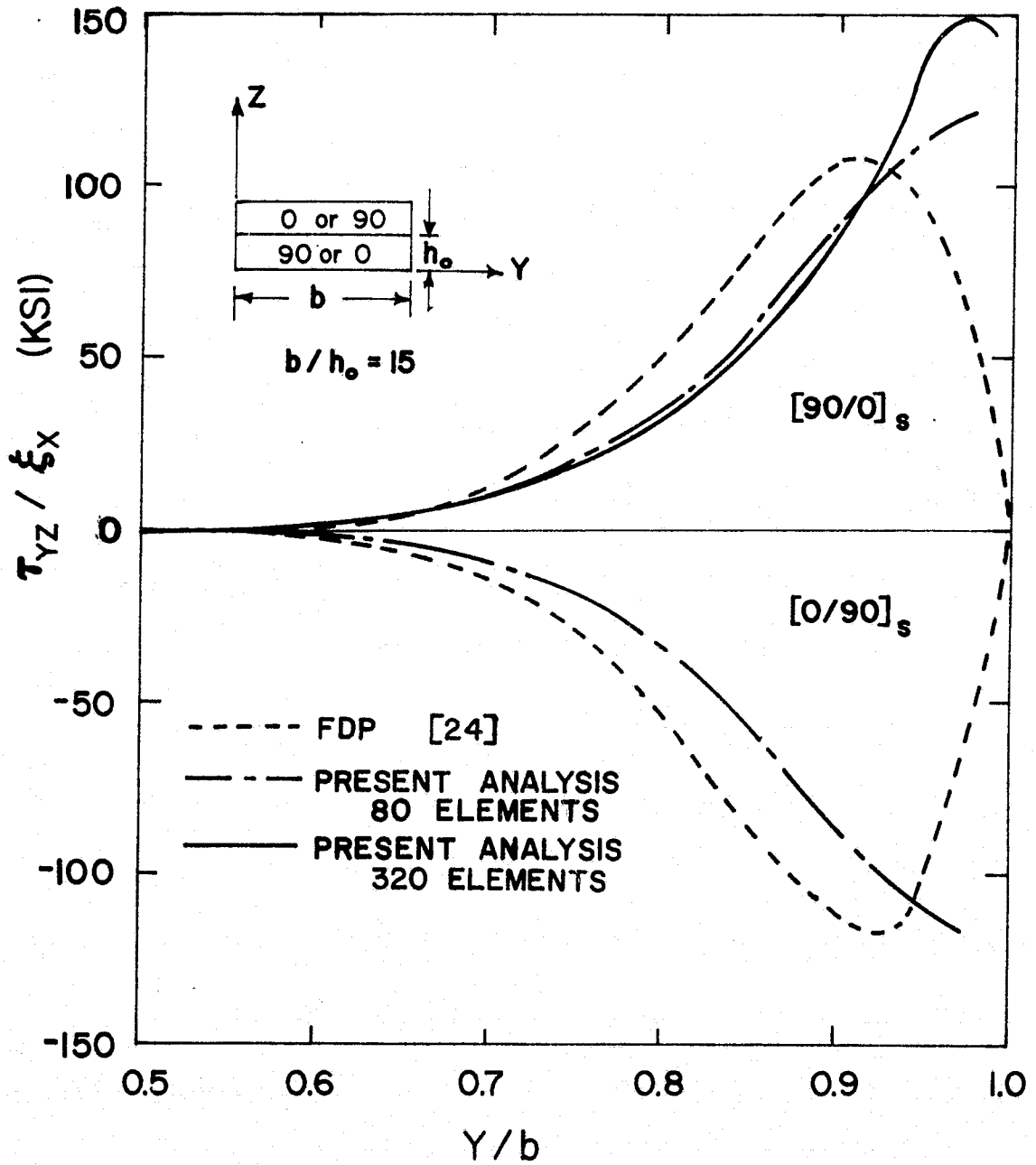
Figure 12. Distribution of τ_{xz} Along Interface $z/h_o = 1.0$ of $[+45/-45]_s$ Graphite/Epoxy Laminate
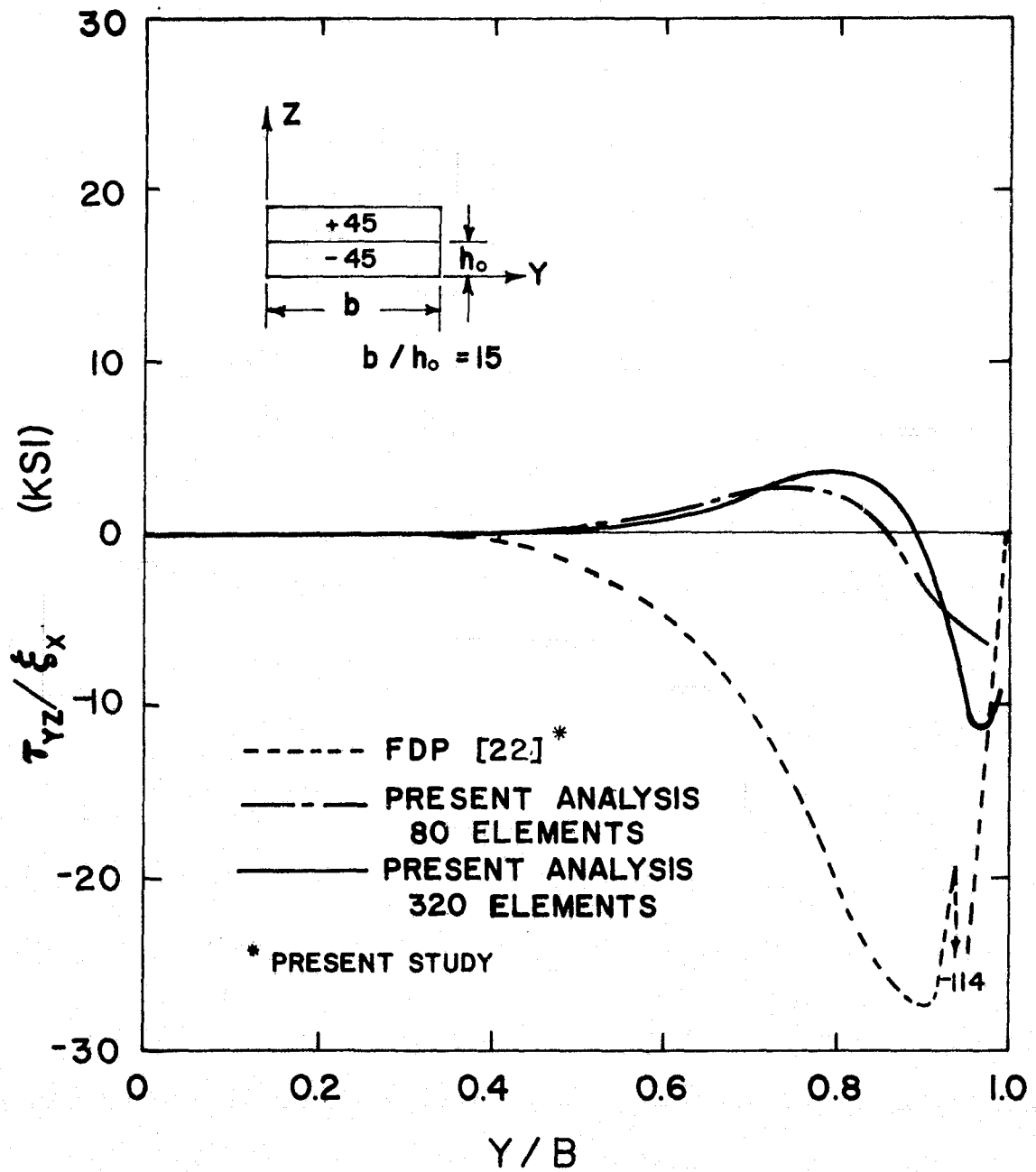
Figure 13. Distribution of τ_{yz} Along Interface $z/h_o=1.0$ of $[+45/-45]_s$ Graphite/Epoxy Laminate

exhibited a distribution which indicates approximate satisfaction of Eq. (5.1). Planimeter analysis showed the 320 element result to have less than 7 percent error.

The σ_z distribution along the interface $z/h_0 = 1.0$ is shown in Fig. 14. As illustrated in the figure, both the present analysis and the finite difference solution of Pipes exhibited a boundary layer initiating at $y/b = 0.3$ and extending to the free-edge with laminate theory being recovered for $y/b < 0.3$. Both solutions indicated possible instability in the results near the free-edge. While the published results of Pipes and Pagano [22] showed the σ_z distribution to remain positive near the free-edge, the stress-distributions in Fig. 14 indicate that the reversal of sign for $y/b > 0.9$ may be possible when the self-equilibrating condition $\Sigma F_z = \int_0^b \sigma_z \, dy = 0$ is considered. However, this is an area where future research endeavors could be undertaken especially when the delamination mode of failure is considered. A relatively coarse grid of 20 elements (not shown) gave a maximum positive value of $\sigma_z/\xi_x = 17$ KSI with no indication of instability.

5.3.4 Six-Layer Graphite/Epoxy Laminate

The influence of stacking sequence on the interlaminar stresses was noted from results obtained for the $[+45/-45/0]_s$, $[+45/0/-45]_s$ and $[0/+45/-45]_s$ graphite/epoxy laminates. The τ_{xz} distributions through the laminate thickness are shown in Fig. 15 near the free edge. As shown in the figure, the results of the present analysis are in good agreement with the results of the finite difference
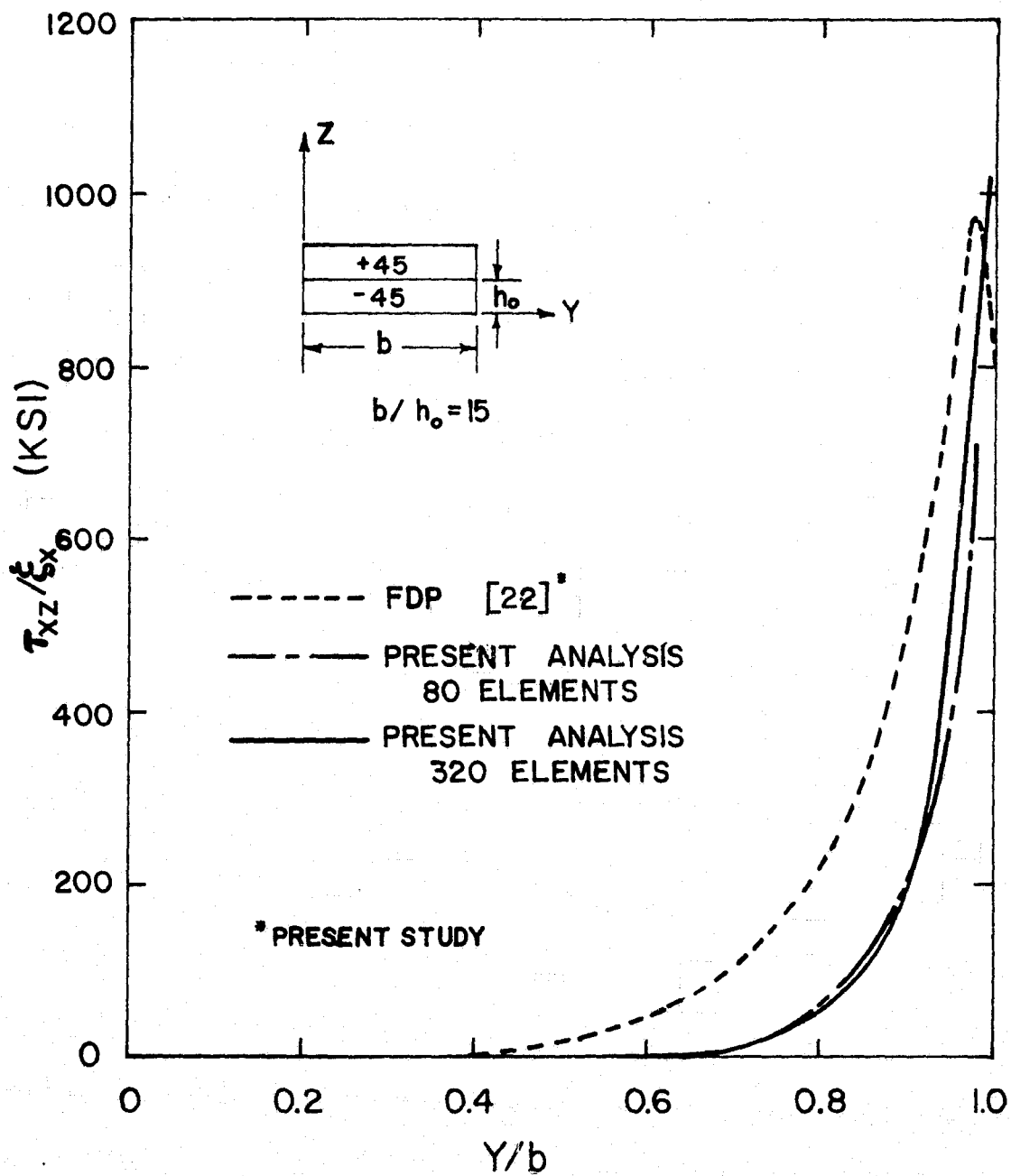
Figure 14. Distribution of σ_z Along Interface $z/h_o = 1.0$ of $[+45/-45]_s$ Graphite/Epoxy Laminate

61
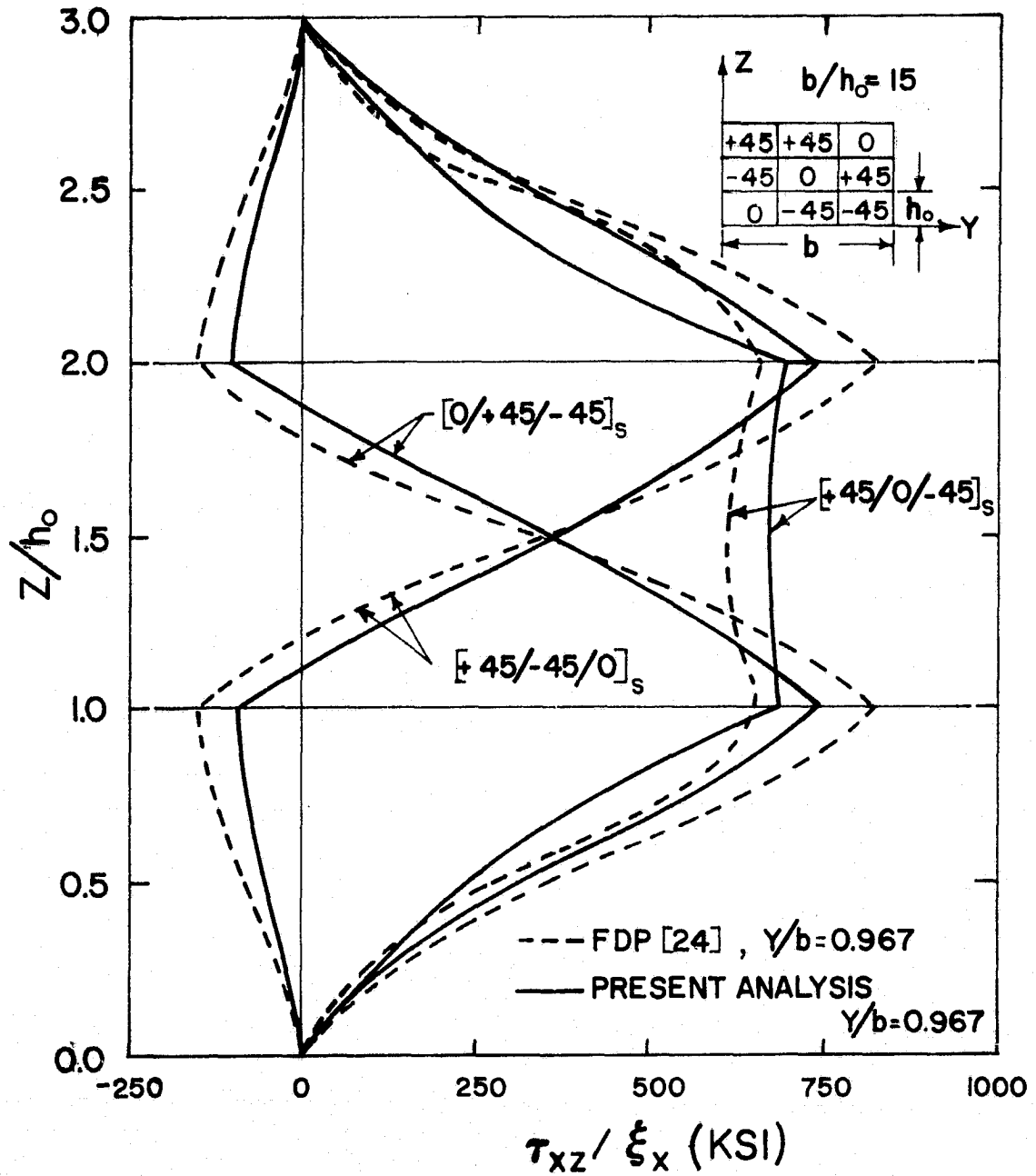
Figure 15. Distribution of τ_{xz} Through Six-Layer Graphite/Epoxy Laminate

solution of Pipes.

The τ_{yz} distributions through the laminate thickness are given in Fig. 16 at various values of y/b. Again, the results of the present analysis agreed quite favorably with the results of the finite difference solution of Pipes.

The σ_z distributions along the interfaces at $z/h_0 = 1.0$ and $z/h_0 = 2.0$ are shown in Figs. 17 and 18 for the $[+45/-45/0]_s$ and $[0/+45/-45]_s$ lay-ups, respectively. The σ_z distributions for the $[+45/0/-45]_s$ were identical at each interface and similar in form and magnitude to the distribution shown at $z/h_0 = 1.0$ in Fig. 18.

The present analysis exhibited, as indicated in Fig. 17, a possible instability in the solution near the free-edge for the σ_z stress at $z/h_0 = 2.0$. Separate results obtained for the finite difference program of Pipes using the VPI&SU computer exhibited a possible high instability in σ_z at the free-edge. The boundary layers for both solutions were approximately equal with the laminate theory being recovered for y/b < 0.3.

It is interesting to note the reversal of the sign of the σ_z distributions for the $[+45/-45/0]_s$ and $[0/+45/-45]_s$ stacking sequences as indicated by Figs. 17 and 18. The delamination mode of failure could be experienced by the $[+45/-45/0]_s$ lay-up because of the tensile nature of σ_z at the free-edge.

63

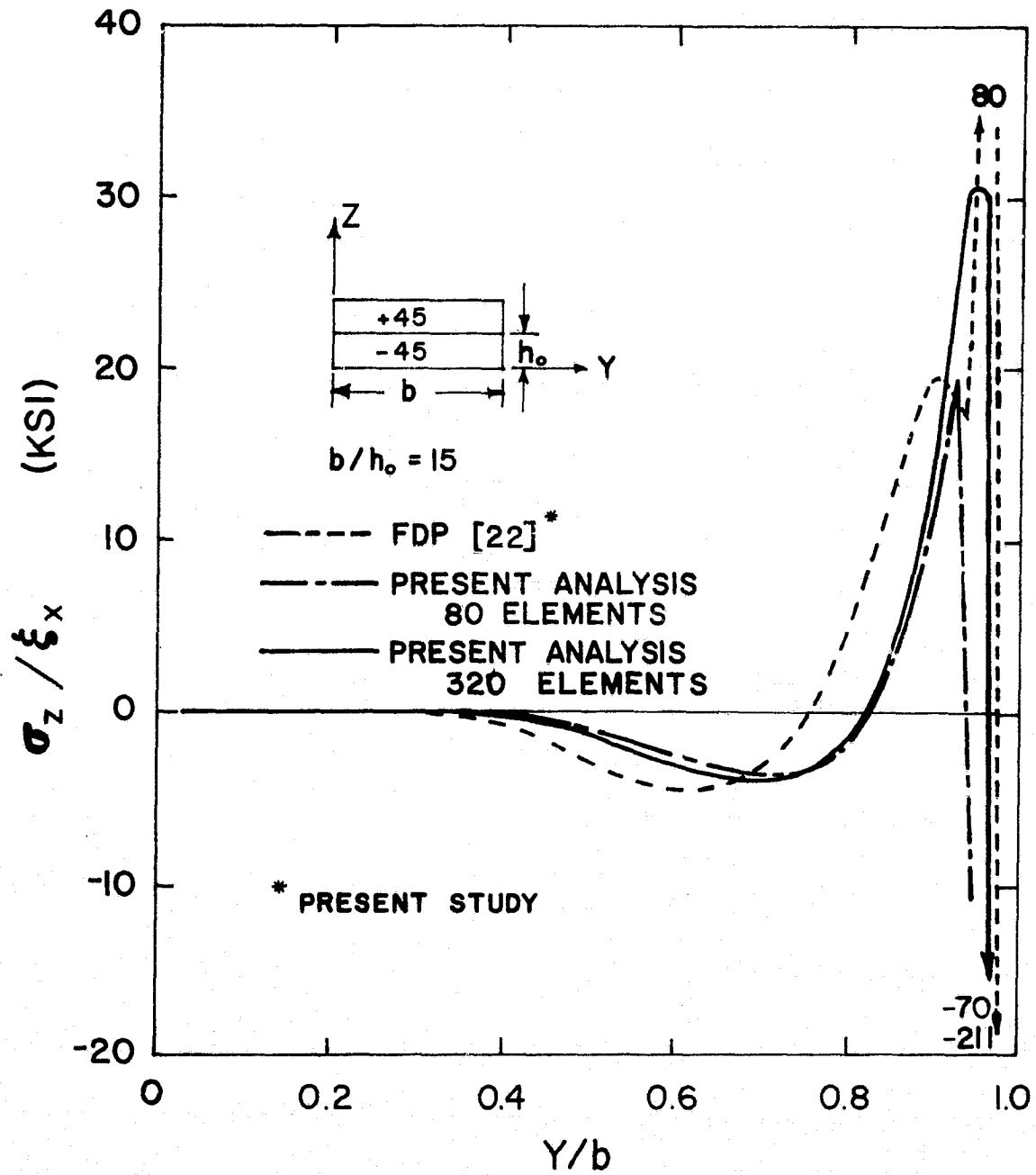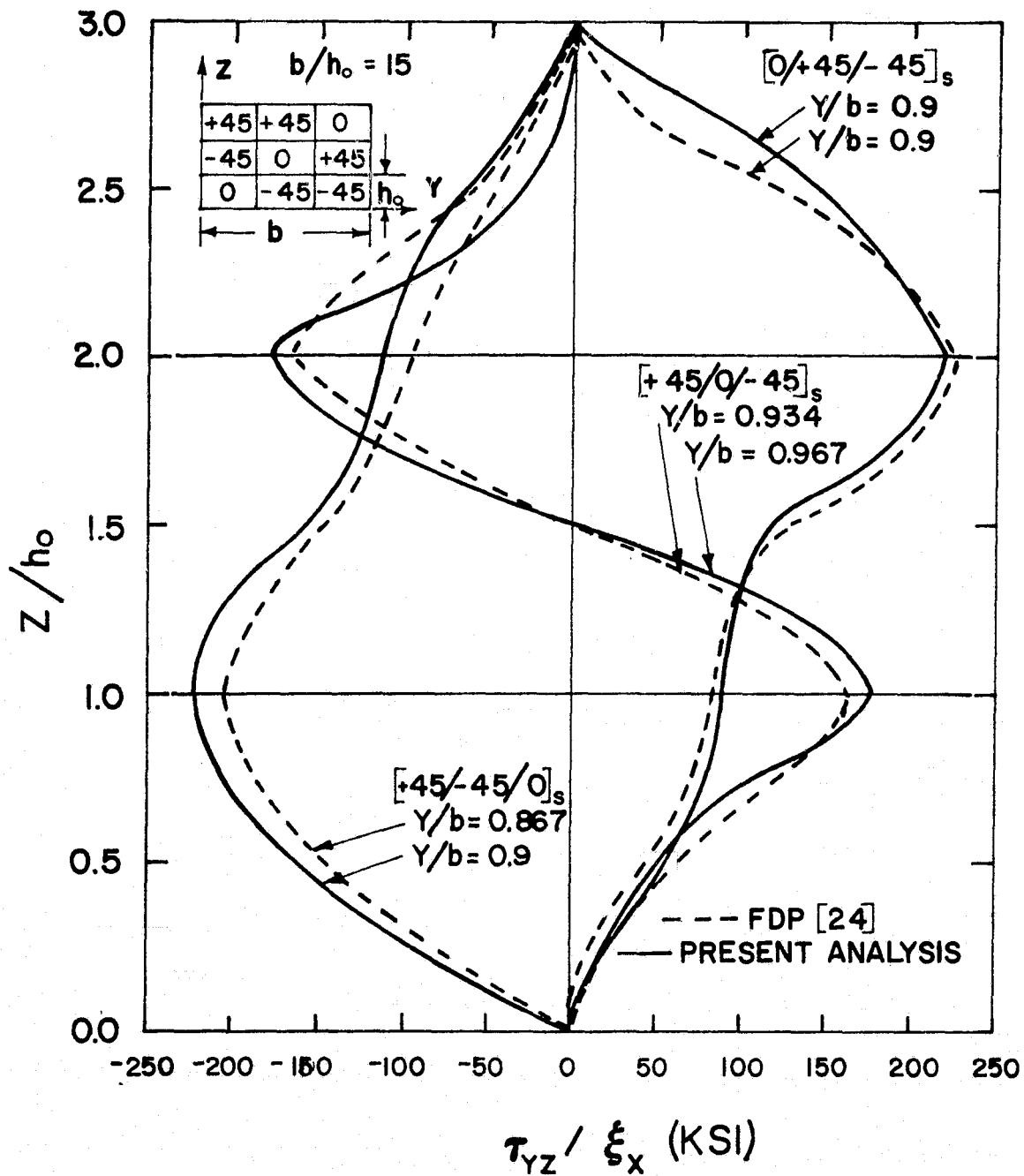Figure 16. Distribution of τ_{yz} Through Six-Layer Graphite/Epoxy Laminate
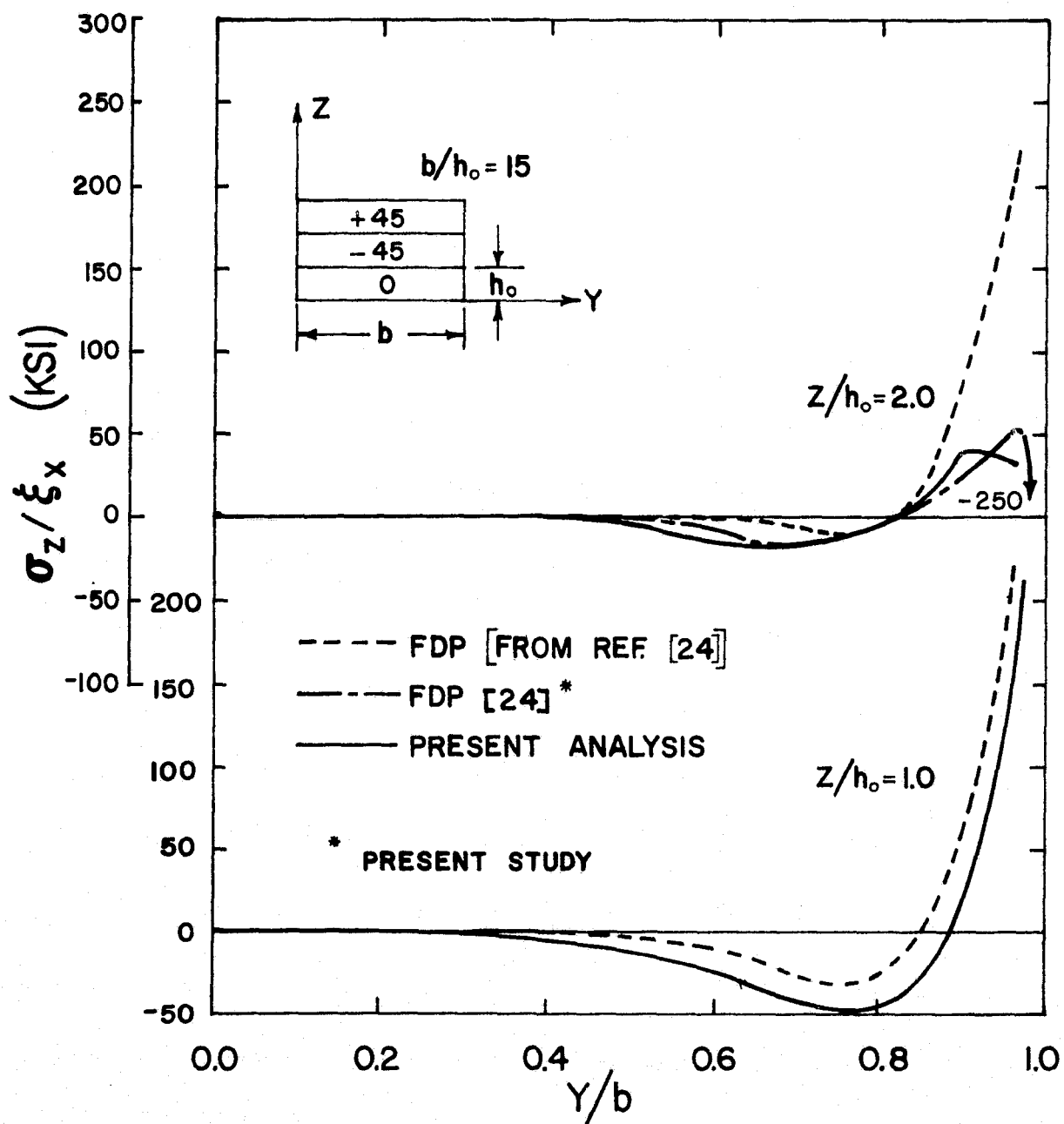
Figure 17. Distribution of σ_z Along Interfaces $z/h_o=1.0$ and $z/h_o=2.0$ of $[+45/-45/0]_s$ Graphite/Epoxy Laminate
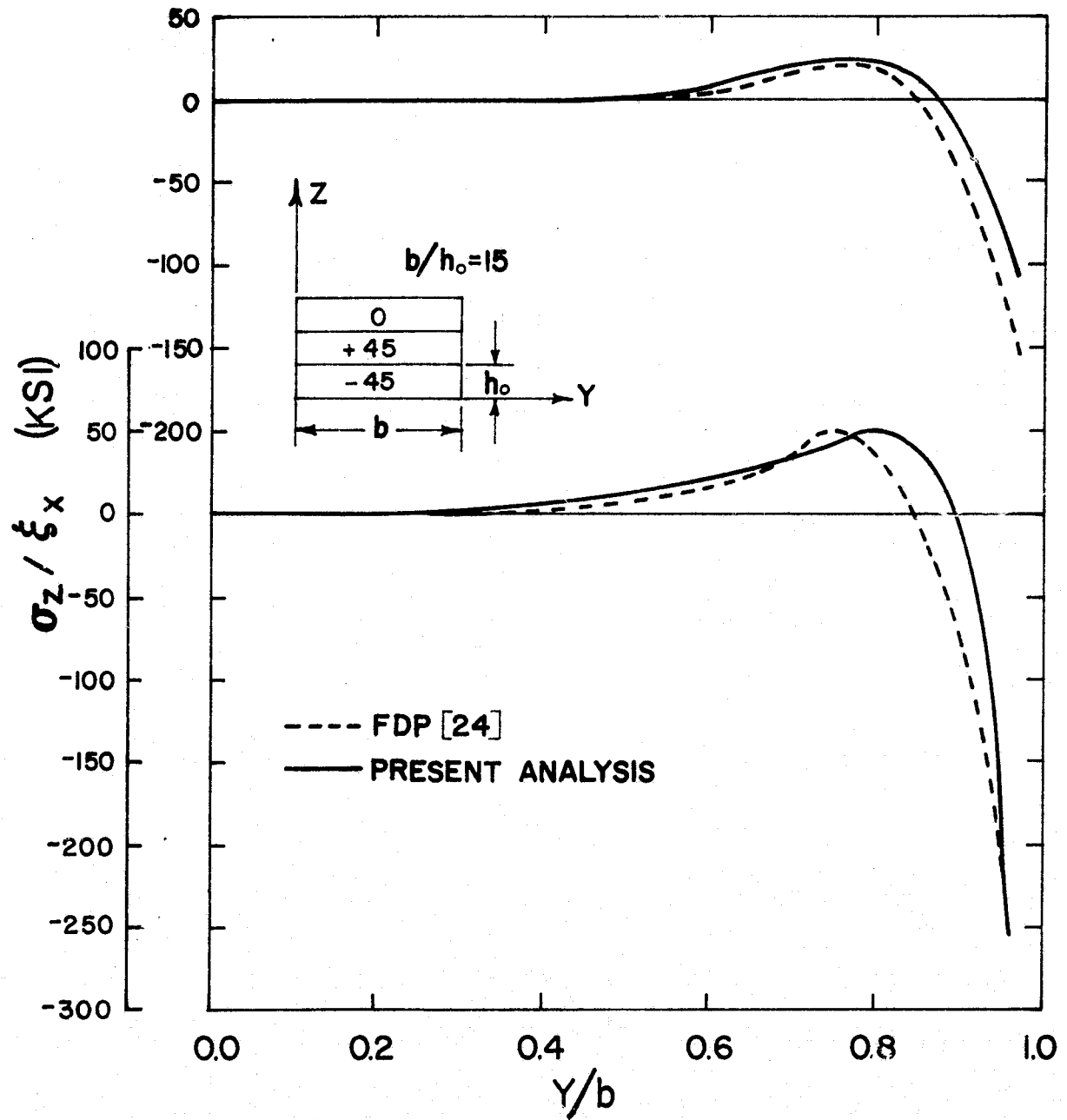
Figure 18. Distribution of σ_z Along Interfaces $z/h_o=1.0$ and $z/h_o=2.0$ of $[0/+45/-45]_s$ Graphite/Epoxy Laminate

5.3.5 Influence of Material and Fiber Orientation on Angle-Ply

Laminates

Linear elastic strain and thermal loading were considered for the $[+\theta/-\theta]_s$ graphite/epoxy, boron/epoxy and borsic/aluminum laminates. The thermal loading consisted of using an increment of temperature change, ΔT, equal to the difference between the stress-free temperature and room temperature with the coefficients of thermal expansion being room temperature values. A value of 0.7% applied strain was considered for uniaxial strain loading.

The thermal results exhibited interlaminar stress distributions similar to the results previously shown in Figs. 12, 13 and 14 but of opposite sign. Figures 19 and 20 show a comparison of normalized results for both the thermal and strain loading problems.

The normalized maximum values of τ_{xz} at the interface $z/h_0 = 1.0$ for given fiber orientations are shown in Fig. 19. As indicated in the figure, the epoxy matrix composites exhibited maximum values occurring at a fiber orientation of approximately 20 degrees for strain loading whereas the metal matrix composite exhibited a maximum value at a fiber orientation of approximately 30 degrees. Thus, it can be seen that the critical fiber angle is a function of the matrix material. The thermal results exhibited similar curves with all maximum values occurring at a fiber orientation of approximately 45 degrees. Thus, the critical angle for thermal loading is independent of the matrix material.

The normalized maximum values of σ_z at the interface $z/h_0 = 1.0$ for given fiber orientations are presented in Fig. 20. It should be
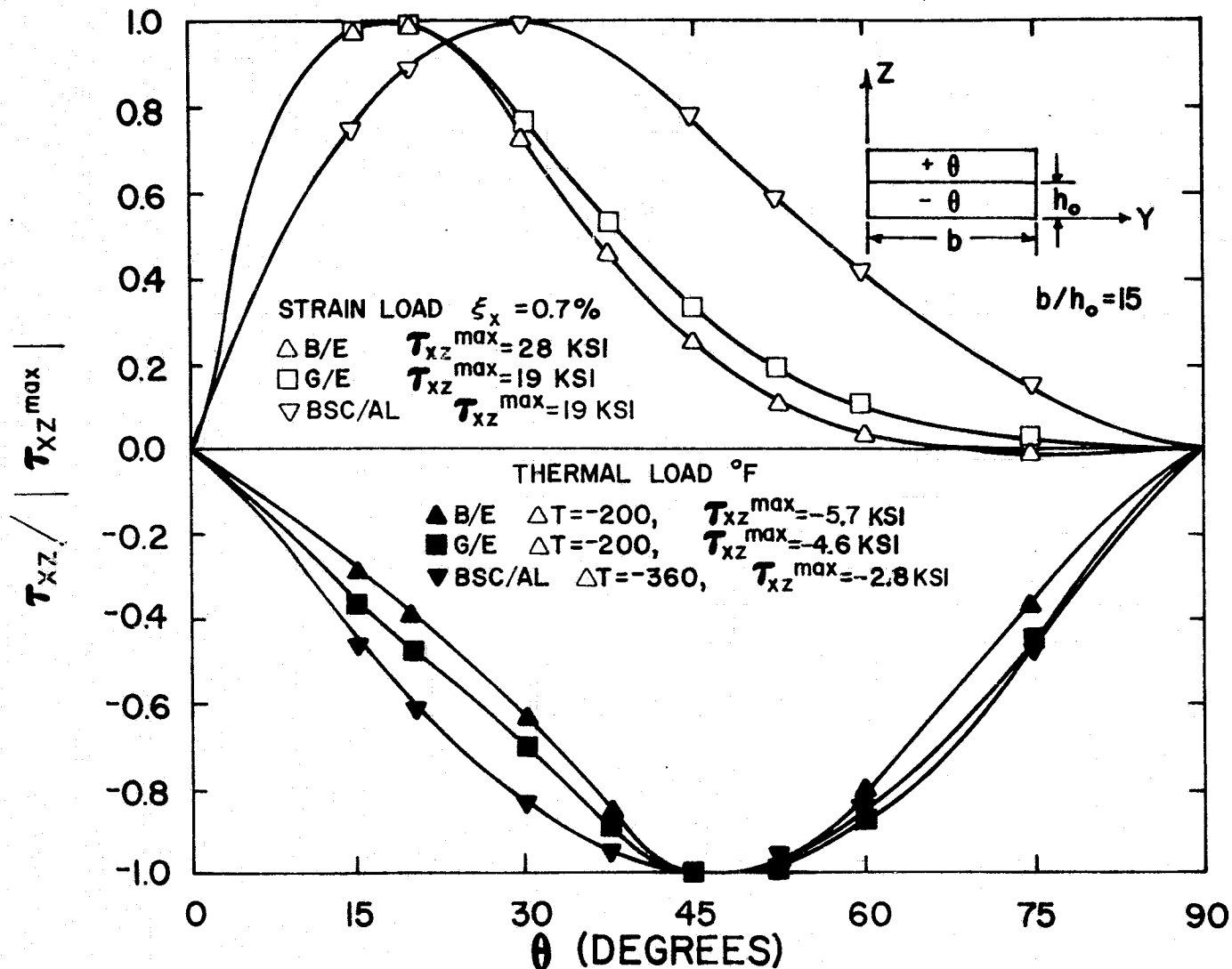
Figure 19. $\tau_{xz}/|\tau_{xz}^{max}|$ at Interface $z/h_o = 1.0$ as a Function of Fiber Orientation
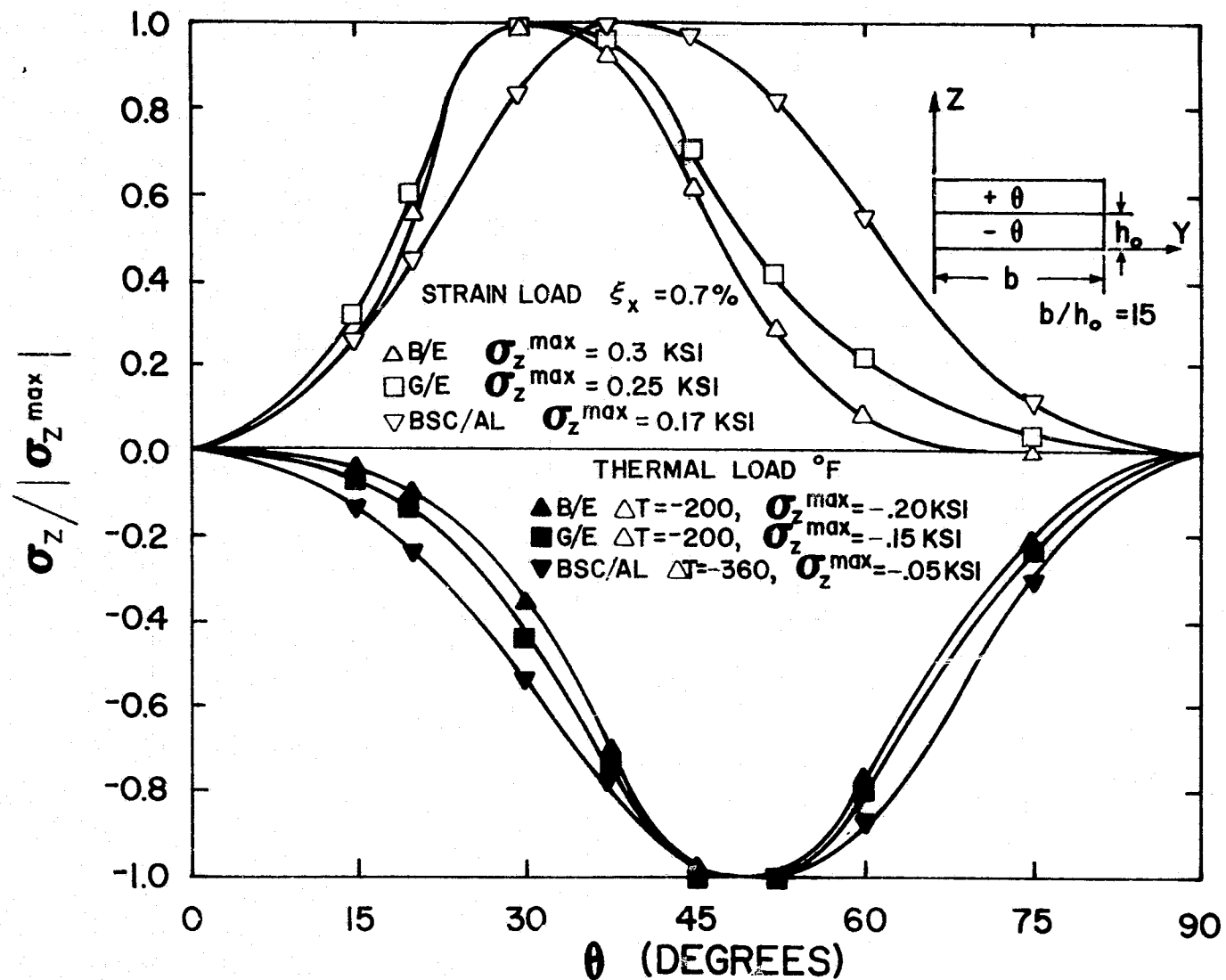
Figure 20. $\sigma_z/|\sigma_z^{max}|$ at Interface $z/h_o=1.0$ as a Function of Fiber Orientation

noted that the results shown in the figure were taken from a region (y/b = 0.933) slightly removed from the free-edge so as to eliminate results which might exhibit the possible instability in the solution. As indicated in the figure, the metal matrix composite exhibited a maximum value at a fiber orientation of approximately 37 degrees whereas the epoxy matrix systems exhibited a maximum value at a fiber orientation of approximately 30 degrees. Again, the critical fiber angle is dependent on the matrix material when σ_z is considered. The thermal results again showed that all maximum values occurred at a fiber orientation of approximately 52 degrees. As indicated in the figure, the strain load results are positive and the thermal load results are negative. Hence, the thermal effect is to delay the de-lamination mode of failure. However, the results indicate that the magnitude of σ_z near the free-edge would be relatively small even for strains well above 0.7%.

The results of the present analysis indicated that the nor-malized τ_{yz} stress exhibited results similar to the results of σ_z in Fig. 20 but of opposite sign. The maximum values occurred at the same fiber orientations and, like the σ_z stress, the τ_{yz} stress magnitude was relatively small.

Thus, for angle-ply laminates the critical interlaminar stress is τ_{xz}. In fact, for some fiber orientations the ultimate value of τ_{xz} was exceeded when an applied strain of 0.7% was considered.

5.4 Nonlinear Results

Nonlinear solutions were obtained for the $[0/90]_s$ and $[+45/-45]_s$ graphite/epoxy laminates. The nonlinear thermal and uniaxial strain loading procedures of Chapter 4 were employed for this analysis. The laminates were loaded until complete failure was exhibited (failure criteria will be discussed in Chapter 6). Results were obtained using the 80 element grid (Fig. 5).

5.4.1 Cross-Ply Graphite/Epoxy Laminate

The nonlinear $[0/90]_s$ graphite/epoxy results exhibited failure at an applied strain of 1.0% which was in good agreement with published experimental results [41]. A comparison of the linear elastic (free of thermal effects) and nonlinear solutions for the τ_{yz} distribution along the interface $z/h_0 = 1.0$ is given in Fig. 21. As indicated in the figure, the complete nonlinear solution (thermal and strain loading) gives a peak value near the free-edge which is approximately three times larger than the linear elastic solution. As shown in Fig. 22, the σ_z distribution at the interface $z/h_0 = 1.0$ exhibited results for the complete nonlinear solution which were nearly three times larger than the linear elastic solution. Thus, a nonlinear solution including thermal effects may be needed to accurately predict the delamination mode of failure.

5.4.2 Angle-Ply Graphite/Epoxy Laminate

The nonlinear $[+45/-45]_s$ graphite/epoxy results indicated failure at an applied strain which agreed quite well with published
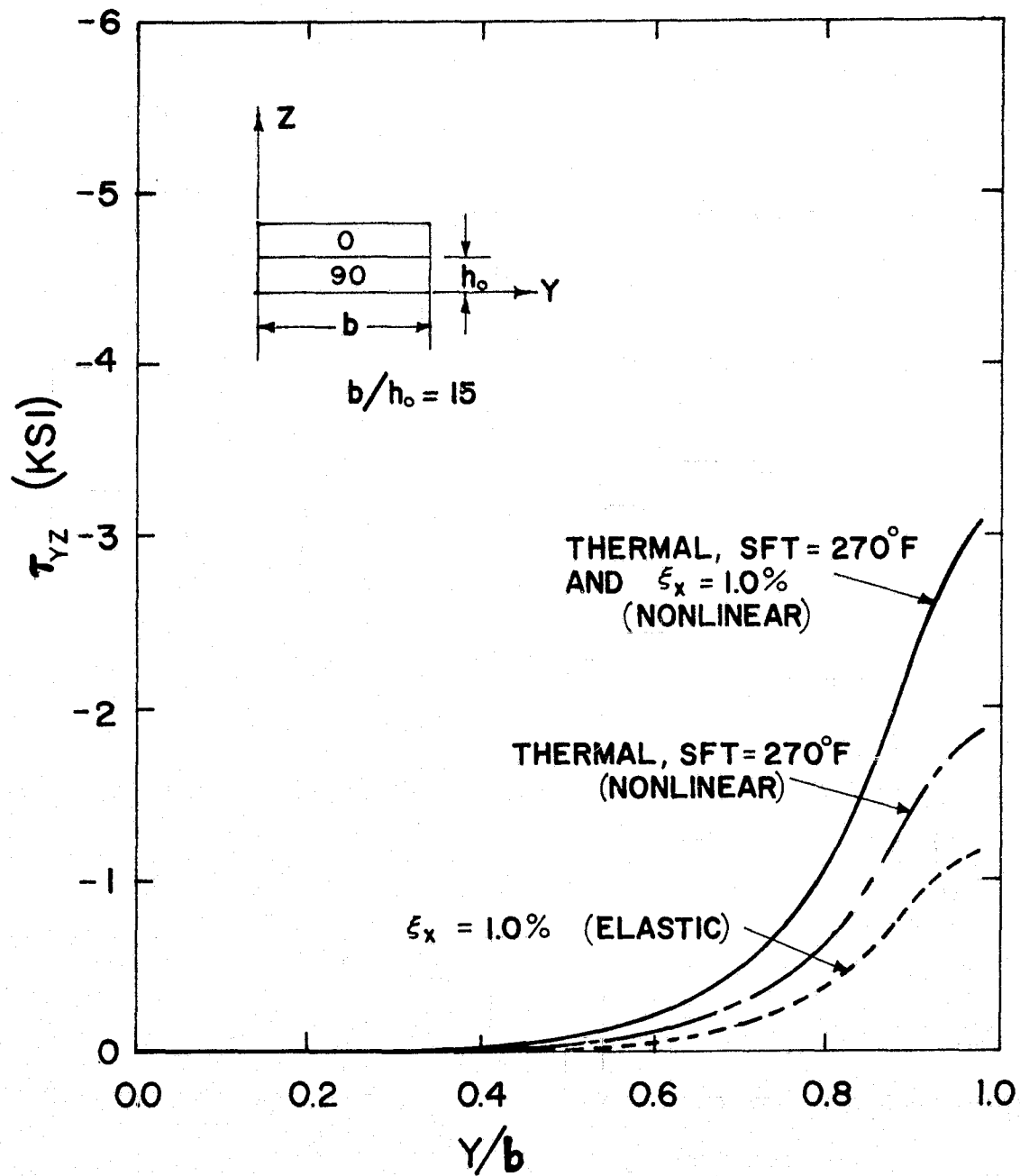
Figure 21. Comparison of Linear Elastic and Nonlinear Results
for τ_{yz} Along Interface $z/h_o = 1.0$ of $[0/90]_s$ Graphite/
Epoxy Laminate
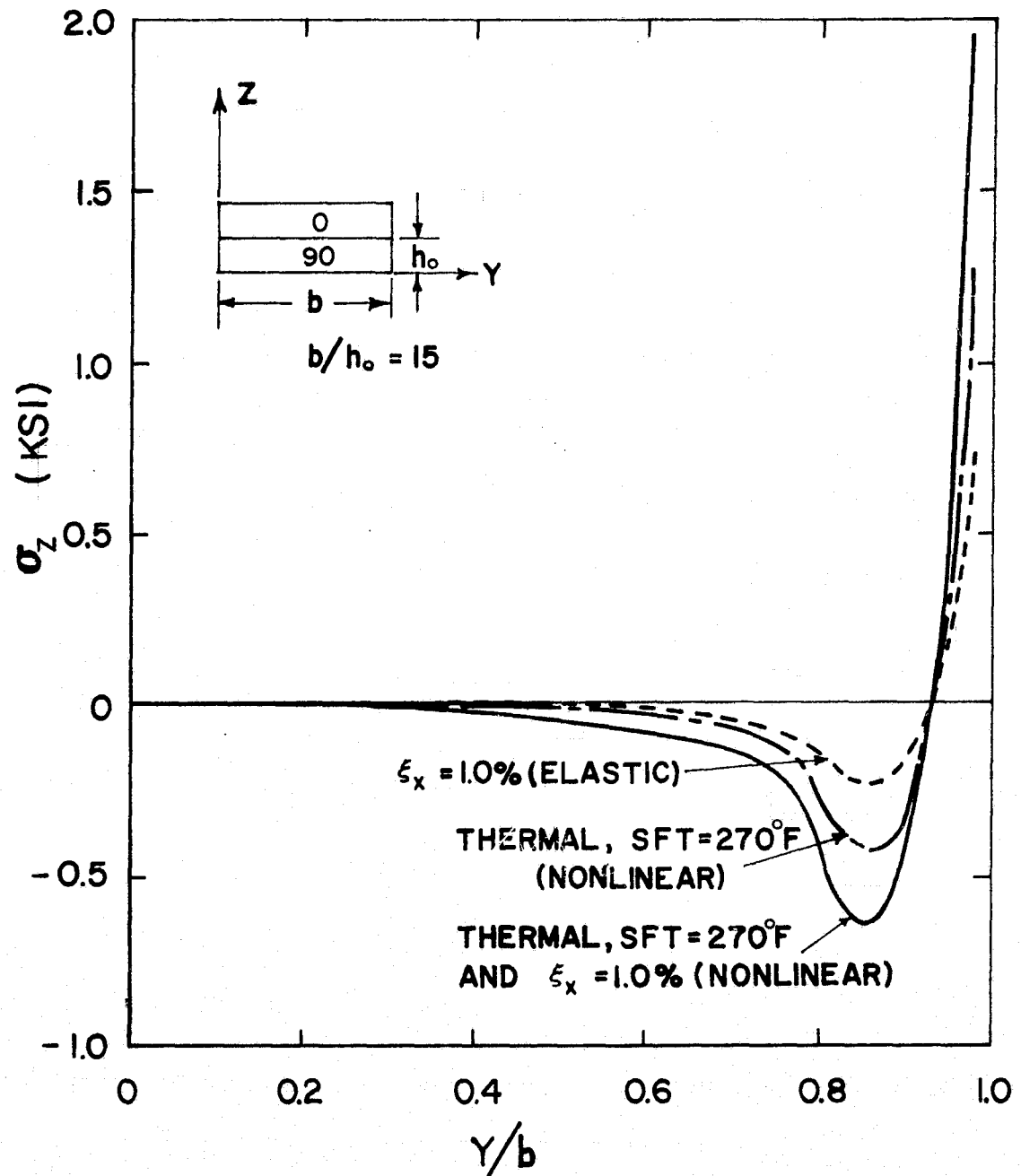
Figure 22. Comparison of Linear Elastic and Nonlinear Results for σ_z Along Interface $z/h_o=1.0$ of $[0/90]_s$ Graphite/Epoxy Laminate

experimental results [41]. A comparison of the interlaminar stress distributions along the interface $z/h_0 = 1.0$ for the linear elastic and complete nonlinear solutions are given in Figs. 23, 24 and 25 for the τ_{xz}, τ_{yz} and σ_z stresses, respectively. The possible instabilities of the σ_z distribution near the free-edge are not shown in Fig. 25. As indicated in the three figures, the distributions of the stresses for linear elastic strain loading of 0.3% were approximately equal to the distributions of the complete nonlinear results at 4.2% applied strain. Thus, the elastic solution significantly over-estimates the stresses at the free-edge for the $[+45/-45]_s$ graphite/epoxy laminate. This over-estimation may also be present for other fiber orientations.
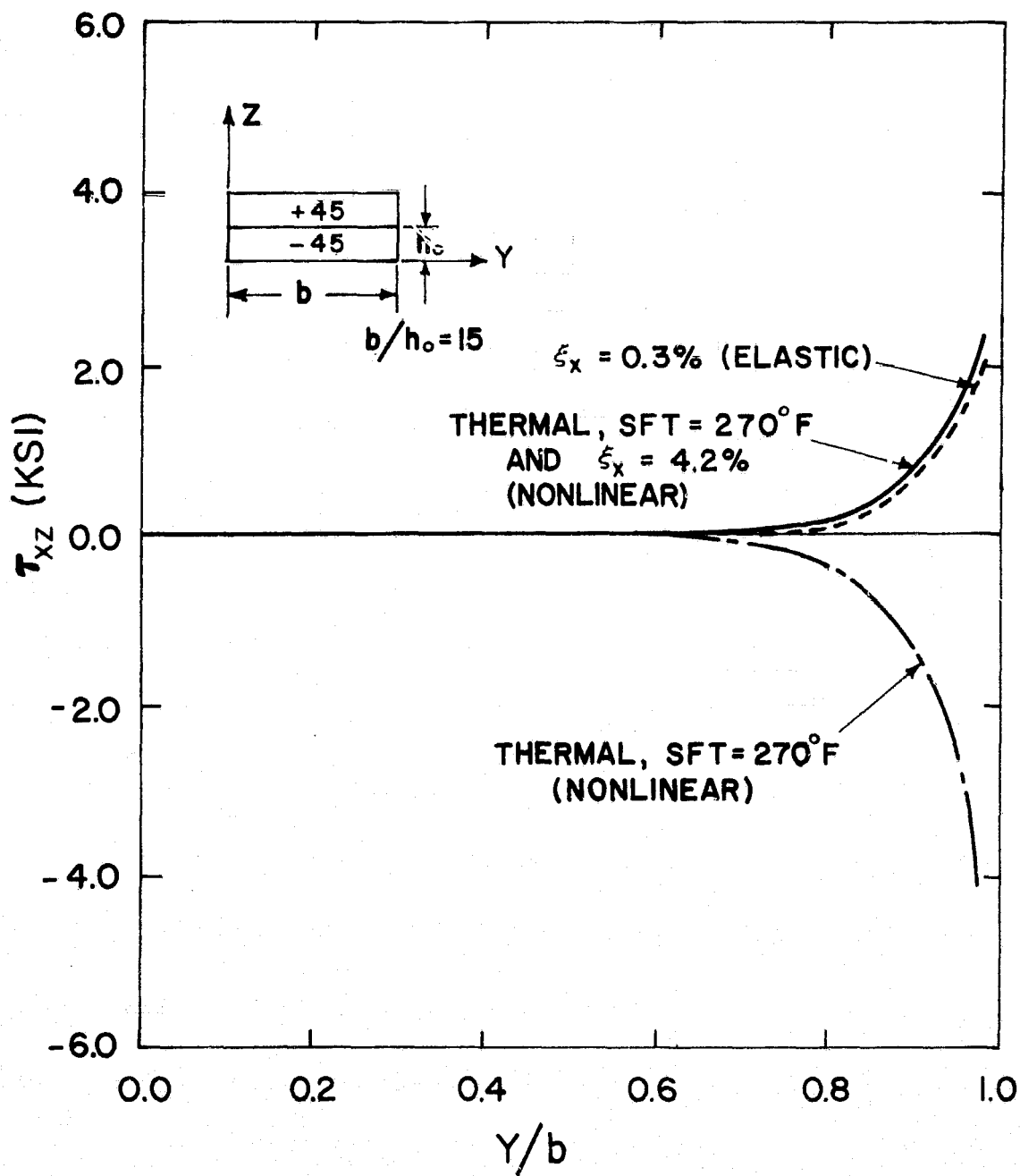
Figure 23. Comparison of Linear Elastic and Nonlinear Results for τ_{xz} Along Interface $z/h_o=1.0$ of $[+45/-45]_s$ Graphite/Epoxy Laminate
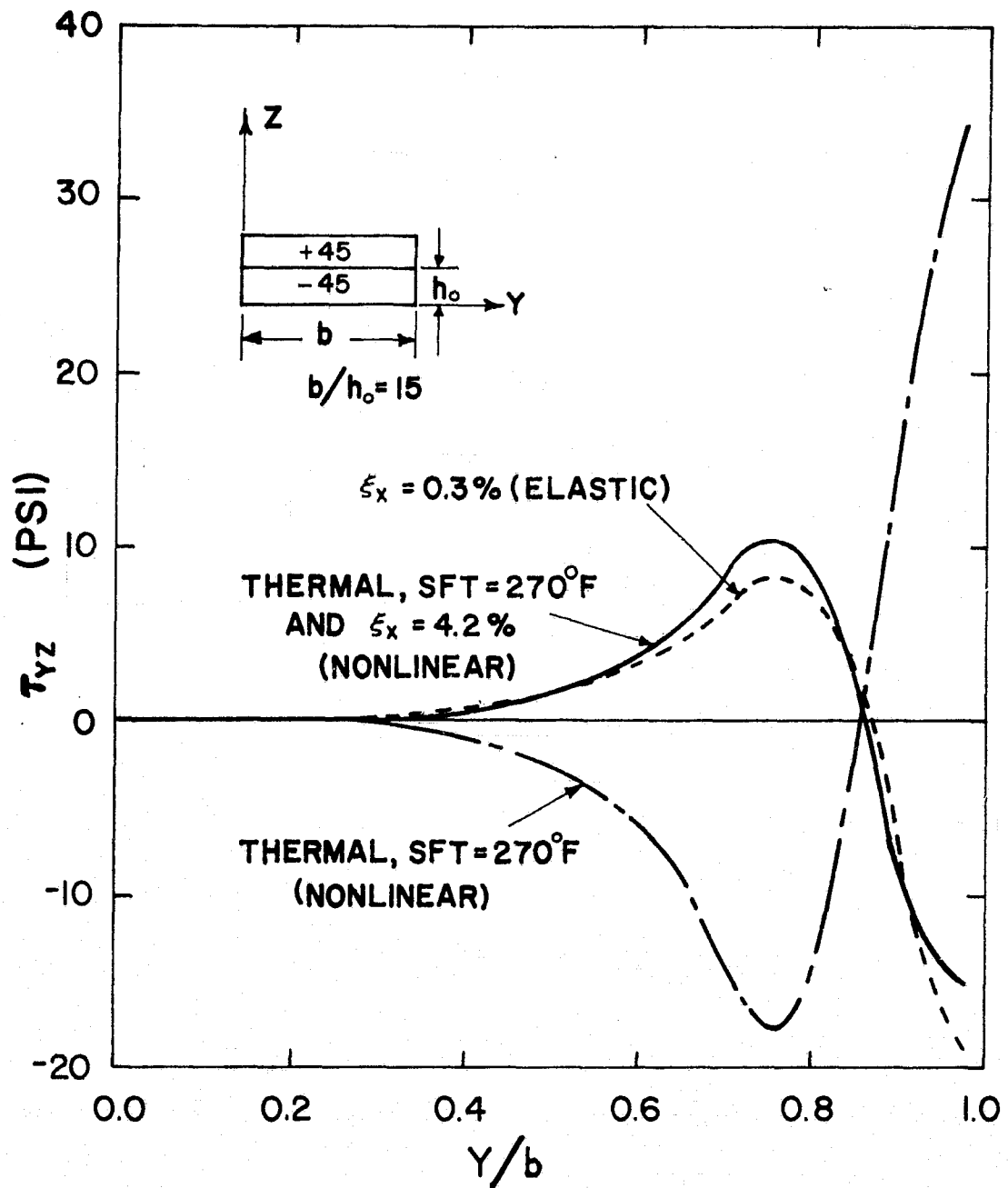
Figure 24. Comparison of Linear Elastic and Nonlinear Results for τ_{yz} Along Interface $z/h_o=1.0$ of $[+45/-45]_s$ Graphite/Epoxy Laminate
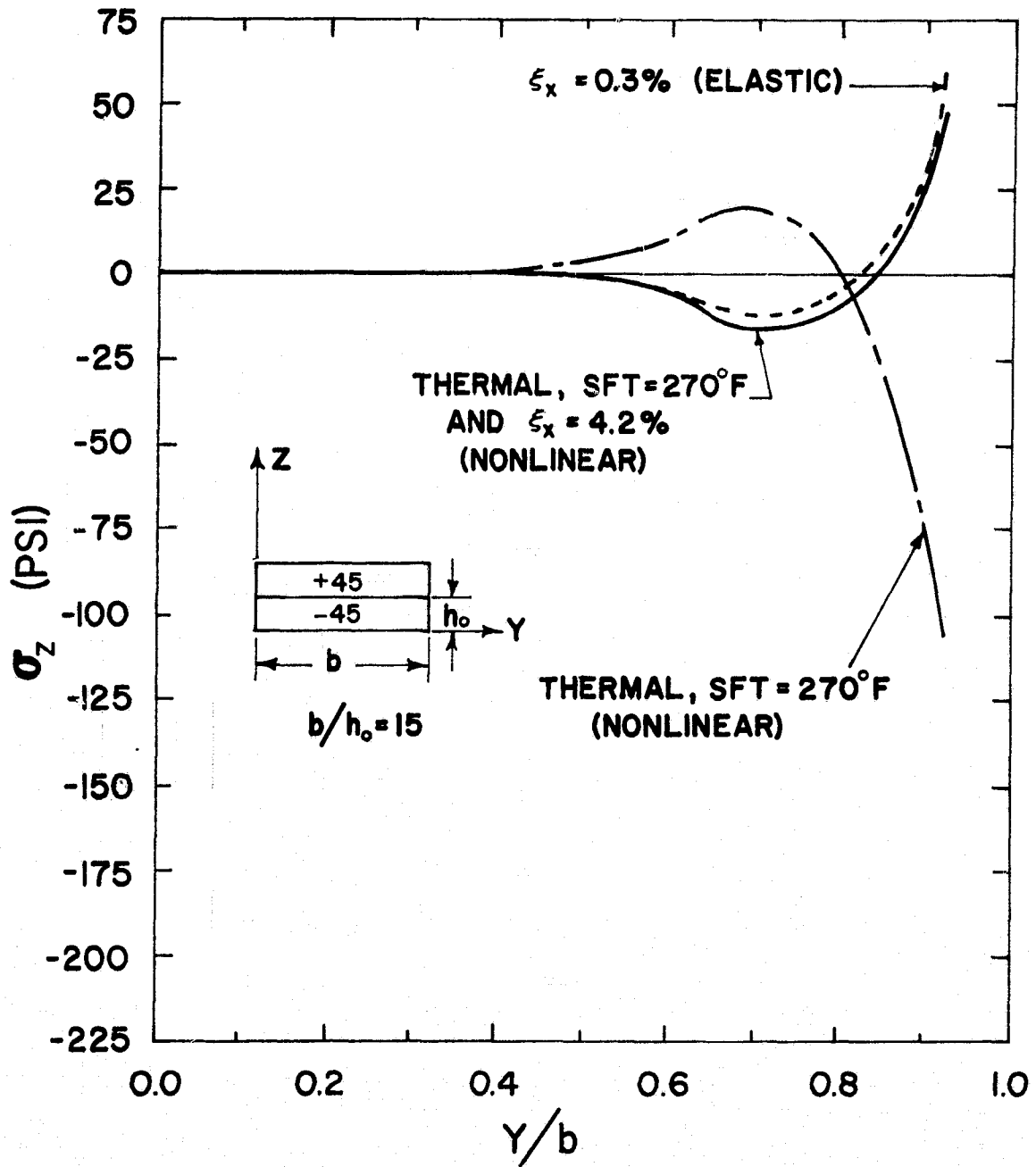
Figure 25. Comparison of Linear Elastic and Nonlinear Results for σ_z Along Interface $z/h_o=1.0$ of $[+45/-45]_s$ Graphite/Epoxy Laminate

Chapter 6

LAMINATE STRESS-STRAIN RESPONSE

This chapter presents results for the prediction of the non-linear stress-strain behavior of a variety of laminates subjected to both tensile and compressive loading. The nonlinear analysis of Chapter 4 was employed and the average stress over the laminate in the loading direction was determined by averaging the stresses over all finite elements. Figure 26 shows the finite element grid that was used for analyses of laminates for up to four layers above the mid-plane.

The results of this investigation indicated that 10 increments of thermal loading and 30 increments of strain loading were reasonable limits for predicting the stress-strain behavior of laminates. Using smaller load increments for either type of loading did not exhibit improved results.

6.1 Sandwich Beam and Tensile Coupon Input Data

The following sections contain results for sandwich beam input data and tensile coupon input data. Lamina data contained in Appendix B show that there is a significant difference between these types of data for the transverse tensile behavior and the shear behavior. The sandwich beam data exhibits an increased stiffness due to honeycomb core reinforcement. Thus, appropriate input data were used when either sandwich beam or tensile coupon laminates were analyzed. However, all compression input data were sandwich beam data.
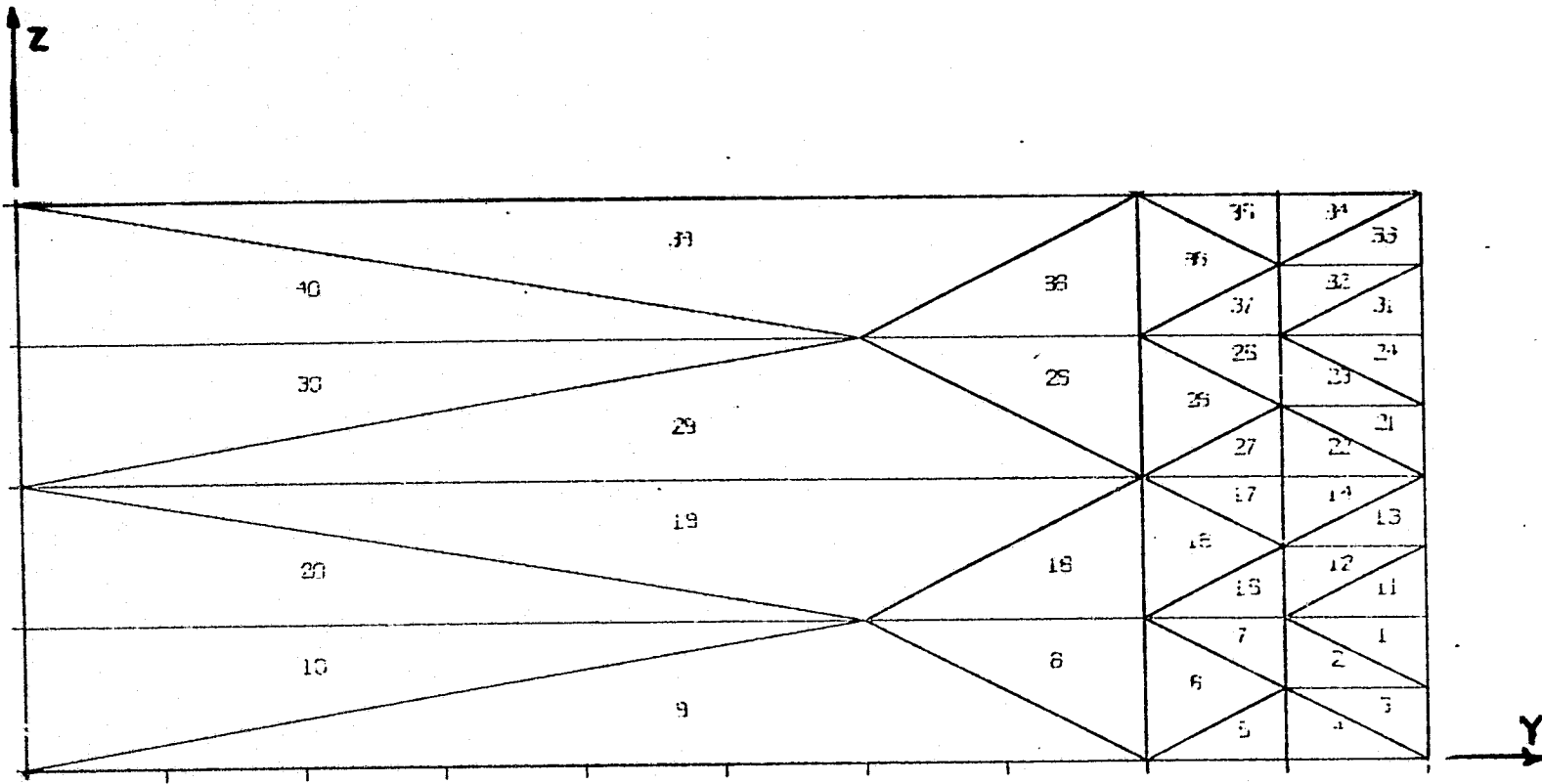
Figure 26. Typical Finite Element Grid

6.2 Material Principal Strain Failure Criteria

Angle-ply laminates of various fiber orientations were considered for each material (boron/epoxy, graphite/epoxy, borsic/ aluminum). Initial results for boron/epoxy exhibited good agreement between theory and experiment for the stress-strain response to failure. The results showed that ultimate failure of a laminate occurred when a certain in-plane material principal strain component had attained its ultimate value in each finite element. This observation led to the development of a failure criteria for angle-ply laminates which was used to predict failure for all materials subsequently investigated.

A material principal strain failure criteria is proposed for angle-ply laminates. The theory proposes that when a component of in-plane material principal strain has attained its ultimate value throughout the laminate (i.e., in all finite elements) ultimate failure has occurred. In equation form the theory states that when any of the strain ratios

$$\varepsilon_1/\varepsilon_1^u \geq 1.0$$
$$\varepsilon_2/\varepsilon_2^u \geq 1.0 \qquad\qquad (6.1)$$
$$\gamma_{12}/\gamma_{12}^u \geq 1.0$$

is attained in all finite elements then the laminate has failed.

Values for both in-plane and interlaminar strain ratios, as well as the absolute value of the sum of the ratios, were calculated at the failure strain, ε_x^f. As expected, the results indicated that interlaminar shear strains were larger at the free-edge and decreased

C-2

to zero at the center of the laminates. It was also noted from the results that the total strain ratio generally had a maximum value at the free-edge and a minimum value at the center of the laminate.

6.2.1 Tensile Loading of Angle-Ply Laminates

This section considers the tensile loading of angle-ply laminates which were initially subjected to thermal cooling. Boron/ epoxy (both tensile coupon input data and sandwich beam input data), graphite/epoxy, and borsic/aluminum angle-ply laminates were considered. Tables 1 through 4 present the strain ratios, $\varepsilon_i/\varepsilon_i{}^u$ (where $\varepsilon_4 = \gamma_{23}$, $\varepsilon_5 = \gamma_{13}$, $\varepsilon_6 = \gamma_{12}$), for the above cases, respectively.

As shown in the tables, the epoxy matrix materials exhibited large γ_{13} strain ratios at the free-edge for the lower fiber orientations, whereas the metal matrix material did not. The epoxy matrix materials also exhibited significantly larger total strain ratios at the free-edge than at the center of the laminate for these same fiber orientations. The metal matrix material did not exhibit significant differences between total strain ratios at the center and free-edge. In fact, the ± 45 degree laminate had a large total strain ratio at the center of the laminate than at the free-edge of the laminate.

Figures 27 through 30 show the graphical representation of the in-plane strain ratios (Tables 1 - 4) as a function of fiber orientation at the theoretically determined failure strain. As indicated in the figures, the curves show that angle-ply laminate failure for

Table 1. STRAIN RATIOS IN BORON/EPOXY ANGLE-PLY LAMINATES LOADED IN TENSION - COUPON DATA

$[+\Theta/-\Theta]_s$ LAY-UP (DEGREES)	FAILURE STRAIN ξ_x (%)	IN-PLANE STRAIN RATIOS*			INTERLAMINAR STRAIN RATIOS**			TOTAL STRAIN RATIO	
		$\varepsilon_1/\varepsilon_1^u$	$\varepsilon_2/\varepsilon_2^u$	$\gamma_{12}/\gamma_{12}^u$	$\varepsilon_3/\varepsilon_3^u$	$\gamma_{23}/\gamma_{23}^u$	$\gamma_{13}/\gamma_{13}^u$	CENTER	FREE-EDGE
0	0.65	1.00 T	0.11 C	0.0	0.11 C [1]	0.0	0.0	1.28	1.28
15	0.70	1.00 T	0.38 C	0.53	0.03 C	0.31	1.00	1.90	3.33
20	0.725	1.00 T	0.53 C	0.66	0.16 T [2]	0.44	1.00	2.35	3.73
30	1.25	1.00 T	0.89 C	0.98	0.74 T [2]	0.73	1.00	3.61	5.21
45	1.56	0.53 T	0.03 C	1.00	0.06 C [1]	0.05	0.05	1.64	1.74
60	0.81	0.33 T	1.00 T	0.53	0.16 C [1]	0.10	0.05	2.07	2.22
75	0.50	0.10 T	1.00 T	0.14	0.13 C [1]	0.05	0.05	1.41	1.47
90	0.425	0.01 C	1.00 T	0.0	0.11 C [1]	0.0	0.0	1.12	1.12

T = Tensile   C = Compressive   Stress Free Temperature = 270 °F
*   Value approximately equal in all elements (unless otherwise noted)
**   Value taken from elements at intersection of interface and free-edge (unless otherwise noted)
1   Value approximately equal in all elements
2   Value taken from elements at intersection of interface and centerline

Table 2. STRAIN RATIOS IN BORON/EPOXY ANGLE-PLY LAMINATES LOADED IN TENSION - SANDWICH BEAM DATA

$[+\Theta/-\Theta]_s$ LAY-UP (DEGREES)	FAILURE STRAIN ξ_x (%)	IN-PLANE STRAIN RATIOS*			INTERLAMINAR STRAIN RATIOS**			TOTAL STRAIN RATIO	
		$\varepsilon_1/\varepsilon_1^u$	$\varepsilon_2/\varepsilon_2^u$	$\gamma_{12}/\gamma_{12}^u$	$\varepsilon_3/\varepsilon_3^u$	$\gamma_{23}/\gamma_{23}^u$	$\gamma_{13}/\gamma_{13}^u$	CENTER	FREE-EDGE
0	0.65	1.00 T	0.25 C	0.0	0.25 C [1]	0.0	0.0	1.52	1.52
15	0.70	1.00 T	0.49 C	0.50	0.16 C	0.23	0.83	2.17	3.27
20	0.725	1.00 T	0.67 C	0.61	0.09 C	0.33	0.87	2.35	3.52
30	1.20	1.00 T	0.82 C	0.98	0.25 T [2]	0.54	0.85	3.10	4.32
40	1.44	0.73 T	0.38 C	1.00	0.02 C	0.28	0.31	2.10	2.70
45	1.56	0.58 T	0.02 C	1.00	0.09 C	0.08	0.07	1.69	1.84
50	1.80	0.46 T	0.96 T	1.00	0.20 C [1]	0.07	0.05	2.63	2.74
60	0.90	0.33 T	1.00 T	0.55	0.18 C [1]	0.07	0.04	2.09	2.19
75	0.55	0.08 T	1.00 T	0.15	0.14 C [1]	0.04	0.01	1.38	1.43
90	0.45	0.02 C	1.00 T	0.0	0.13 C [1]	0.0	0.0	1.13	1.13

T = Tensile   C = Compressive   Stress Free Temperature = 270 $^\circ$F
*   Value approximately equal in all elements (unless otherwise noted)
**   Value taken from elements at intersection of interface and free-edge (unless otherwise noted)
1   Value approximately equal in all elements
2   Value taken from elements at intersection of interface and centerline

Table 3. STRAIN RATIOS IN GRAPHITE/EPOXY ANGLE-PLY LAMINATES LOADED IN TENSION – COUPON DATA

$[+\theta/-\theta]_s$ LAY-UP (DEGREES)	FAILURE STRAIN ξ_x (%)	IN-PLANE STRAIN RATIOS*			INTERLAMINAR STRAIN RATIOS**			TOTAL STRAIN RATIO	
		ϵ_1/ϵ_1^u	ϵ_2/ϵ_2^u	$\gamma_{12}/\gamma_{12}^u$	ϵ_3/ϵ_3^u	$\gamma_{23}/\gamma_{23}^u$	$\gamma_{13}/\gamma_{13}^u$	CENTER	FREE-EDGE
0	0.85	1.00 T	0.16 C	0.0	0.16 C [1]	0.0	0.0	1.32	1.32
15	0.95	1.00 T	0.50 C	0.41	0.08 C [1]	0.19	0.69	2.00	2.90
20	1.00	1.00 T	0.71 C	0.53	0.04 C	0.28	0.75	2.27	3.32
30	1.55	1.00 T	1.00 C	0.78	0.30 T [2]	0.42	0.68	3.05	4.08
45	4.20	0.65 T	0.06 C	1.00	0.09 C [1]	0.05	0.05	1.80	1.89
60	0.95	0.40 T	1.00 T	0.38	0.13 C [1]	0.08	0.04	1.93	2.04
75	0.55	0.13 T	1.00 T	0.08	0.09 C [1]	0.04	0.01	1.30	1.35
90	0.425	0.01 C	1.00 T	0.0	0.07 C [1]	0.0	0.0	1.15	1.15

T = Tensile   C = Compressive   Stress Free Temperature = 270 $^{\circ}$F
*   Value approximately equal in all elements (unless otherwise noted)
**   Value taken from elements at intersection of interface and free-edge (unless otherwise noted)
1   Value approximately equal in all elements
2   Value taken from elements at intersection of interface and centerline

83

Table 4. STRAIN RATIOS IN BORSIC/ALUMINUM ANGLE-PLY LAMINATES LOADED IN TENSION - COUPON DATA

$[+\Theta/-\Theta]_s$ LAY-UP (DEGREES)	FAILURE STRAIN ε_x (%)	IN-PLANE STRAIN RATIOS*			INTERLAMINAR STRAIN RATIOS**			TOTAL STRAIN RATIO	
		$\varepsilon_1/\varepsilon_1^u$	$\varepsilon_2/\varepsilon_2^u$	$\gamma_{12}/\gamma_{12}^u$	$\varepsilon_3/\varepsilon_3^u$	$\gamma_{23}/\gamma_{23}^u$	$\gamma_{13}/\gamma_{13}^u$	CENTER	FREE-EDGE
0	0.55	1.00 T	0.20 C	0.0	0.02 C [1]	0.0	0.0	1.44	1.44
15	0.45	1.00 T	0.40 C	0.32	0.25 T [1]	0.08	0.31	1.86	2.30
20	0.45	1.00 T	0.47 C	0.40	0.35 T [1]	0.11	0.31	2.26	2.67
30	0.60	1.00 T	0.51 C	0.53	0.60 T [1]	0.12	0.20	2.70	3.00
45	3.20	1.00 T	0.13 C	1.00	0.70 T [1]	0.02	0.02	2.62	2.38
60	1.275	0.61 T	1.00 T	0.50	0.03 C [1]	0.08	0.05	2.48	2.61
75	0.8	0.19 T	1.00 T	0.25	0.03 C [1]	0.0	0.0	1.77	1.78
90	0.8	0.01 C	1.00 T	0.0	0.03 C [1]	0.0	0.0	1.33	1.33

T = Tensile   C = Compressive   Stress Free Temperature = 430 °F
*   Value approximately equal in all elements (unless otherwise noted)
**   Value taken from elements at intersection of interface and free-edge (unless otherwise noted)
1   Value approximately equal in all elements
2   Value taken from elements at intersection of interface and centerline
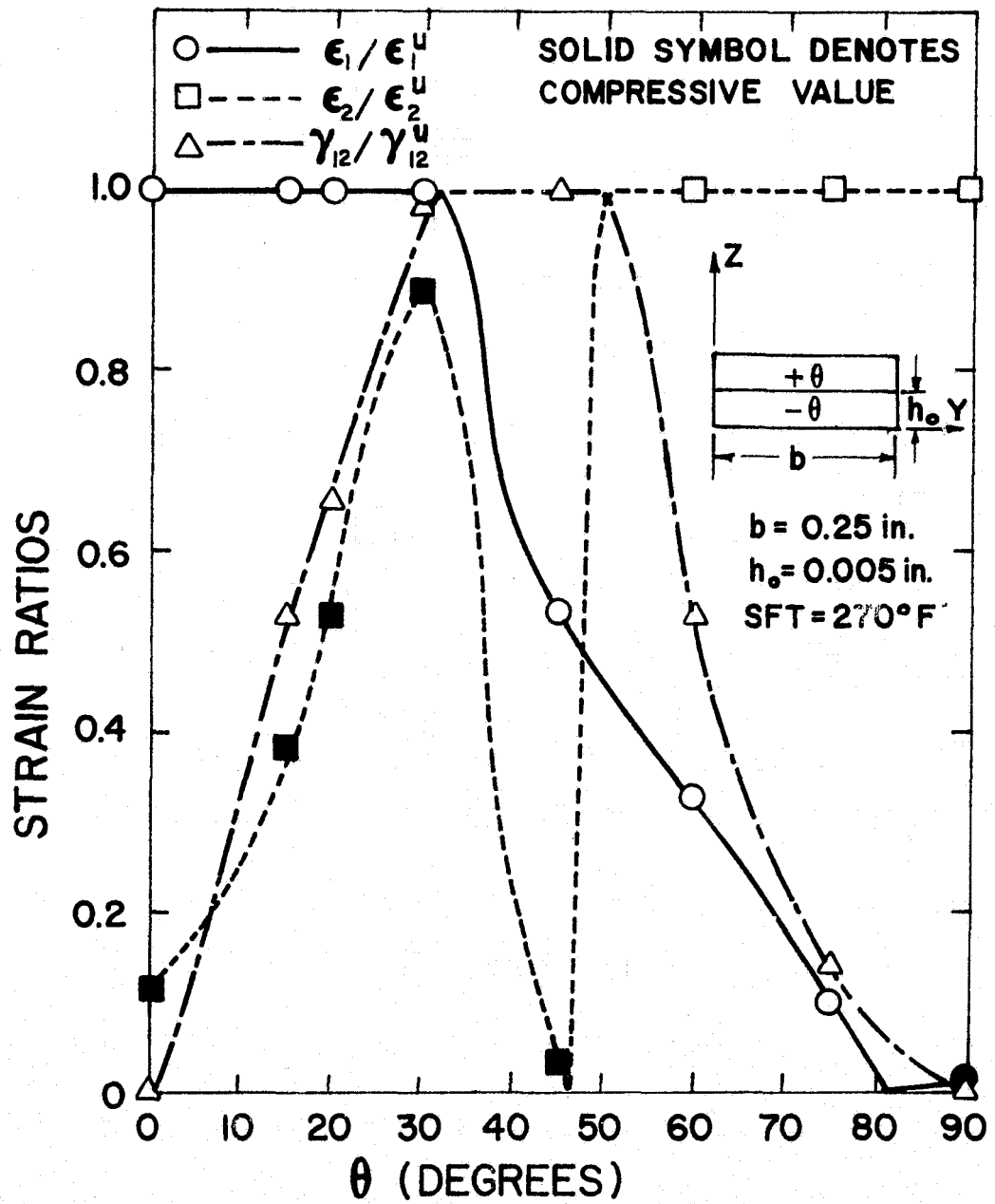
Figure 27. In-Plane Strain Ratios in Boron/Epoxy Angle-Ply Laminates
Loaded in Tension - Coupon Data
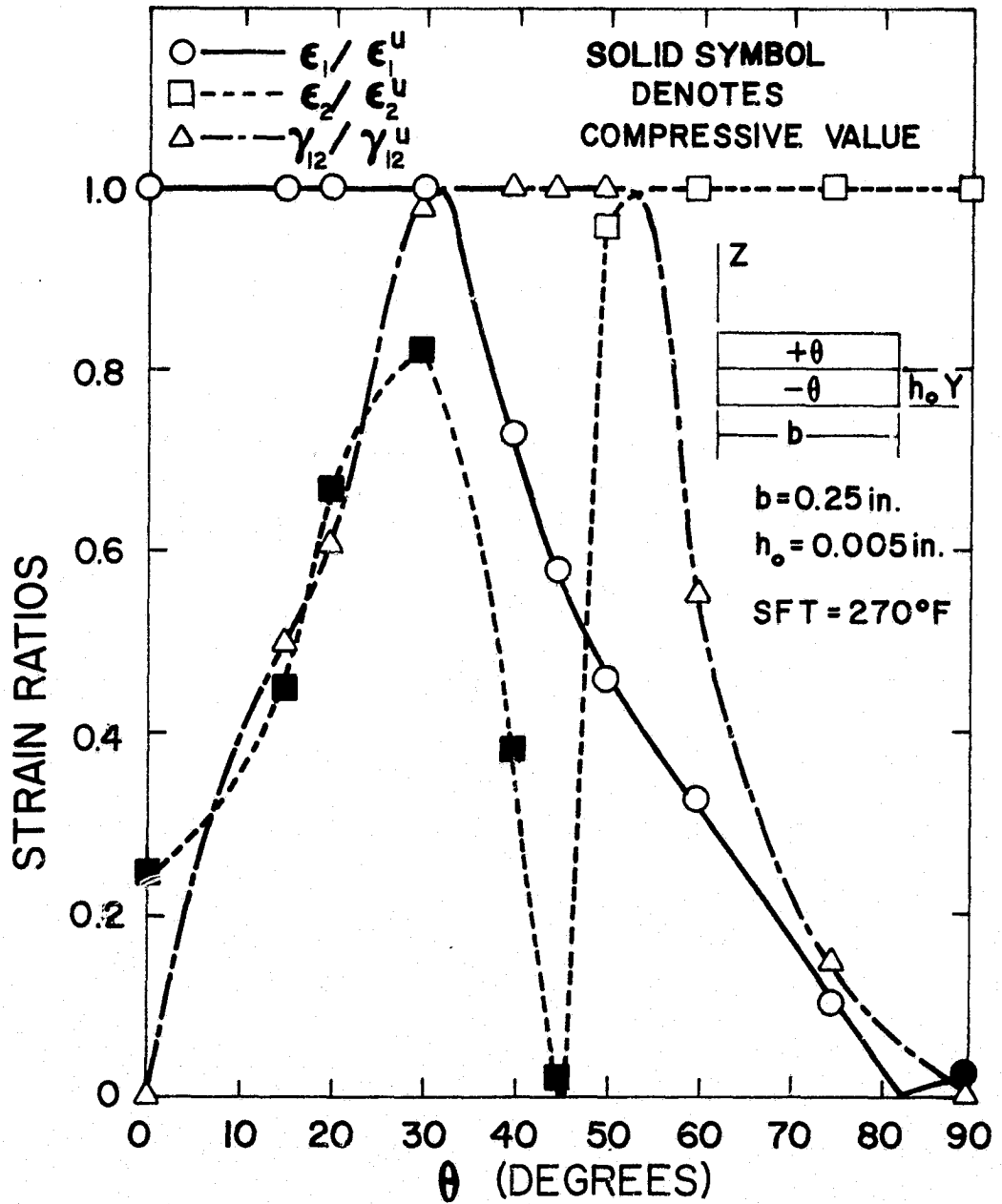
Figure 28. In-Plane Strain Ratios in Boron/Epoxy Angle-Ply Laminates Loaded in Tension - Sandwich Beam Data
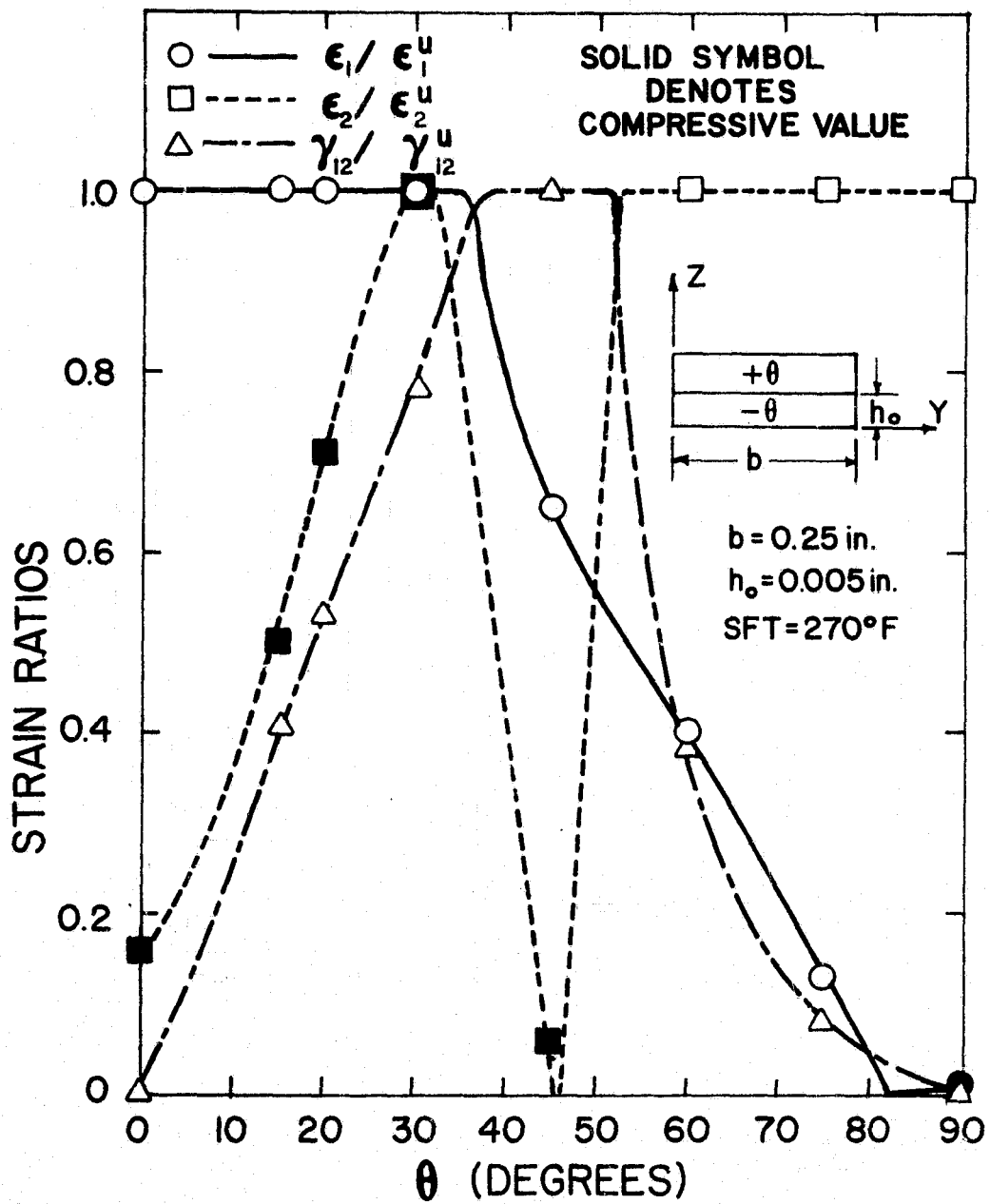
Figure 29. In-Plane Strain Ratios in Graphite/Epoxy Angle-Ply
Laminates Loaded in Tension - Coupon Data
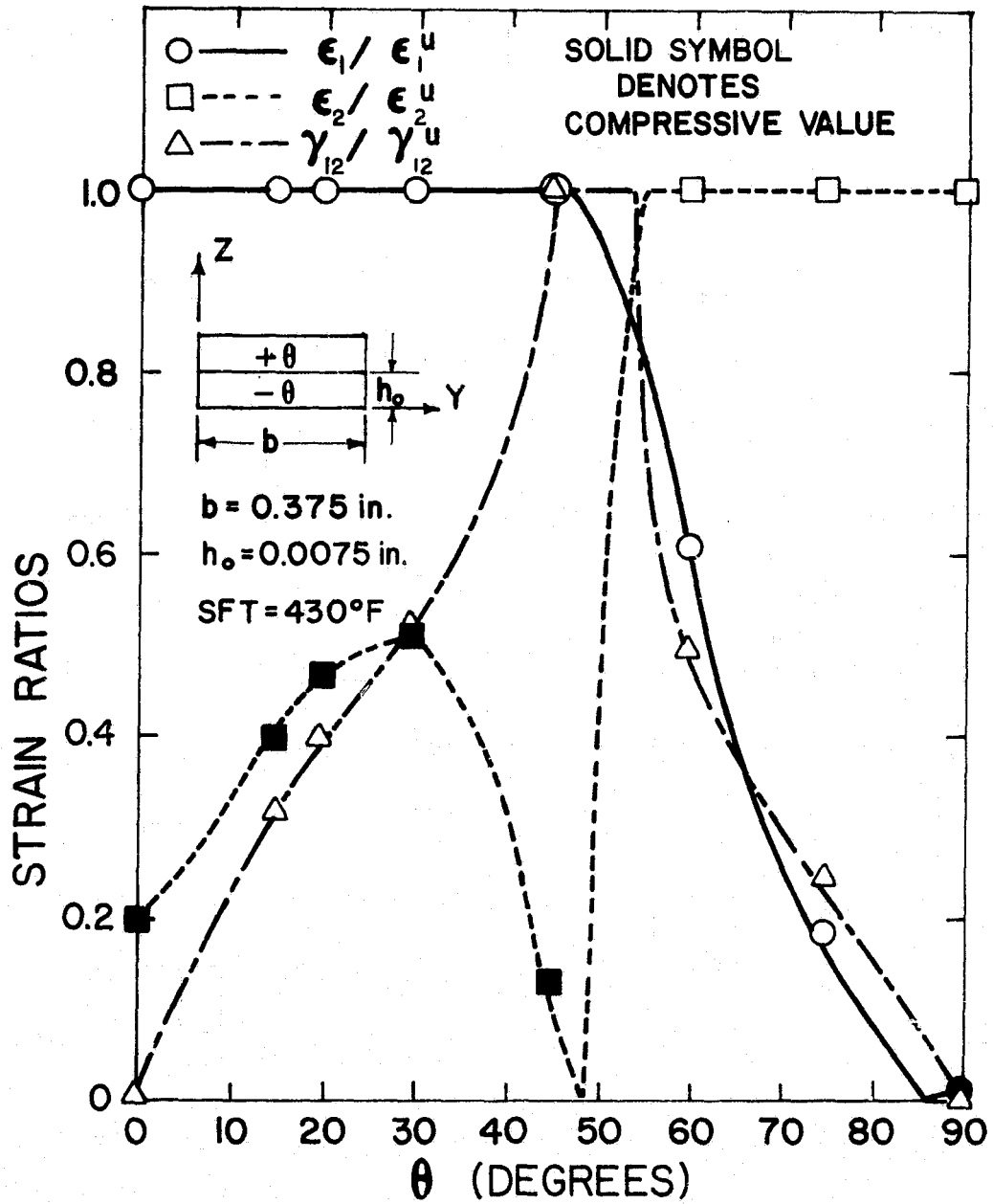
Figure 30. In-Plane Strain Ratios in Borsic/Aluminum Angle-Ply
Laminates Loaded in Tension - Coupon Data

tensile loading can be classified as ε_1 tensile failure for small angles, γ_{12} shear failure for intermediate angles, and ε_2 tensile failure for large angles. The figures also show that tensile coupon and sandwich beam results for boron/epoxy are quite similar (± 40 and ± 50 degree laminates were analyzed for the sandwich beam to determine the form of the ε_2 curve). The graphite/epoxy results were very much like the boron/epoxy results but exhibited overlapping of ε_1 tensile and ε_2 compressive failure at ± 30 degrees. As shown in Fig. 30, the metal matrix laminates exhibited a much smaller intermediate region than the epoxy matrix laminates. Thus, as expected, the failure mode in angle-ply laminates subjected to tensile loading is material dependent.

6.2.2 Compressive Loading of Angle-Ply Laminates

This section considers the compressive loading of angle-ply laminates which were initially subjected to thermal cooling. All lamina input data were taken from sandwich beam experimental results.

Tables 5 through 7 present the values of the strain ratios at the theoretically predicted failure strain for boron/epoxy, graphite/ epoxy and borsic/aluminum laminates, respectively. The tables indicate that all the material systems exhibited similar behavior with respect to strain ratios. Fiber orientations of $\leq |45|$ degrees exhibited significantly higher total strain ratios at the free-edge than at the center of the laminate for all materials. The strain ratios for the ε_3 strain which attained a value of 1.0 (boron/epoxy, borsic/aluminum) were assumed to indicate delamination and the

Table 5. STRAIN RATIOS IN BORON/EPOXY ANGLE-PLY LAMINATES LOADED IN COMPRESSION - SANDWICH BEAM DATA

[+Θ/-Θ]$_s$ LAY-UP (DEGREES)	FAILURE STRAIN ξ_x (%)	IN-PLANE STRAIN RATIOS*			INTERLAMINAR STRAIN RATIOS**			TOTAL STRAIN RATIO	
		ϵ_1/ϵ_1^u	ϵ_2/ϵ_2^u	$\gamma_{12}/\gamma_{12}^u$	ϵ_3/ϵ_3^u	$\gamma_{23}/\gamma_{23}^u$	$\gamma_{13}/\gamma_{13}^u$	CENTER	FREE-EDGE
0	-1.1	1.00 C	1.00 T	0.0	1.00 T [1]	0.0	0.0	3.0	3.0
15	-0.60	0.50 C	1.00 T	0.37	0.41 T [1]	0.20	0.74	2.25	3.18
20	-0.55	0.26 C	1.00 T	0.46	0.17 T	0.26	0.70	1.91	2.87
30	-0.60	0.14 C [3]	1.00 T	0.60	0.04 C [2]	0.32	0.54	1.56	2.35
45	-1.60	0.34 T	0.12 C	0.100	0.11 T	0.21	0.19	1.58	2.00
60	-2.25	0.45 T	1.00 C	0.98	1.00 T [2]	0.16	0.08	3.45	3.70
75	-1.6	0.22 T	1.00 C	0.58	1.00 T [1]	0.07	0.02	2.84	2.93
90	-1.7	0.11 T	1.00 C	0.0	1.00 T [1]	0.0	0.0	2.1	2.1

T = Tensile C = Compressive Stress Free Temperature = 270 °F
* Value approximately equal in all elements (unless otherwise noted)
** Value taken from elements at intersection of interface and free-edge (unless otherwise noted)
1 Value approximately equal in all elements
2 Value taken from elements at intersection of interface and centerline
3 Value taken from elements at intersection of mid-plane and centerline

90

Table 6.   STRAIN RATIOS IN GRAPHITE/EPOXY ANGLE-PLY LAMINATES LOADED IN COMPRESSION -
SANDWICH BEAM DATA

[+Θ/-Θ]$_s$ LAY-UP (DEGREES)	FAILURE STRAIN ξ_x (%)	IN-PLANE STRAIN RATIOS*			INTERLAMINAR STRAIN RATIOS**			TOTAL STRAIN RATIO	
		ϵ_1/ϵ_1^u	ϵ_2/ϵ_2^u	$\gamma_{12}/\gamma_{12}^u$	ϵ_3/ϵ_3^u	$\gamma_{23}/\gamma_{23}^u$	$\gamma_{13}/\gamma_{13}^u$	CENTER	FREE-EDGE
0	-1.30	1.00 C	0.60 T	0.0	0.60 T [1]	0.0	0.0	2.21	2.21
15	-0.90	0.55 C	1.00 T	0.30	0.17 T [1]	0.18	0.65	2.20	3.03
20	-0.75	0.34 C	1.00 T	0.36	0.05 T	0.23	0.61	1.77	2.53
30	-0.90	0.15 C [3]	1.00 T	0.55	0.06 C [2]	0.33	0.55	1.85	2.59
45	-4.2	0.35 T	0.24 C	1.00	0.03 T	0.24	0.02	1.66	2.14
60	-2.2	0.42 T	1.00 C	0.73	0.68 T [1]	0.07	0.04	2.88	3.00
75	-1.6	0.17 T	1.00 C	0.44	0.75 T [1]	0.03	0.01	2.38	2.43
90	-1.6	0.04 T	1.00 C	0.0	0.82 T [1]	0.0	0.0	1.86	1.86

T = Tensile   C = Compressive   Stress Free Temperature = 270 °F
*   Value approximately equal in all elements (unless otherwise noted)
**   Value taken from elements at intersection of interface and free-edge (unless otherwise noted)
1   Value approximately equal in all elements
2   Value taken from elements at intersection of interface and centerline
3   Value taken from elements at intersection of mid-plane and centerline

Table 7. STRAIN RATIOS IN BORSIC/ALUMINUM ANGLE-PLY LAMINATES LOADED IN COMPRESSION - SANDWICH BEAM DATA

$[+\Theta/-\Theta]_s$ LAY-UP (DEGREES)	FAILURE STRAIN ξ_x (%)	IN-PLANE STRAIN RATIOS*			INTERLAMINAR STRAIN RATIOS**			TOTAL STRAIN RATIO	
		ϵ_1/ϵ_1^u	ϵ_2/ϵ_2^u	$\gamma_{12}/\gamma_{12}^u$	ϵ_3/ϵ_3^u	$\gamma_{23}/\gamma_{23}^u$	$\gamma_{13}/\gamma_{13}^u$	CENTER	FREE-EDGE
0	-1.20	1.00 C	0.81 T	0.0	0.81 T [1]	0.0	0.0	2.64	2.64
15	-1.15	0.52 C	1.00 T	0.48	0.21 T [1]	0.15	0.54	2.20	2.80
20	-0.925	0.32 C	1.00 T	0.52	0.06 T [2]	0.05	0.42	1.75	2.32
30	-1.0	0.16 C [3]	1.00 T	0.70	0.28 C [1]	0.28	0.48	2.10	2.85
45	-2.1	0.46 T	0.33 C	1.00	0.28 T [1]	0.20	0.20	2.11	2.52
60	-3.5	0.53 T	0.82 C	1.00	1.00 T [1]	0.11	0.06	3.34	3.52
75	-3.2	0.26 T	1.00 C	0.75	1.00 T [1]	0.01	0.02	2.84	2.94
90	-4.25	0.07 T	1.00 C	0.0	1.00 T [1]	0.0	0.0	2.00	2.00

T = Tensile   C = Compressive   Stress Free Temperature = 430 °F
*   Value approximately equal in all elements (unless otherwise noted)
**   Value taken from elements at intersection of interface and free-edge (unless otherwise noted)
1   Value approximately equal in all elements
2   Value taken from elements at intersection of interface and centerline
3   Value taken from elements at intersection of mid-plane and centerline

laminate was allowed to continue loading until an in-plane strain failure occurred. However, the 3-direction stiffness was reduced in accordance with the progressive failure theory of Section 4.2.

Figures 31 through 33 show the graphical representation of the in-plane strain ratios (Tables 5 - 7) as a function of fiber orientation at the theoretically predicted failure strain. As shown in the figures, the results indicate that failure of angle-ply-laminates subjected to compressive loading can be classified as ε_1 compressive failure for extremely small angles, ε_2 tensile failure for small angles, γ_{12} shear failure for intermediate angles, and ε_2 compressive failure for large angles. As indicated by the figures, the results were quite similar for all materials.

However, the materials containing boron fibers exhibited results which were nearly identical. These materials also exhibited a larger shear region than the graphite/epoxy system. It is interesting to note from the figures the dominance of ε_2 failure modes in angle-ply laminates subjected to compressive loading.

6.3 Stress-Strain Behavior of Angle-Ply Boron/Epoxy Laminates

This section presents results for the theoretical prediction of the nonlinear stress-strain behavior for a variety of boron/epoxy angle-ply laminates. The present analysis is compared where applicable to the theoretical and experimental results of Petit and Waddoups [11] and Kaminski, et al. [14], and the theoretical results of Hashin, et al. [15]. The type of input data (sandwich beam or tensile coupon) is noted on the figures.
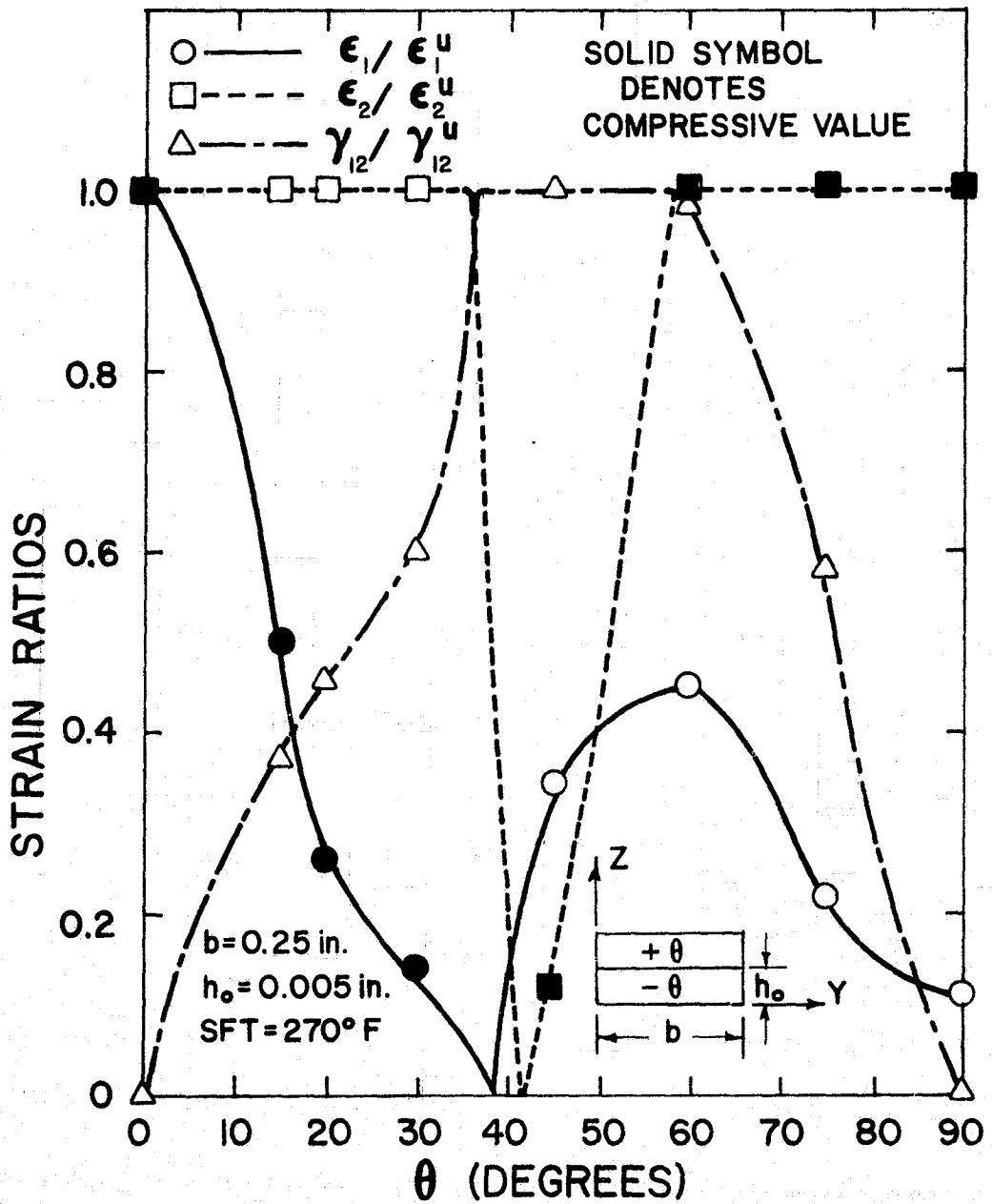
Figure 31. In-Plane Strain Ratios in Boron/Epoxy Angle-Ply
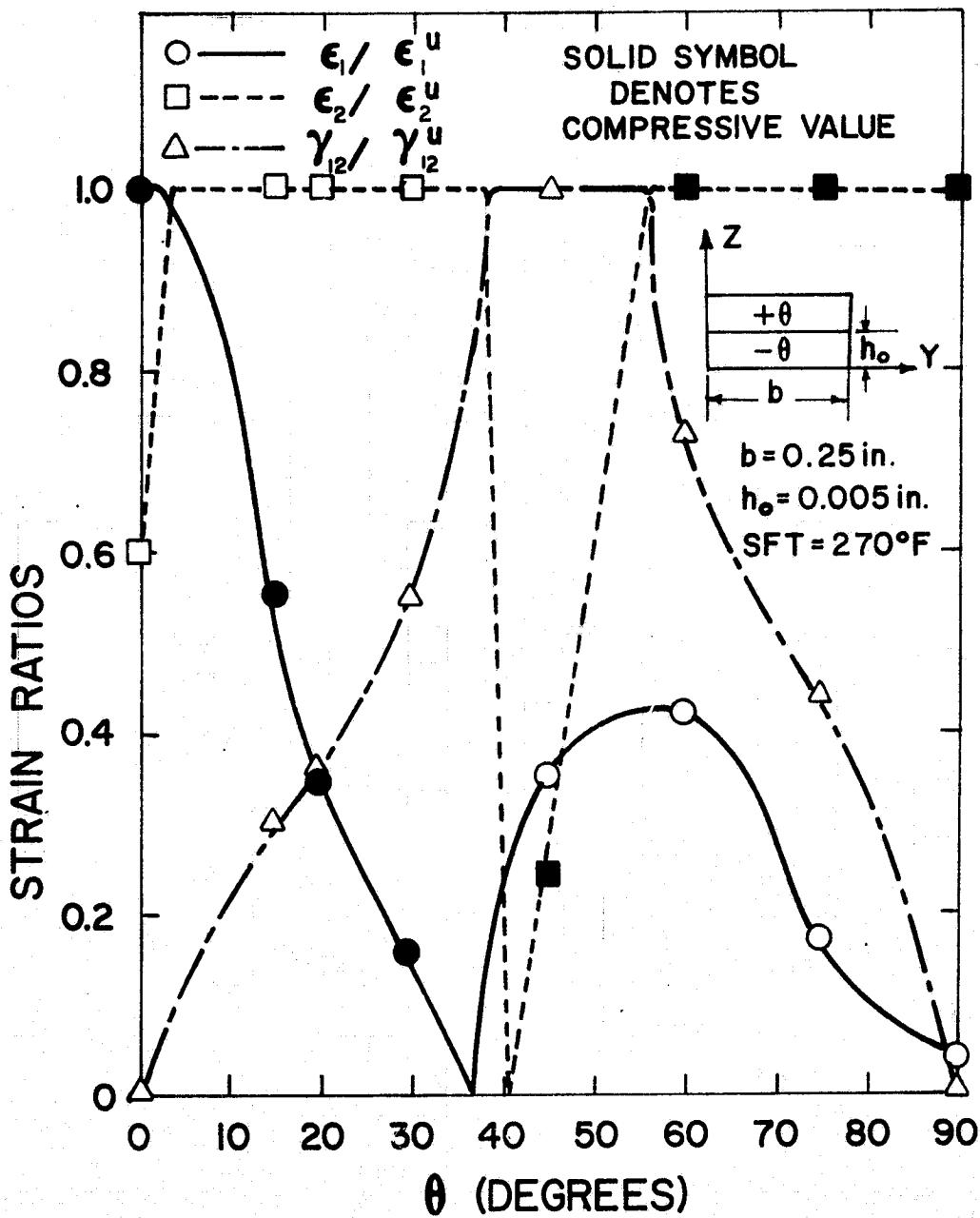Laminates Loaded in Compression - Sandwich Beam Data

Figure 32. In-Plane Strain Ratios in Graphite/Epoxy Angle-Ply Laminates Loaded in Compression - Sandwich Beam Data
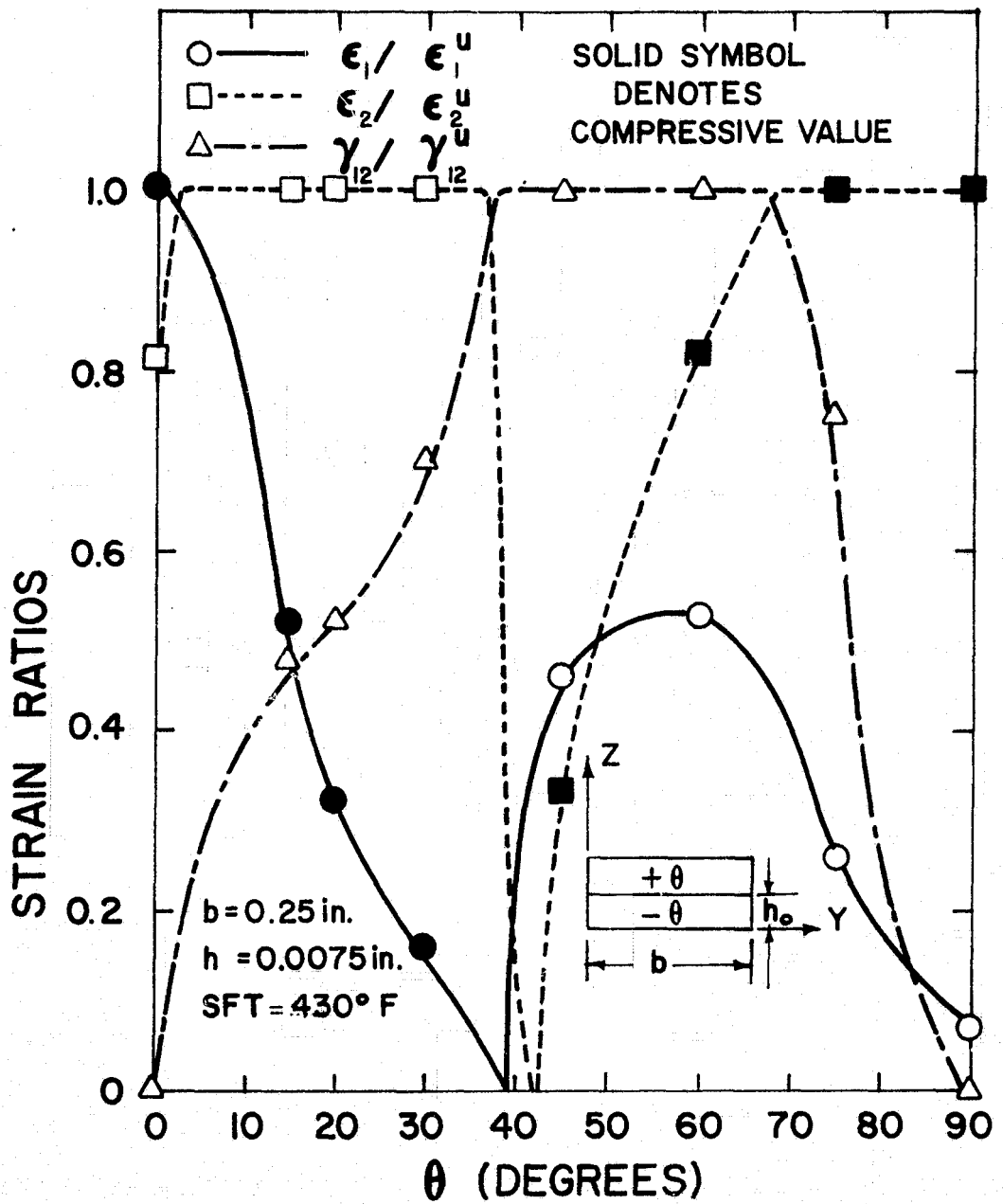
Figure 33. In-Plane Strain Ratios in Borsic/Aluminum Angle-Ply Laminates Loaded in Compression - Sandwich Beam Data

The theoretical analysis of this investigation is inherently dependent on input lamina properties. Thus, the analysis cannot account for experimental anomalies such as poor bonding, variable fiber volume fraction, initial cracks or voids in the laminate, and improper alignment of fibers. Also, when sandwich beam results are considered there is some reinforcement present due to the honeycomb core. The effect of this reinforcement is undoubtedly a function of the specimen ply orientations.

Tensile and compressive loading was considered and all laminates were assumed to have a stress-free temperature of 270°F. It should be noted that the theoretical results of References [11, 14, 15] did not consider thermal effects for room temperature loading. The predicted failure strains, ε_x^f, for the present analysis are given in Tables 1, 2 and 5.

[+20/-20]$_s$ Laminate

The tensile results for this laminate are shown in Fig. 34. As indicated in the figure, both theories adequately predict the shape of the curve. However, the theory of Reference 11 overestimates the ultimate strength whereas the present analysis accurately predicts the ultimate strength.

The individual theories each indicated that laminate failure was a result of ε_1 tensile failure. However, better agreement for the failure strain is exhibited by the present analysis. The thermal analysis indicated initial ε_1 tensile strains existed after cooldown and, hence, the range of strain available for loading in tension is
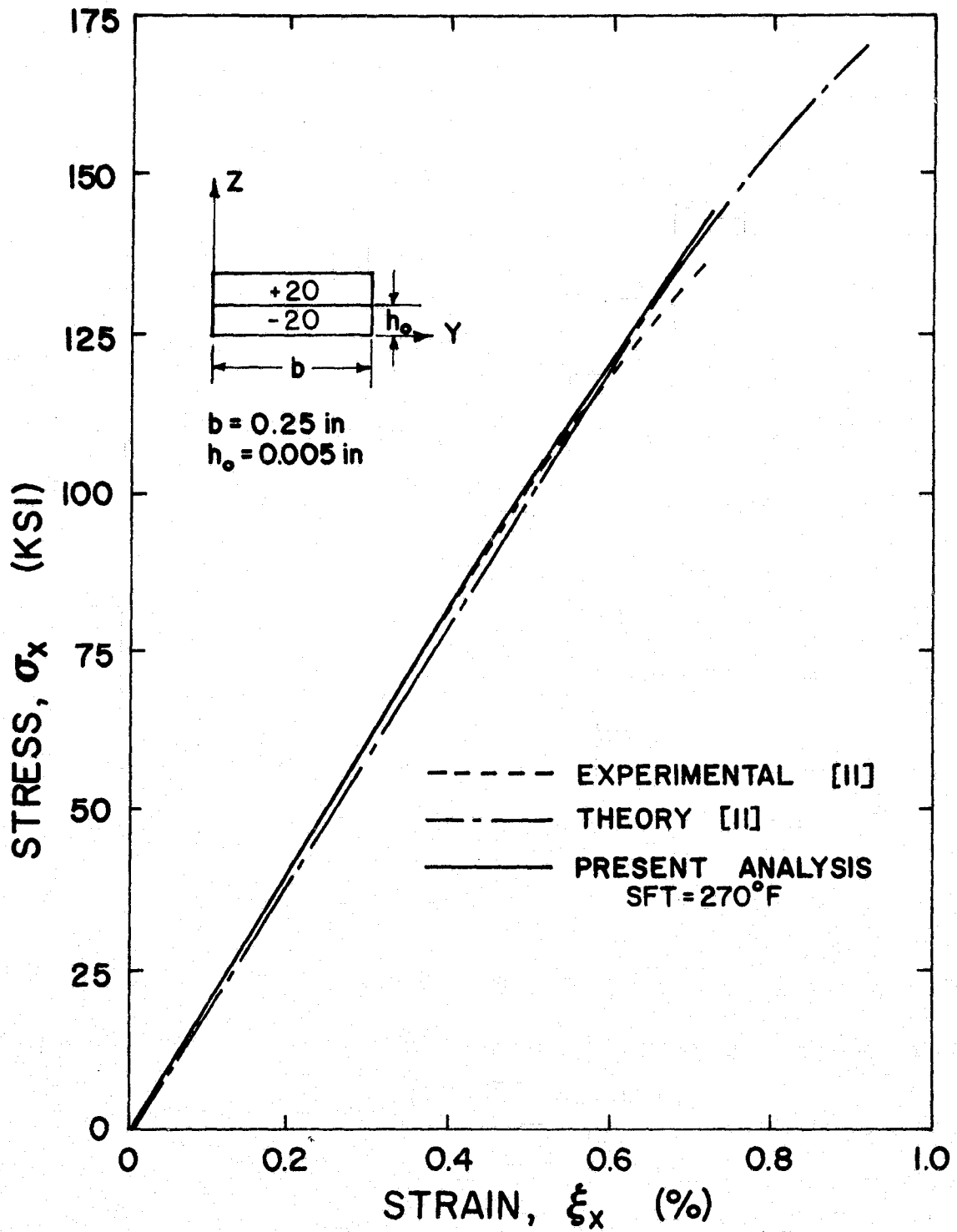
Figure 34. Tensile Stress-Strain Behavior of [+20/-20]$_s$ Boron/ Epoxy Laminate - Sandwich Beam Data

limited accordingly. The results of this figure indicate the importance of thermal effects for predicting failure of this laminate.

Figure 35 shows the compressive results for this laminate. As can be seen in the figure, the theory of Reference [11] predicts the initial laminate modulus more closely than does the present analysis. However, the present analysis more accurately predicts the ultimate strength of the laminate.

Both theories predicted that laminate failure was a result of ε_2 tensile failure. However, the thermal results of the present analysis indicated that initial ε_2 compressive strain existed in the laminate, hence, the better prediction of ultimate strength. And, again it is seen that inclusion of thermal effects provides a better prediction of failure. The higher stiffness exhibited by the experimental curve may possibly be attributed to more pronounced honeycomb reinforcement for the laminate compared to individual reinforcement inherent in the lamina data.

A comparison of the tensile and compression results for this laminate reveals that the thermal effect increases the compressive strength but decreases the tensile strength.

$[+30/-30]_s$ Laminate

Figure 36 shows the tensile results for this laminate. It can be seen from the figure that both the present analysis and the theory of Reference [11] exhibit good correlation between theory and experiment whereas the theory of Reference [15] does not exhibit the degree of nonlinearity of the experimental curve.
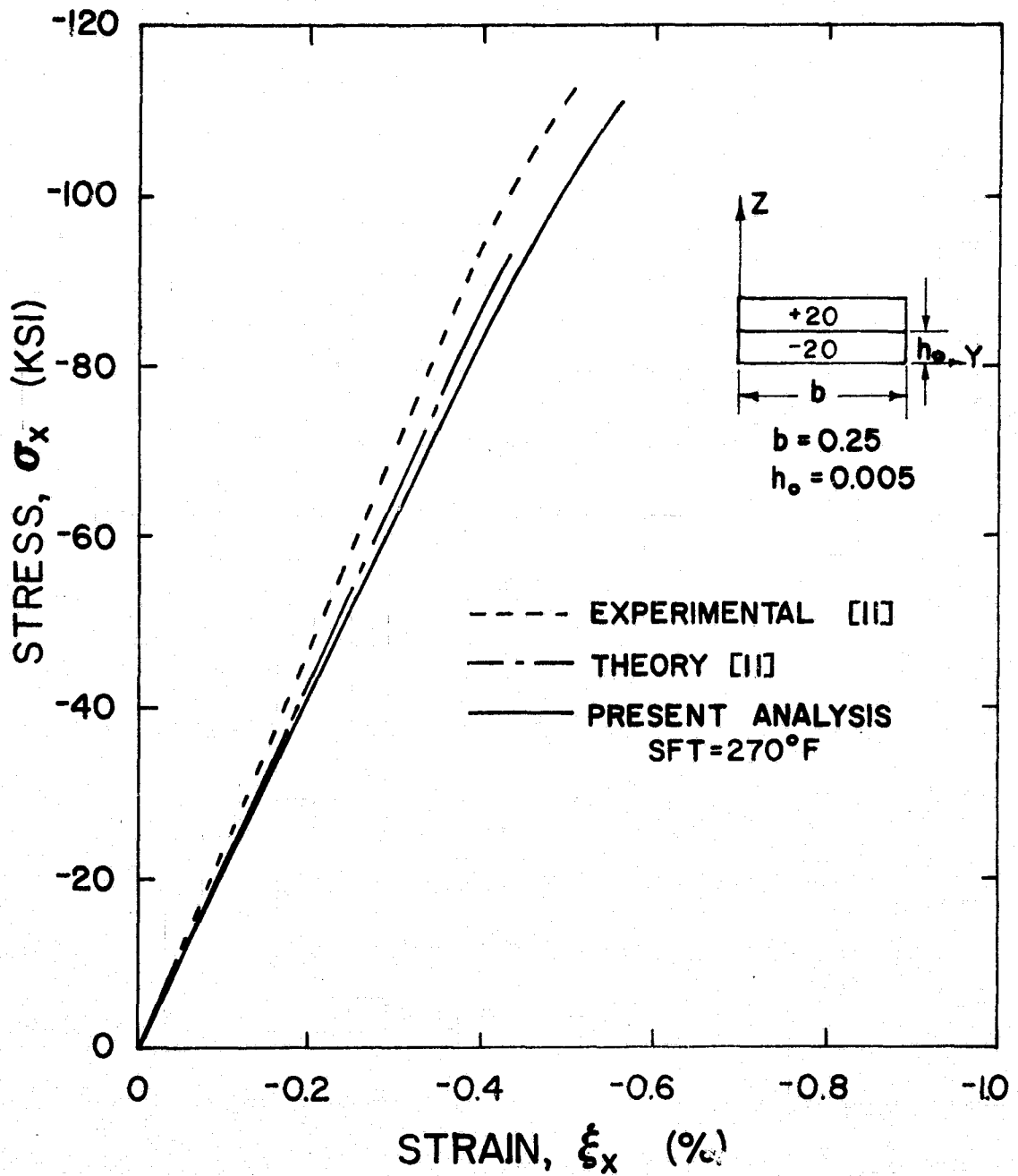
Figure 35. Compressive Stress-Strain Behavior of [+20/-20]$_s$ Boron/
Epoxy Laminate - Sandwich Beam Data

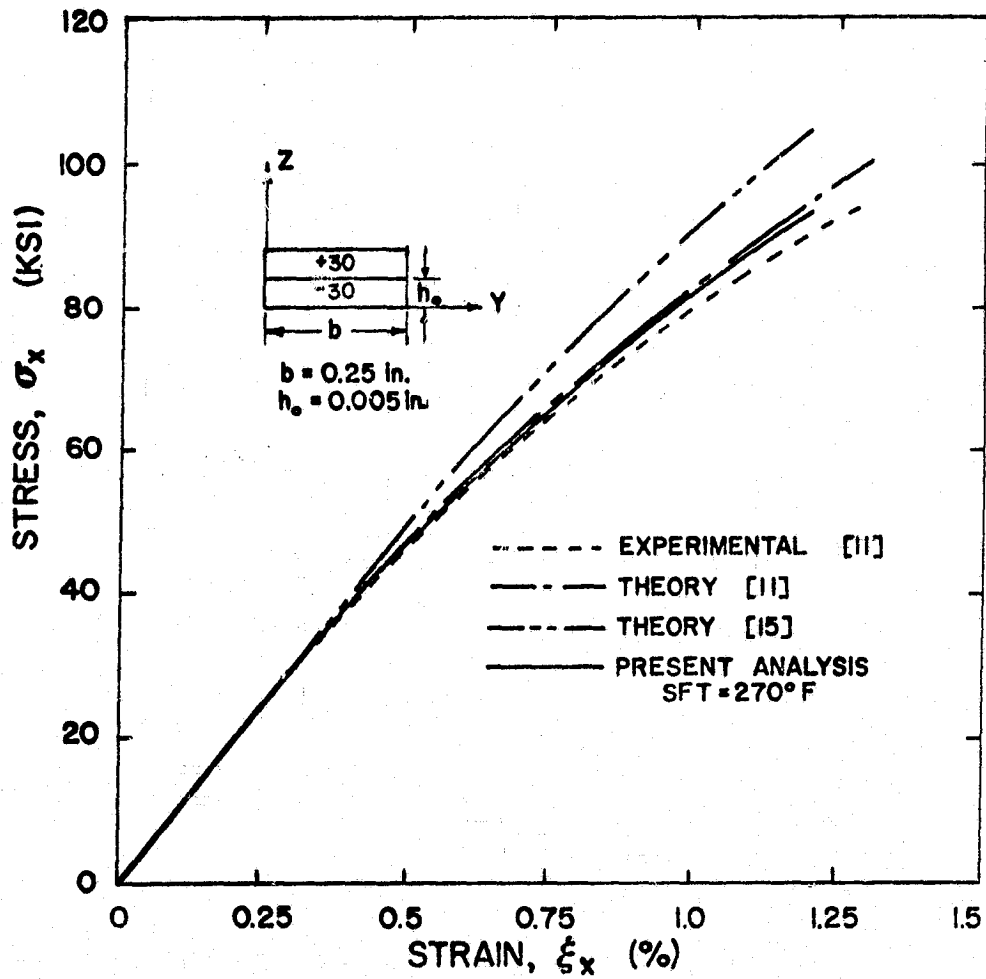Figure 36. Tensile Stress-Strain Behavior of [+30/-30]s Boron/Epoxy Laminate - Sandwich Beam Data

The present analysis and the theory of Reference [15] predicted that laminate failure was a result of ε_1 tensile failure whereas the theory of Reference [11] predicted that laminate failure was a result of ε_2 compressive failure. These differences can be attributed to the method in which the lamina stress-strain data was input for the analysis. The present analysis and the method of Reference [15] used Ramberg-Osgood [16] approximations whereas the method of Reference [11] involved linear segments. The present analysis indicated that the in-plane shear strain, γ_{12}, had attained a strain ratio of 0.1 throughout the laminate after thermal cooling. The subsequent strain loading yielded an in-plane shear strain of the same sign as the initial in-plane shear strain. Since the shear data exhibits a highly nonlinear curve, the present analysis would reflect the non-linearity sooner.

The compressive results for this laminate are shown in Fig. 37. As indicated in the figure, both analyses exhibit nonlinearity comparable to the experimental curve. However, the results of Reference [11] agreed more favorably than the present analysis in predicting both the nonlinearity and the ultimate strength.

The theories indicated that laminate failure was due to ε_2 tensile failure. However, the present analysis indicated that initial ε_2 compressive strain resulted from thermal cooling, hence, the overestimation of laminate strength. It may be possible that assumed stress-free temperature was too high for this laminate.
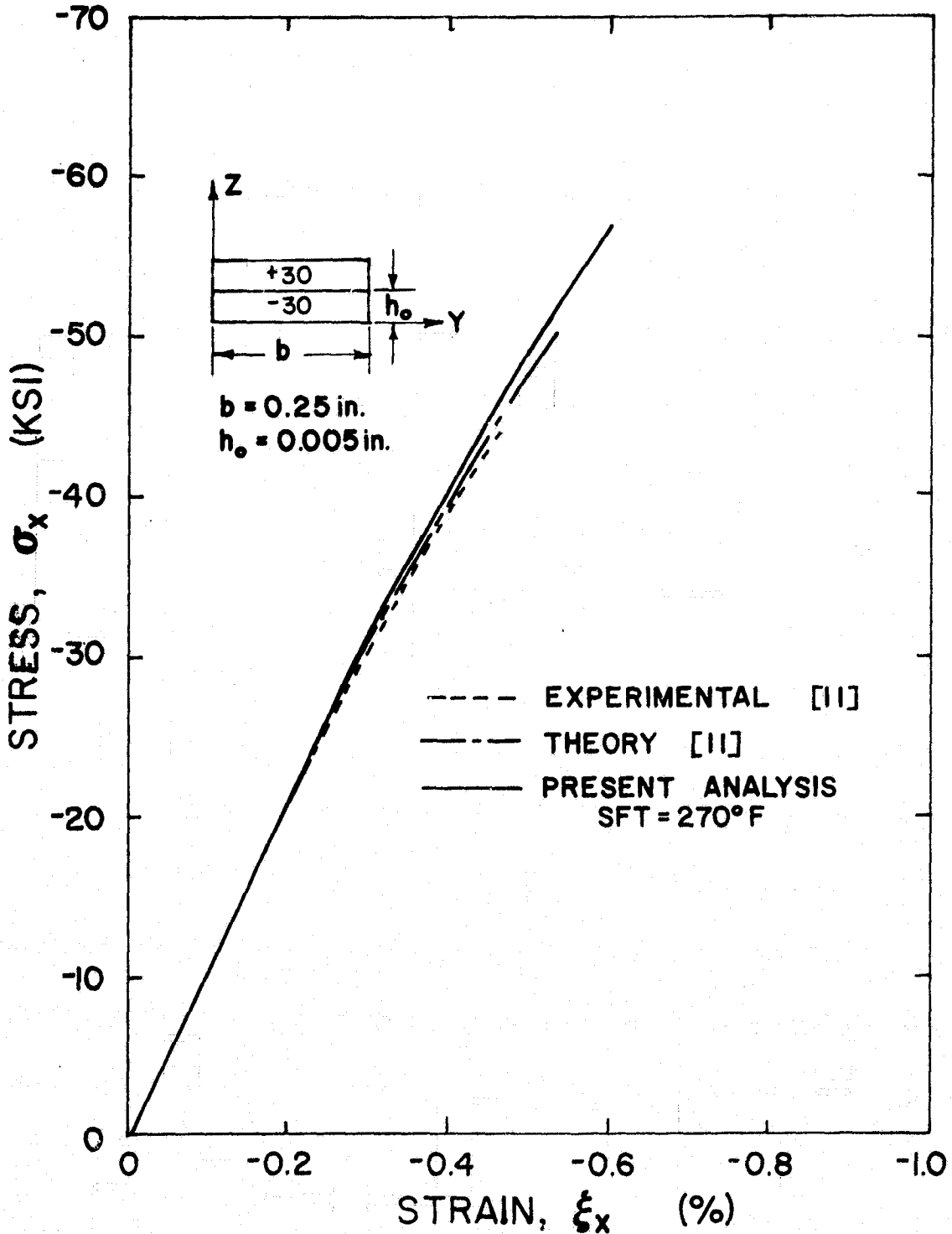
Figure 37. Compressive Stress-Strain Behavior of [+30/-30]$_s$ Boron/ Epoxy Laminate - Sandwich Beam Data

[+45/-45]$_s$ Laminate

The tensile results, Fig. 38, show the comparison of theoretical and experimental results for both sandwich beam and tensile coupon lamina input data. The results of the present analysis as well as the results of the theory of Reference [14] adequately represent the experimental curve. However, the present analysis does exhibit better results for the sandwich beam curve. Both analyses predicted that failure occurred as a result of in-plane shear, γ_{12}, failure.

It is interesting to note the significant difference between sandwich beam and tensile coupon behavior. This difference is attributed to honeycomb core reinforcement of the laminate. Compressive results (not shown) exhibited behavior similar to the results for the sandwich beam curve.

[+60/-60]$_s$ Laminate

The tensile results for this laminate, Fig. 39, show that both theoretical curves adequately represent the experimental curve up to 0.3% strain. However, the present analysis accurately predicts the ultimate strain but overestimates the ultimate stress. The theory of Reference [11] underestimates both the ultimate stress and strain.

Both analyses indicated that laminate failure was due to ε_2 tensile failure. However, the present analysis indicated that initial ε_2 compressive strain resulted from thermal cooling, hence, the better agreement with respect to the applied failure strain. Thus, the thermal effect provides a wider range of strain for tensile loading of this laminate. The lower stiffness shown by the
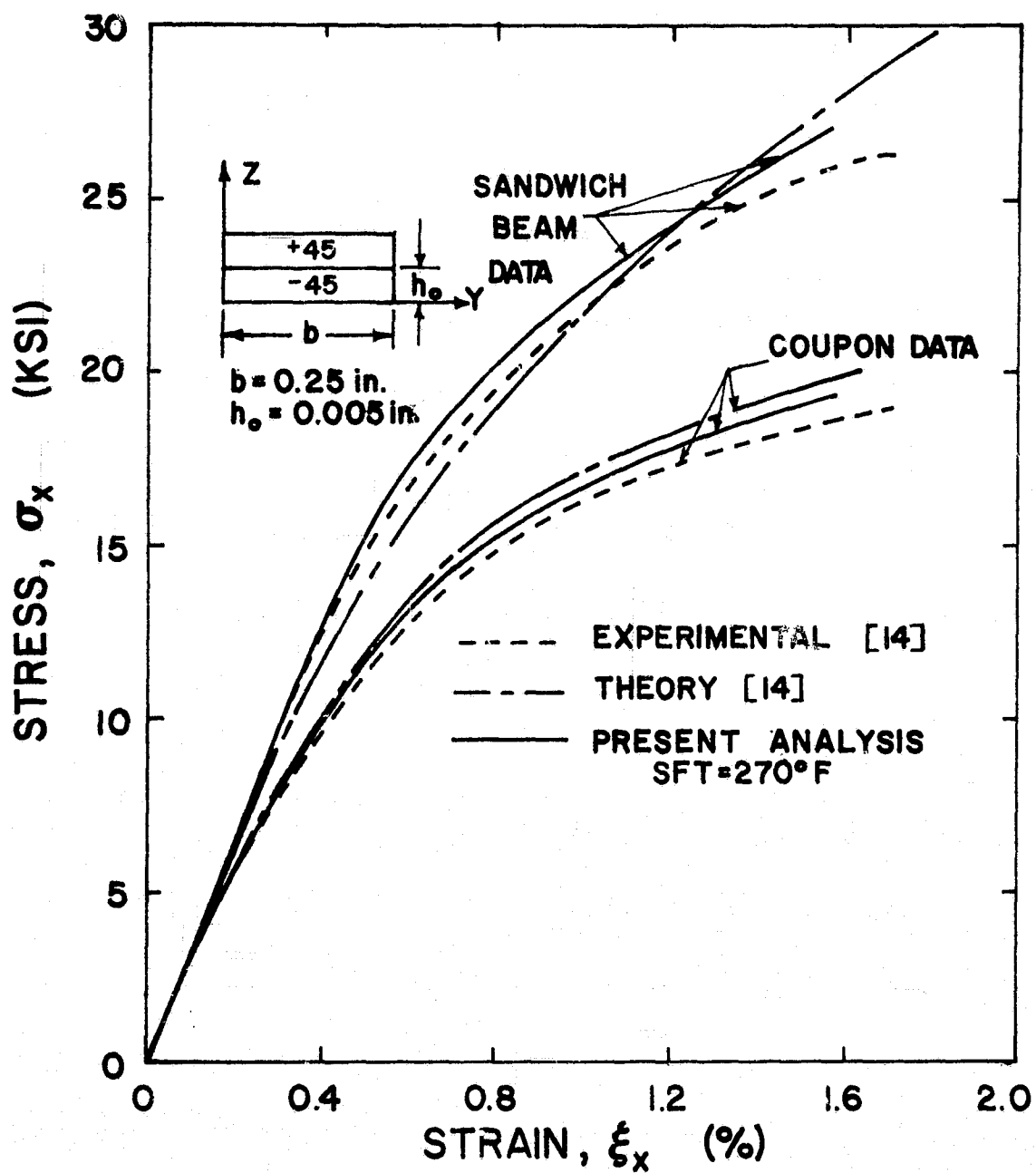
Figure 38. Tensile Stress-Strain Behavior of [+45/-45]$_s$ Boron/Epoxy Laminate
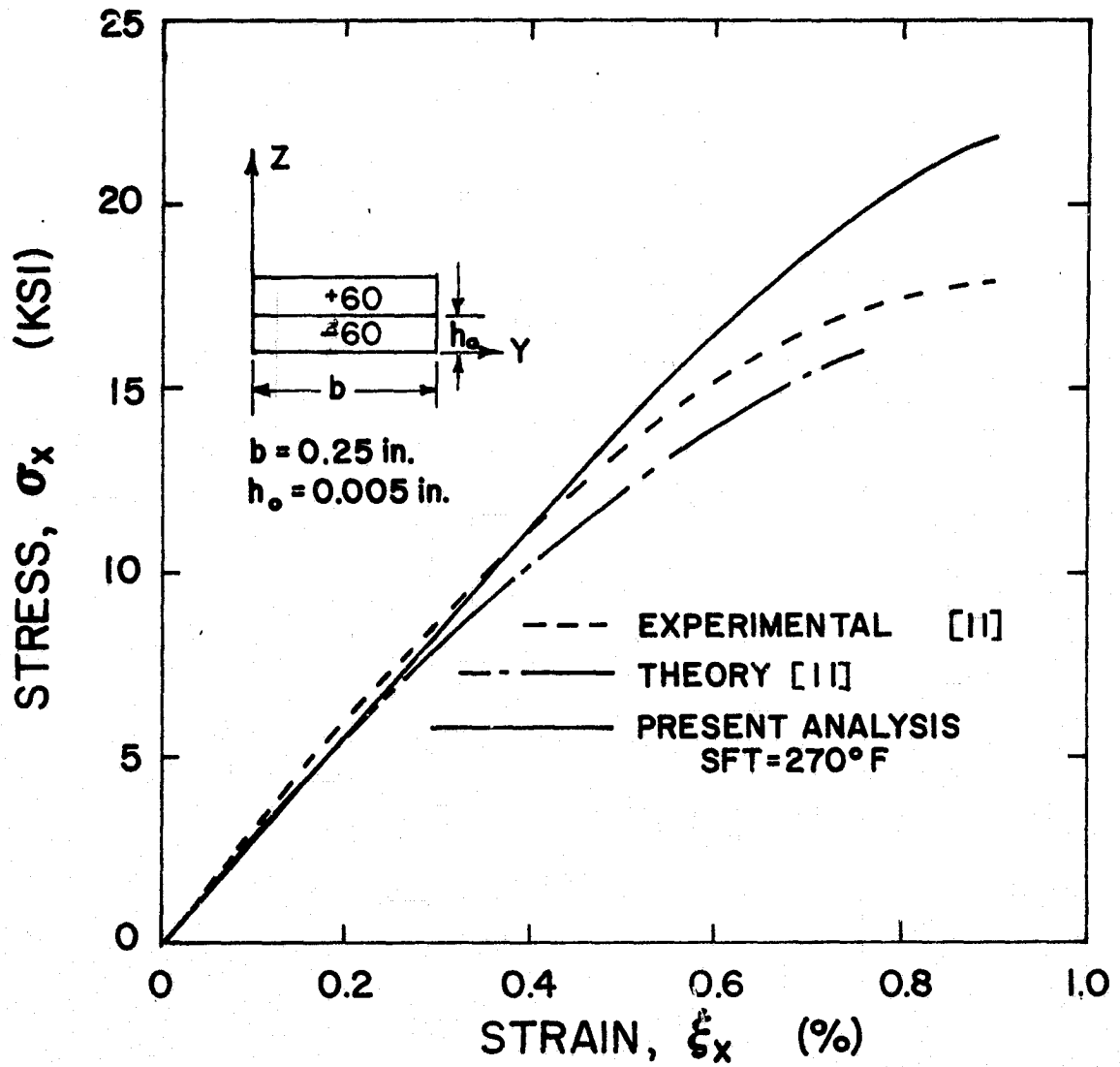
Figure 39.   Tensile Stress-Strain Behavior of [+60/-60]$_s$ Boron/Epoxy
Laminate - Sandwich Beam Data

experimental curve may possibly be attributed to less pronounced honeycomb reinforcement for the laminate compared to individual reinforcement inherent of the lamina data.

Figure 40 shows that neither theory gave a good prediction of the ultimate compressive strength of this laminate. It can be seen in the figure that the theory of Reference [11] more closely resembles the experimental curve whereas the present analysis exhibits a better indication of the ultimate strain.

The theories predicted that ε_2 compressive failure would cause laminate failure. It may be possible that the sandwich beam method of determining experimental data allows additional loading of angle-ply laminates by supporting the compressive ε_2 mode of failure. Noting Table 5, the present analysis shows that subsequent in-plane shear failure will occur upon additional loading. This mode of failure may also be supported by the sandwich beam test method.

6.4 Stress-Strain Behavior of Cross-Ply and Other Boron/Epoxy Laminates

It was stated in the previous sections that angle-ply laminates exhibit total laminate failure when all layers fail at the same applied strain level. This fact is generally not true for more complex laminates.

A study of various boron/epoxy laminates by Kaminski, et al., [14] showed that first ply failure was a sufficient technique to predict laminate failure for some boron/epoxy laminates subjected to tensile loading. However, results of Reference [14] also showed
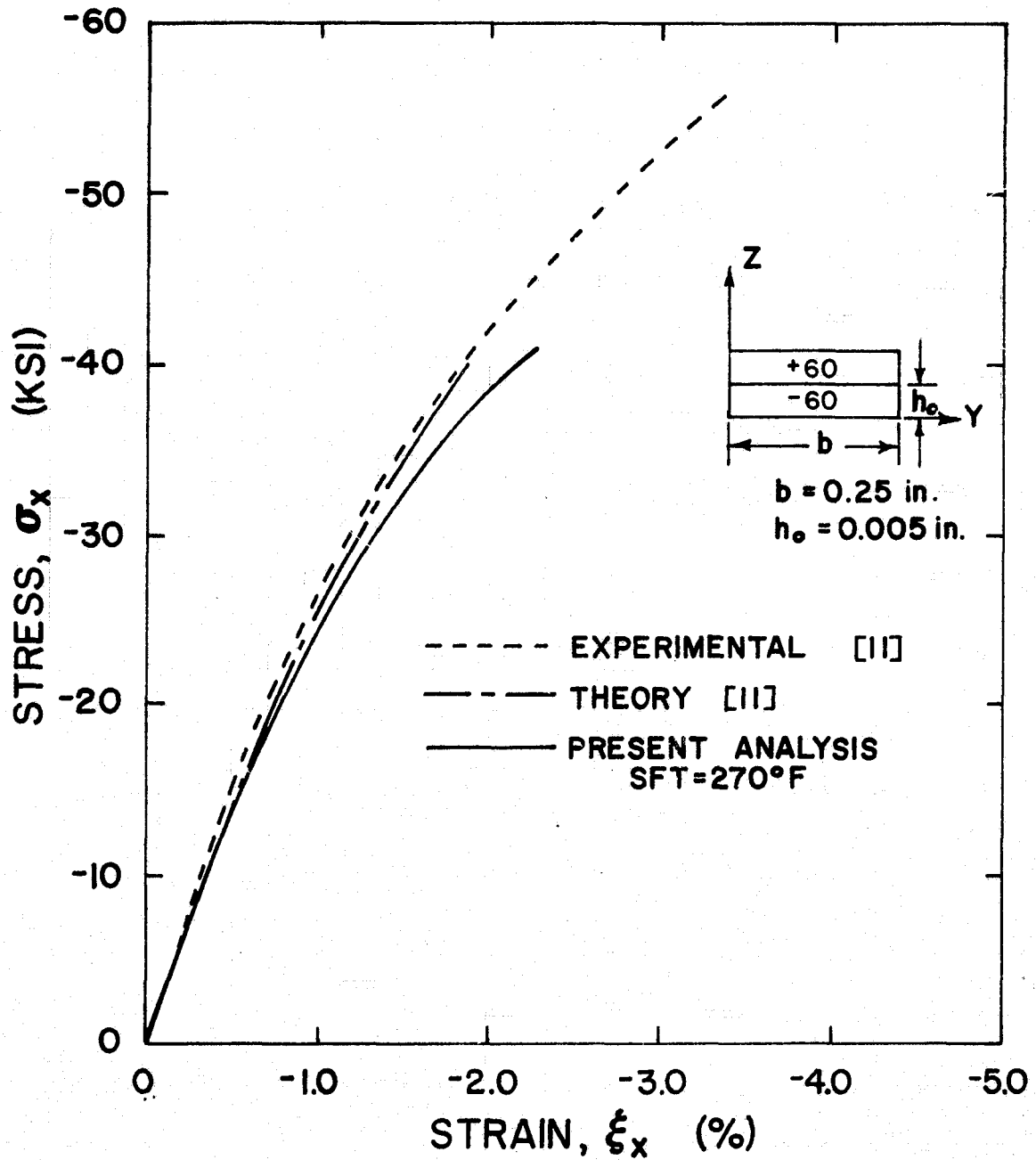
Figure. 40. Compressive Stress-Strain Behavior of [+60/-60]$_s$ Boron/ Epoxy Laminate - Sandwich Beam Data

that the first ply failure theory was not a viable technique to use in predicting laminate failure when compressive loading was considered for laminates comprised of angle-plies in combination with 0 degree plies or angle-plies in combination with 90 degree plies. It was also shown in Reference [14] that first ply failure could not accurately predict failure when tensile loading was considered for laminates comprised of angle-plies in combination with both 0 and 90 degree layers.

Using experimental results of References [11, 14] and theoretical results of this investigation a qualitative analysis was undertaken to determine failure modes of more complex boron/epoxy laminates subjected to tensile and compression loading. For the present analysis all the laminates were assumed to have a stress-free temperature of 270°F.

A comparison of experimental and theoretical results was conducted on laminates which were comprised of angle-plies in combination with 0 and/or 90 degree plies. The cross-ply laminate was also considered. The results indicated that failure of the laminates could be attributed to either first-ply failure, progressive failure, or failure due to edge effects. Table 8 shows the laminates which were considered and the type of failure mode that was observed in the present theory. The results shown in Table 8 are discussed in the following sections. It should be noted that the experimental anomalies previously mentioned in Section 6.3 must be considered.

Table 8. TYPES OF LAMINATE FAILURE

LAMINATE (BORON/EPOXY)	LOADING	TYPE OF FAILURE OBSERVED IN PRESENT THEORY
$[0_2/+45/-45]_s$ $[0/+60/-60]_s$ $[+45/-45/90_2]_s$ $[+30/-30/90]_s$	TENSION	FIRST PLY FAILURE
$[0/90]_s$ $[0/+45/-45/90]_s$	TENSION	PROGRESSIVE FAILURE
$[0_2/+45/-45]_s$ $[0/+60/-60]_s$	COMPRESSION	PROGRESSIVE FAILURE
$[+45/-45/90_2]_s$ $[+30/-30/90]_s$	COMPRESSION	FAILURE DUE TO EDGE EFFECTS

6.4.1 First Ply Failure

The results of the present analysis as well as the results of Reference [14] indicated that the $[0_2/+45/-45]_s$, $[0/+60/-60]_s$, $[+45/-45/90_2]_s$ and $[+30/-30/90]_s$ laminates failed due to first ply failure when loaded in tension. It is interesting to note that each of the laminates contained angle-plies in combination with 0 degree layers or angle-plies in combination with 90 degree layers. It was these 0 or 90 layers which failed first and, thereby, brought about total failure. Figures 41 through 44 show the theoretical and experimental stress-strain behavior of the above laminates for tensile loading.

$[0_2/+45/-45]_s$ Laminate

As shown in Fig. 41, both theoretical analyses exhibited good agreement when compared to the experimental curves. The slightly better agreement of the theory of Reference [14] could be attributed to analytical procedures.

Both analyses indicated the ε_1 tensile failure of the 0 degree layers occurred at approximately 0.65% strain load. The present analysis also showed that both the in-plane shear, γ_{12}, and ε_1 (tensile) had reached strain ratios of over 0.60 throughout the ± 45 degree layers with ε_1 having a higher strain ratio of nearly 0.70 near the free-edge. It can be concluded that the ± 45 degree layers could not support additional load after the 0 degree layer began to fail. It would also seem likely that upon failure of the 0 degree layer that failure of the ± 45 degrees would initiate at the free-edge.
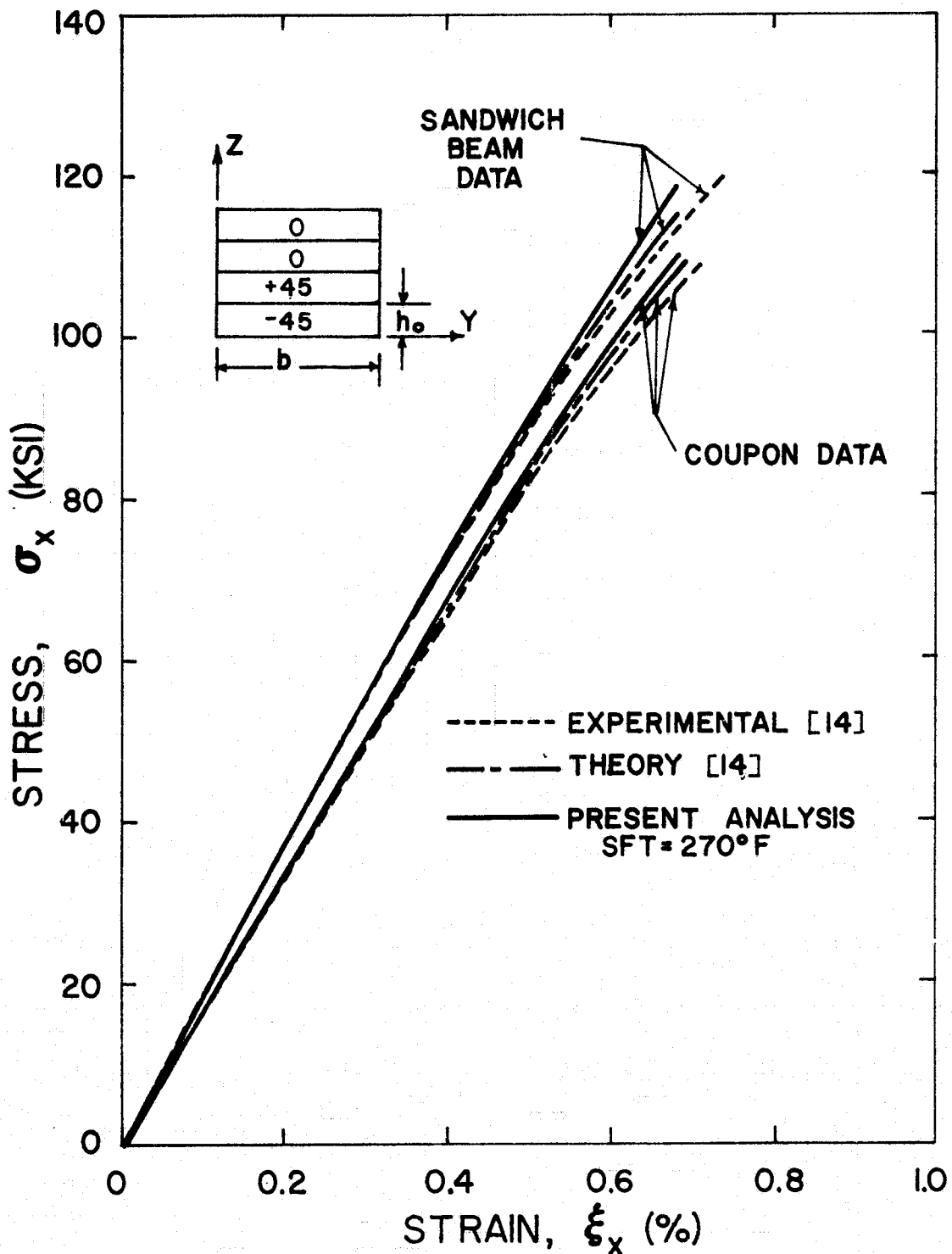
Figure 41. Tensile Stress-Strain Behavior of $[0_2/+45/-45]_s$ Boron/Epoxy Laminate

$[0/+60/-60]_s$ Laminate

The tensile results for this laminate, Fig. 42, indicated that both theoretical analyses exhibited good agreement up to 0.3% strain. However, neither analysis exhibited the nonlinearity above this strain.

The results of Reference [14] showed that laminate failure was a result of ϵ_1 tensile failure of the 0 degree layer. However, the theory of Reference [14] indicated that high ϵ_2 tensile strain existed in the ± 60 degree layers whereas the present analysis showed that simultaneously failure of the ± 60 degree layers occurred due to ϵ_2 tensile failure. The thermal results of the present analysis showed initial ϵ_2 tensile strain in the ± 60 degree layers and ϵ_1 compressive strain in the 0 degree layer. These two facts would account for the better agreement of the ultimate strain and the simultaneous failure. At this time, however, the absence of nonlinearity for the present analysis cannot be explained.

$[+45/-45/90_2]_s$ Laminate

· As shown in Fig. 43, the present analysis exhibited better agreement than the theory of Reference [14] with respect to the initial modulus and nonlinearity of the laminate behavior for tensile loading. The present analysis exhibited better agreement for tensile coupon results than sandwich beam results.

Laminate failure was observed to occur due to ϵ_2 tensile failure in the 90 degree layers for both theoretical analyses. However, the present analysis showed that high in-plane shear strain, γ_{12}, was
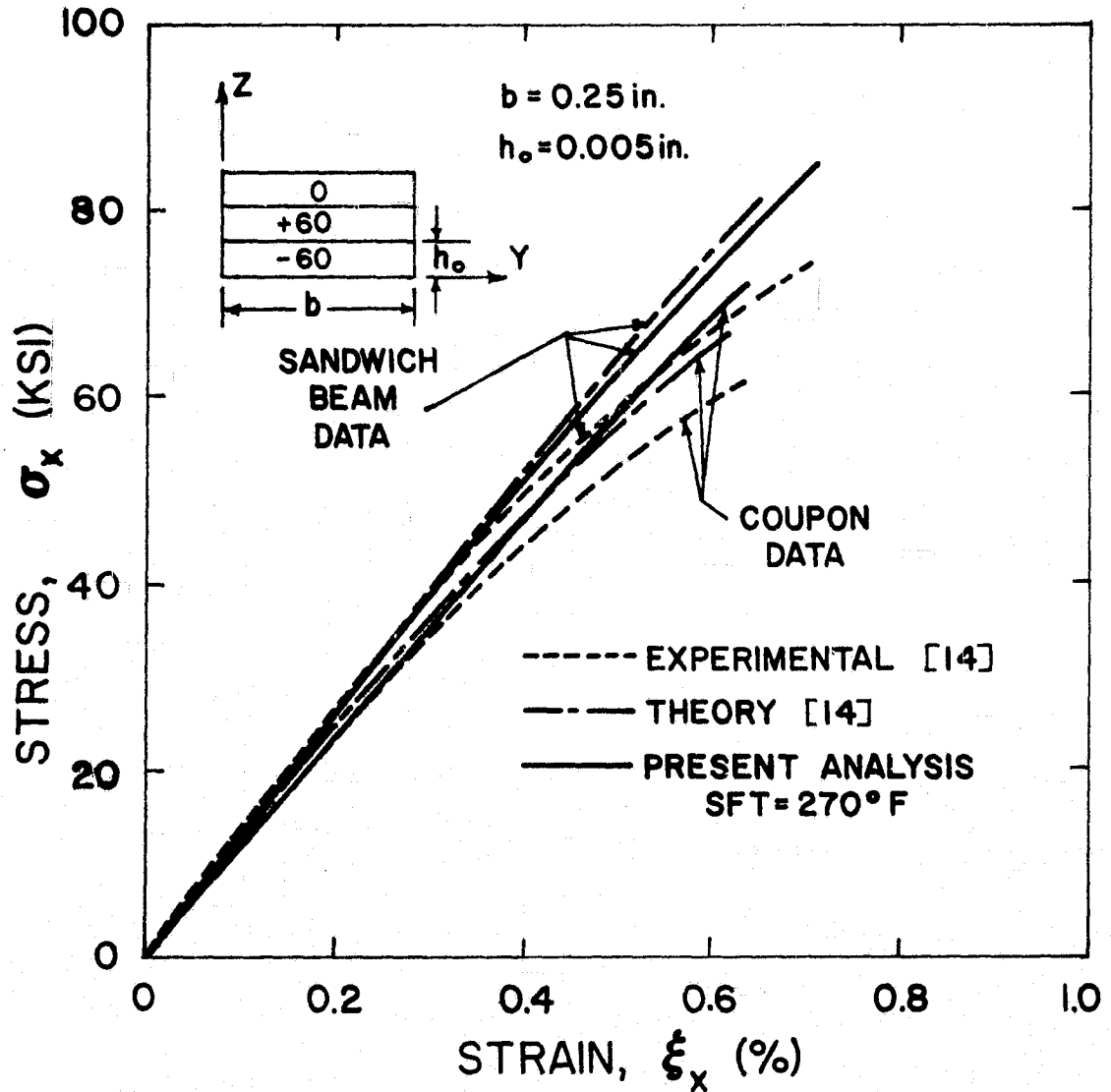
Figure 42. Tensile Stress-Strain Behavior of [0/+60/-60]$_s$ Boron/Epoxy Laminate
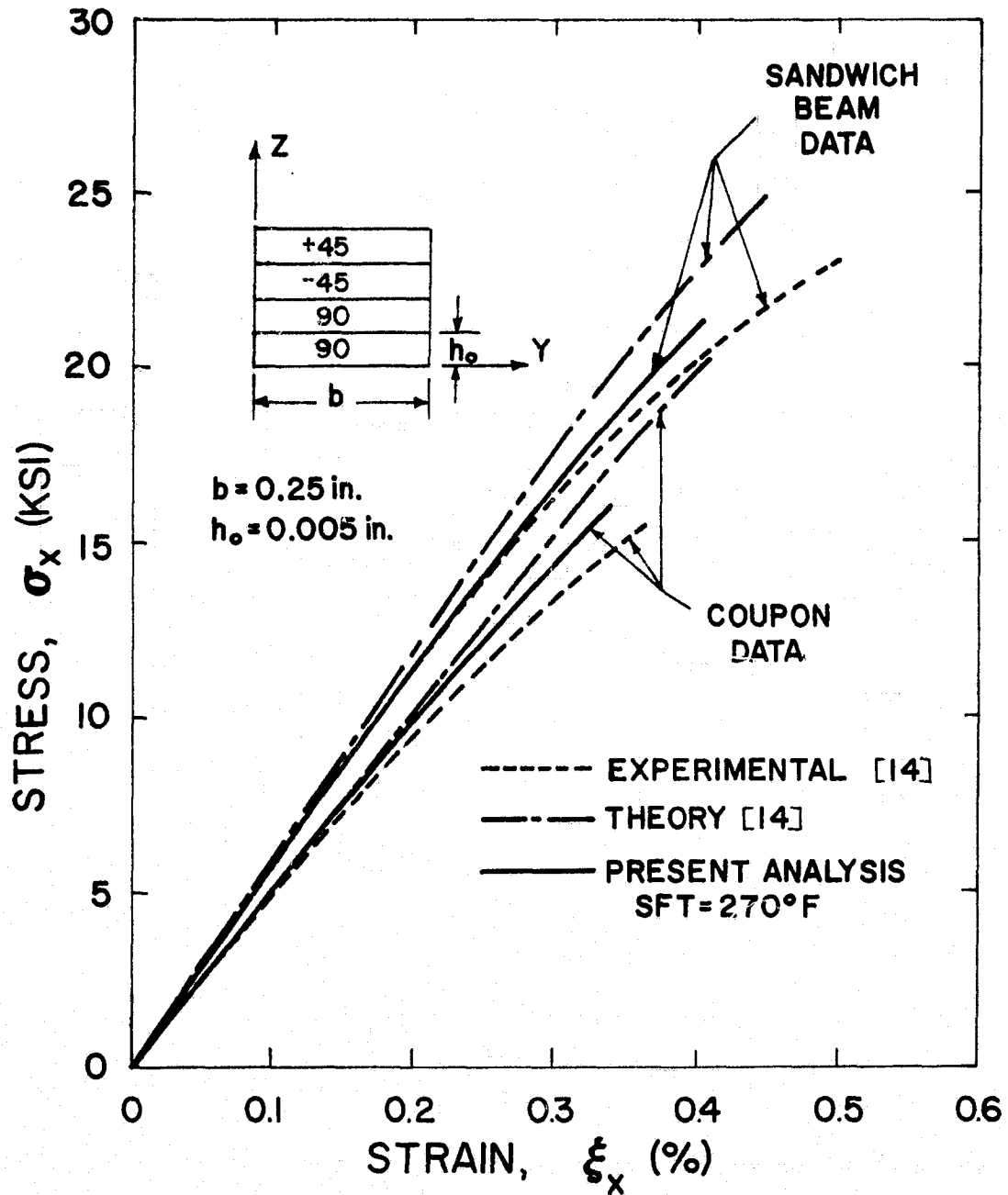
Figure 43. Tensile Stress-Strain Behavior of $[+45/-45/90_2]_s$ Boron/Epoxy Laminate

experienced by the ± 45 degree layers. As indicated in the figure, first ply failure would adequately predict failure for the coupon laminate but the results of the present analysis show that the ± 45 degree layers may support additional load for the sandwich beam laminate. The thermal results of the present analysis also indicated that initial ϵ_2 tensile strain existed in the 90 degree layers which would account for the early ultimate failure based on first-ply failure and the higher degree of nonlinearity.

[+30/-30/90]$_s$ Laminate

The tensile results for this laminate, Fig. 44, show that above 0.7% strain load neither theory predicted the nonlinearity of the experimental curves adequately even though the present analysis was slightly more favorable. The present analysis did predict the ultimate stress quite well when first ply failure was considered.

Laminate failure was observed to occur due to ϵ_2 tensile failure in the 90 degree layer. The lower failure strain exhibited by the present analysis was a result of initial ϵ_2 tensile strain in the 90 degree layer as a result of thermal cooling. A paradox is apparent here in that while a higher value of stress-free temperature would increase the nonlinearity it would decrease the failure strain. The absence of nonlinearity for the present solution cannot be explained at this time.

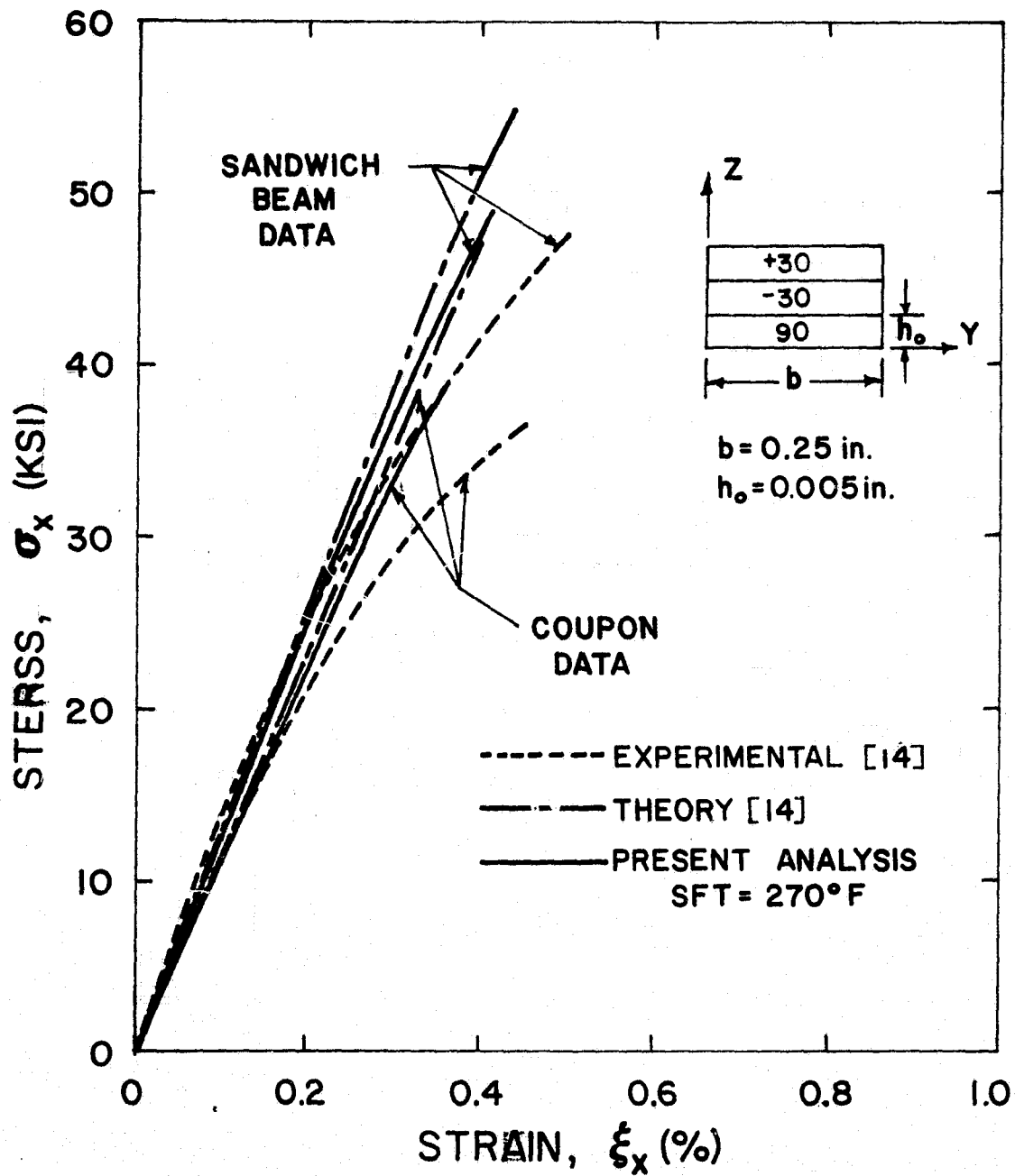Figure 44. Tensile Stress-Strain Behavior of $[+30/-30/90]_s$ Boron/Epoxy Laminate

6.4.2 Progressive Failure for Tensile Loading

The theoretical results of the present analysis as well as the results of References [11, 14, 15] have indicated that when tensile loading of boron/epoxy laminates containing both 0 and 90 degree layers is considered first-ply failure is not sufficient for predicting total laminate failure. The 90 layers usually fail first followed by the 0 degree layers at an increased load level. The progressive failure theory of Section 4.2 was employed in the present analysis for the $[0/90]_s$ and $[0/+45/-45/90]_s$ laminates. It will also be noted that significant edge-effects are present for the latter laminate.

$[0/90]_s$

Figure 45 shows the tensile results for this laminate. All the theories exhibited good agreement up to 0.4% strain. However, the results of the present analysis and the results of Reference [15] underestimated the nonlinearity whereas the results of Reference [11] overestimated the nonlinearity above 0.4% strain load.

The theory of Reference [15] assumed that first fiber failure (ϵ_1) would result in total laminate failure. Thus, the 90 degree stiffness in the loading direction (E_{22}) was not degraded as it failed. The theory of Reference [11] allowed the 90 degree layer to unload after it failed at an applied strain of 0.42%. The 90 degree layer was then assigned an E_{22} value of zero and the laminate was allowed to continue to sustain load until the 0 degree layer failed. The present analysis indicated that the 90 degree layer began to exceed
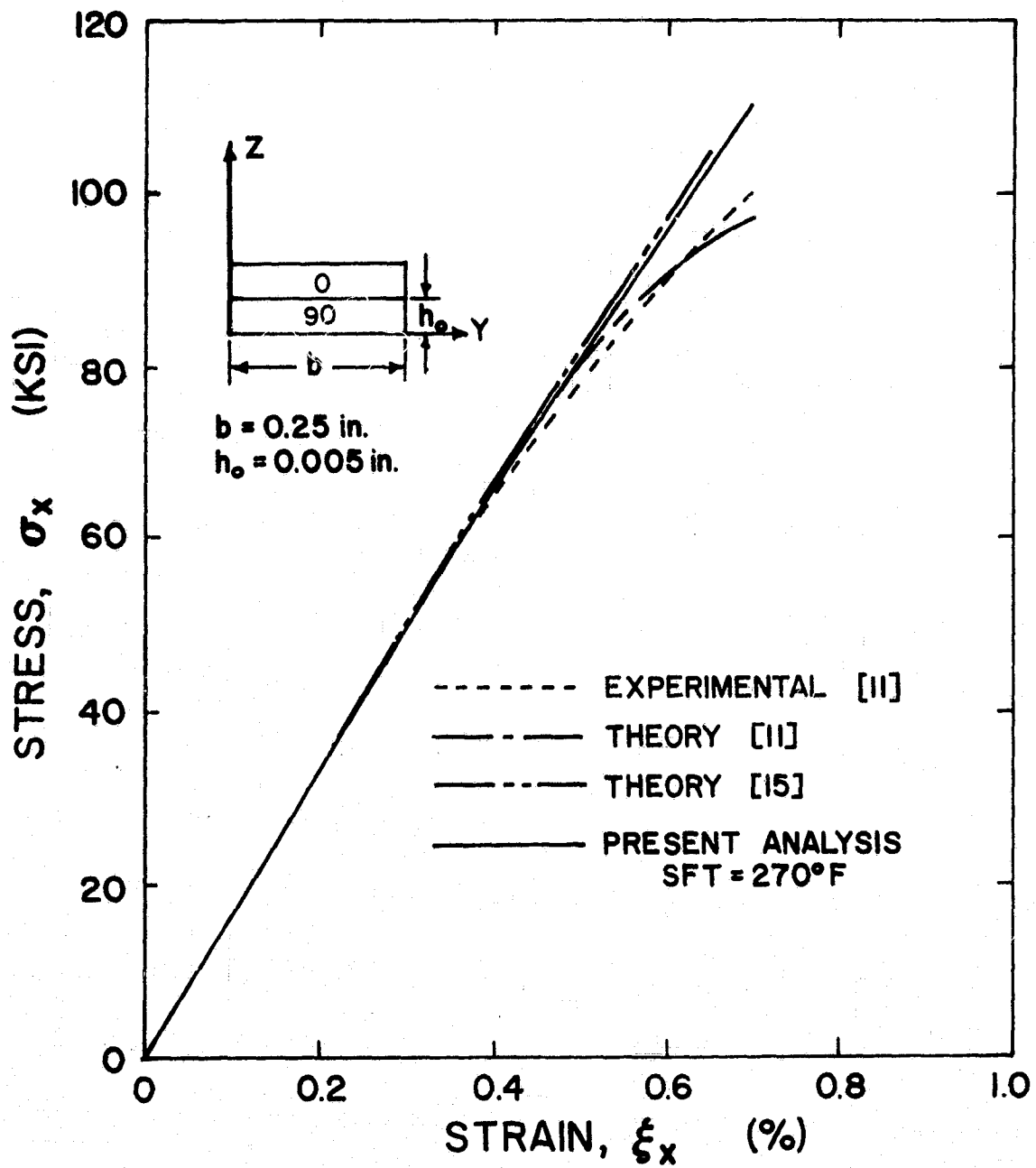
Figure 45. Tensile Stress-Strain Behavior of [0/90]$_s$ Boron/Epoxy Laminate

the ε_2 tensile ultimate at an applied strain of 0.35% (initial ε_2 tensile strain of 0.07% due to thermal loading). Applying the progressive failure theory the 0 degree layer subsequently failed at 0.7% applied strain. For this laminate the stiffness degradation mechanism of the progressive failure theory did not allow enough reduction in stiffness. However, the results obtained by the present analysis accurately predicted the ultimate strain while accounting for total laminate failure.

$[0/+45/-45/90]_s$ Laminate

Figure 46 shows the tensile results for this laminate. The theory of Reference [11] exhibited the best results above 0.3% strain with all theories showing good agreement up to this strain.

The theory of Reference [14] predicted that failure would result from ε_2 tensile failure in the 90 degree layer at a strain of 0.42%. It can be seen from the figure that this first ply failure does not accurately predict the ultimate strength of the laminate. The theory of Reference [11] allowed the 90 degree layer to unload after failure was noted at 0.42% strain. The layer then continued to support additional load with a modulus E_{22} of zero. The present analysis differed from Reference [11] in that failure of the 90 degree layer initiated at 0.35% strain (initial thermal tensile strain for ε_2) and was allowed to support additional load according to the progressive failure theory of Section 4.2. Both the present analysis and the theory of Reference [11] then showed ε_1 tensile failure occurred in the 0 degree layer. The present analysis also showed that considerable
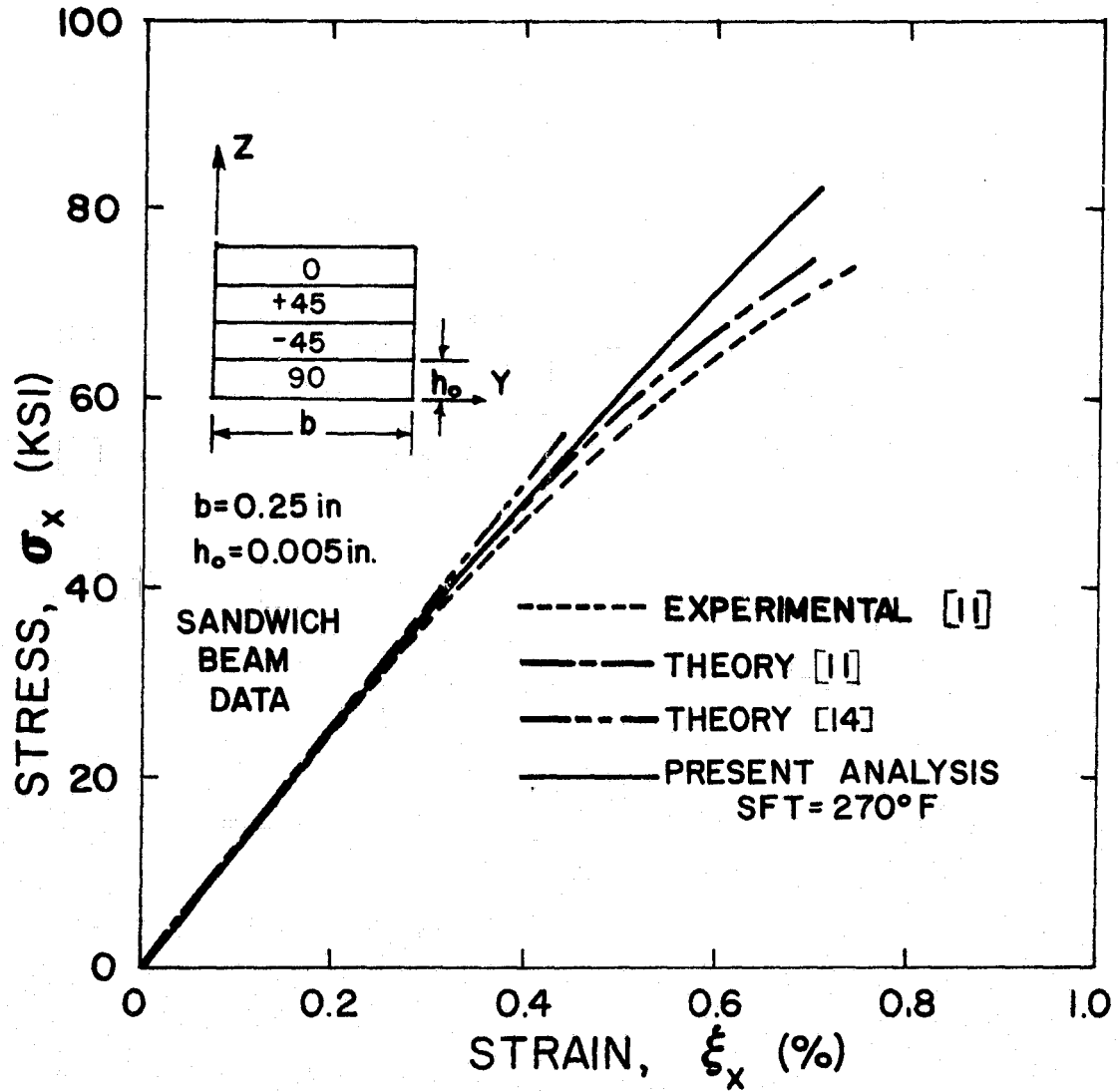
Figure 46. Tensile Stress-Strain Behavior of [0/+45/-45/90]$_s$ Boron/Epoxy Laminate

ε_1 tensile and in-plane shear, γ_{12} existed in the $\pm$ 45 degree layers. Also, the ε_1 tensile strain ratio had reached a value of 1.0 near the free-edge of the $\pm$ 45 degree layers. Thus, while the method of Reference [11] gives better agreement for the nonlinearity due to its greater reduction of stiffness technique, the method cannot show the edge-effects exhibited by the present analysis. These edge-effects give more insight into the failure of this laminate.

6.4.3 Progressive Failure for Compressive Loading

Theoretical results for both the present analysis and the theory of Reference [14] have indicated that first-ply failure theory considerably under-estimates the compressive strength of boron/epoxy laminates which contain an angle-ply laminate in combination with 0 degree layers. The results of applying the progressive failure theory of this investigation for the compression loading of the $[0_2/+45/-45]_s$ and $[0/+60/-60]_s$ laminate showed considerable improvement for the prediction of strength. Also, the theory could account for complete failure of the laminate.

$[0_2/+45/-45]$ Laminate

Figure 47 shows the compressive results for this laminate. The theory of Reference [14] (first-ply failure) considerably under-estimates the strength of the laminate whereas the present analysis with progressive failure exhibits good agreement for both the shape of the curve and the ultimate stress and strain of the laminate.
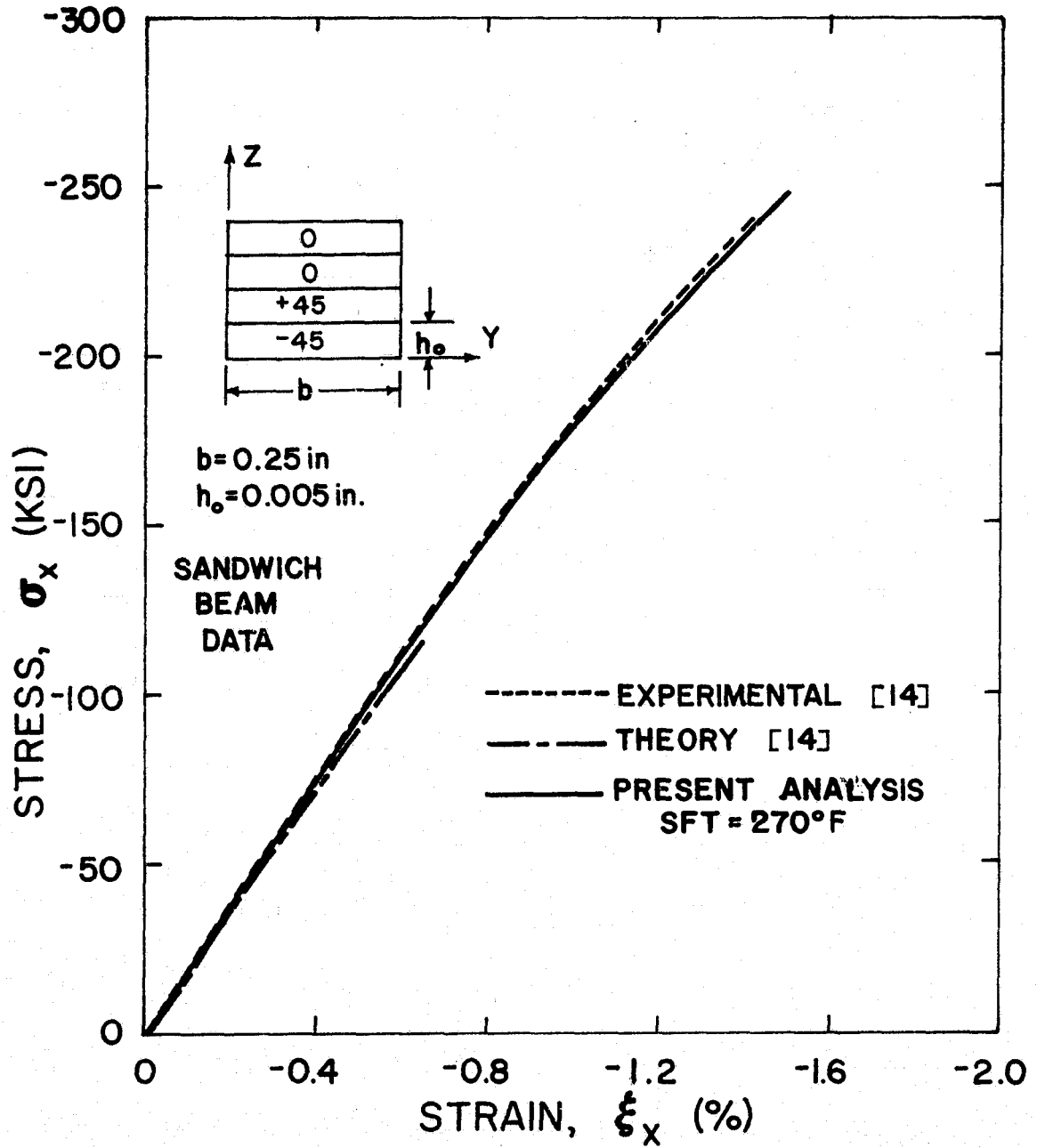
Figure 47. Compressive Stress-Strain Behavior of $[0_2/+45/-45]_s$ Boron/Epoxy Laminate

The theory of Reference [14] predicted that laminate failure was a result of ϵ_2 tensile failure of the 0 degree layers. The results of the present analysis showed that there was an edge-effect in the 0 degree layers with ϵ_2 tensile failure initiating near the free-edge at -0.48% strain with all elements eventually failing (using progressive failure) at a strain of -0.6%. Allowing the laminate to continue to load through progressive failure, the present analysis indicated that ϵ_1 compressive failure began to occur throughout the 0 degree layer at -1.2% strain load. Still allowed to support additional load, the laminate sustained in-plane shear, γ_{12}, failure throughout the ± 45 degree layers at -1.5% strain. Thus, all layers were experiencing failure at -1.5% strain, hence, laminate failure.

It should be noted that since this was a sandwich beam laminate there is honeycomb reinforcement. Thus, the progressive failure theory, while predicting the behavior of this laminate quite well, may actually introduce a similar type reinforcement accounting for the agreement. However, the theory proved to be a viable technique for predicting this laminate behavior in compression.

$[0/+60/-60]_s$ Laminate

The results for the compressive loading of this laminate, Fig. 48, indicate fairly good agreement between both theoretical results and the experimental curve up to -1.0% strain load. The theory of Reference [14] again under-estimates the strength of the laminate. The present analysis, as shown in the figure, does give a more accurate estimation of the ultimate strength of the laminate.
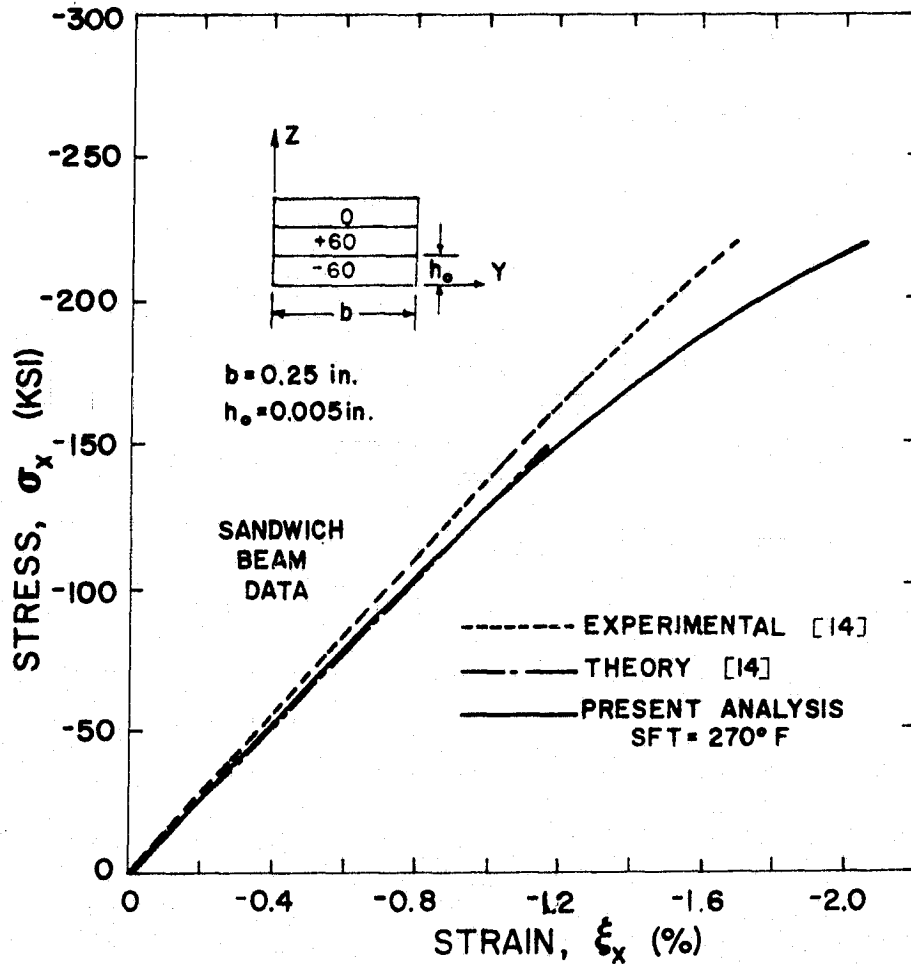
Figure 48. Compressive Stress-Strain Behavior of [0/+60/-60]$_s$
Boron/Epoxy Laminate

The theory of Reference [14] predicted laminate failure was the result of ε_1 compressive failure in the 0 degree layer whereas results of the present analysis indicated that the 0 degree layer was experiencing ε_1 compressive, ε_2 tensile, and ε_3 tensile failures throughout the laminate at an applied strain of -1.1%. Again, employing the progressive failure theory, total laminate failure was exhibited, as shown in the figure, at an applied strain of -2.1% when the ± 60 degree layers failed due to simultaneous ε_3 tensile and in-plane, γ_{12}, shear failure throughout the layers.

As noted for the $[0_2/+45/-45]_s$ case, the progressive failure theory could introduce reinforcement similar to sandwich beam reinforcement. The difference in the curves could be attributed to sandwich beam differences in lamina reinforcement compared to laminate reinforcement, the laminate having more pronounced reinforcement. However, the progressive failure theory gave better results than the theory of Reference [11] for the ultimate strength.

6.4.4 Failure Due to Edge Effects

Theoretical results for both the present analysis and the theory of Reference [14] have indicated that the first ply failure theory substantially over-estimates the laminate strength for compressive loading of boron/epoxy laminates which contain an angle-ply laminate in combination with 90 degree layers. The results of the present analysis indicated that relatively high in-plane strain ratios were present throughout the laminate at the experimentally determined failure strain for the $[+45/-45/90_2]_s$ and $[+30/-30/90]_s$ cases.

However, results also showed that interlaminar strain ratios had attained values of 1.0 near the free-edge of the laminates. It is likely that laminate failure will occur due to these edge-effects and the high in-plane strains. It should be noted that previously the ε_3 (delamination) strain was allowed to be supported for sandwich beam input considerations. However, those cases were for laminates where ε_3 was uniform throughout. Thus, in concentrated form (free-edge) its failure mode may be more significant when acting in conjunction with other interlaminar failure modes.

$[+45/-45/90_2]_s$ Laminate

Figure 49 shows the results for the compressive loading of this laminate. It can be seen that the theory of Reference [14] over-estimates the strength whereas, when edge-effects are considered, the present analysis exhibits excellent agreement between theory and experiment.

The theory of Reference [14] predicted failure due to ε_2 compressive failure of the 90 degree layers. The results of the present analysis indicated that at a strain of -1.25% the laminate was experiencing an ε_2 compressive strain ratio of 0.8 in the 90 degree layers and an in-plane shear strain, γ_{12}, ratio of 0.9 in the ± 45 degree layers. However, the results showed that interlaminar shear strains, γ_{12} and γ_{13}, had attained ratios of 1.0 in ± 45 layer near the free-edge and ε_3 had attained a ratio of 1.0 at the 90 degree and 45 degree interface near the free-edge. The failure of this laminate can be directly attributed to the numerous edge-effects
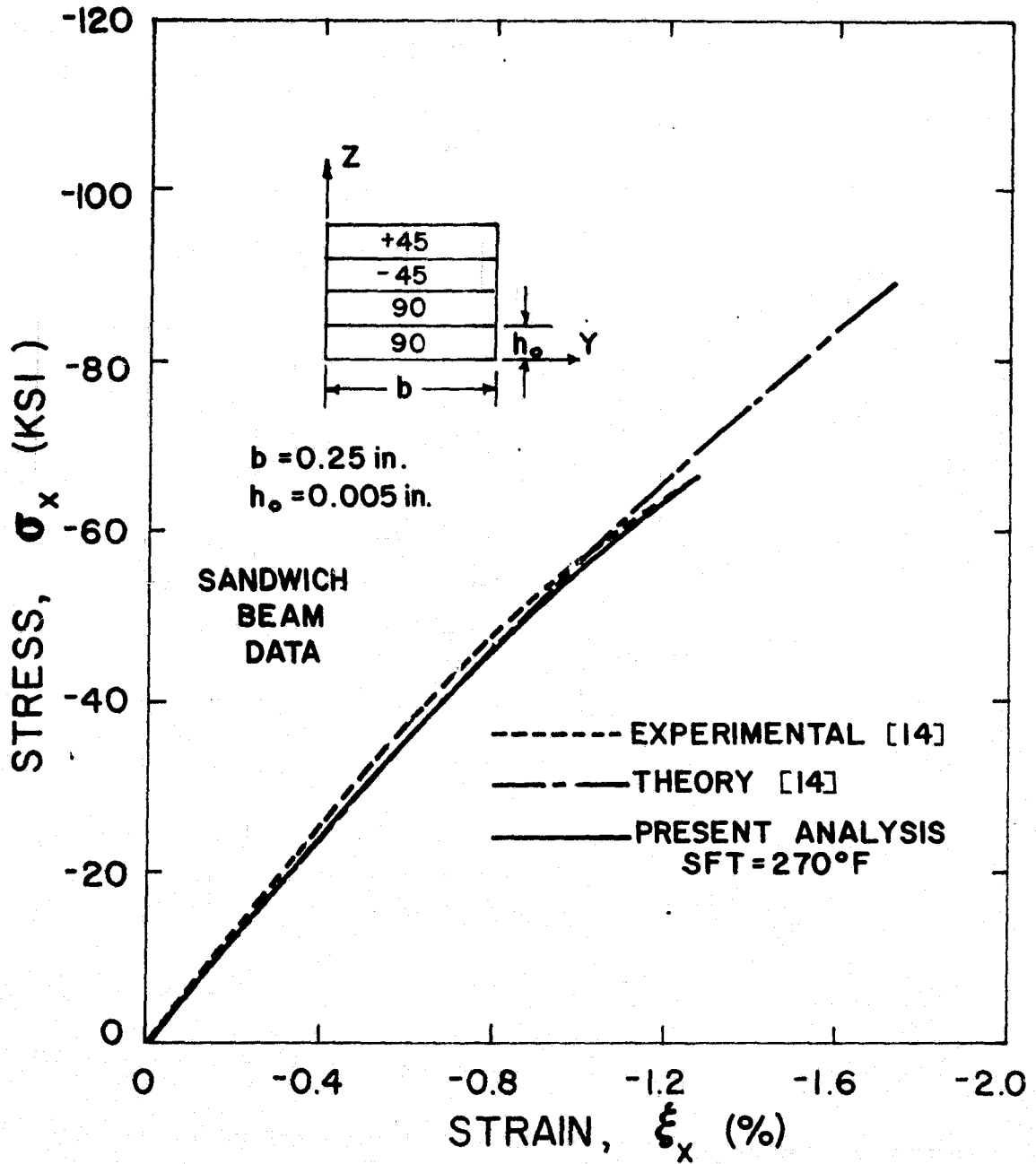
Figure 49. Compressive Stress-Strain Behavior of $[+45/-45/90_2]_s$ Boron/Epoxy Laminate

occurring while high in-plane ratios existed.

$[+30/-30/90]_s$ Laminate

Figure 50 shows the compressive results for this laminate. As indicated in the figure, the theory of Reference [14] considerably over-estimates the laminate strength. When edge effects are considered, the present analysis can accurately predict the laminate strength.

The theory of Reference [14] predicts that laminate failure will result from ε_1 compressive failure in the ± 30 degree layers. The results obtained from the present analysis indicated that at the applied strain of -0.84% numerous strain ratios had attained a value of 1.0 near the free-edge. The ε_2 tensile strain ratios had attained a value of 1.0 near the free-edge in the ± 30 degree layers. A value of 1.0 was also exhibited for the γ_{23} strain ratio at the interfaces near the free-edge. The γ_{13} strain ratio had also reached a value of 1.0 at the ± 30 degree interface at the free-edge. The + 30 degree layers were also experiencing high in-plane, γ_{12}, shear strain with elements at the free-edge attaining 0.75 ratios. The early failure of this laminate in compression can be attributed to these edge-effects. It is interesting to note that the edge-effect was a result of both in-plane and interlaminar strains.

6.5 Stress-Strain Behavior of Two Borsic/Aluminum Laminates

The tensile loading of the $[(0/90)_2]_s$ and $[0/+45/-45]_s$ laminates were studied. Significant differences were noted for the failure
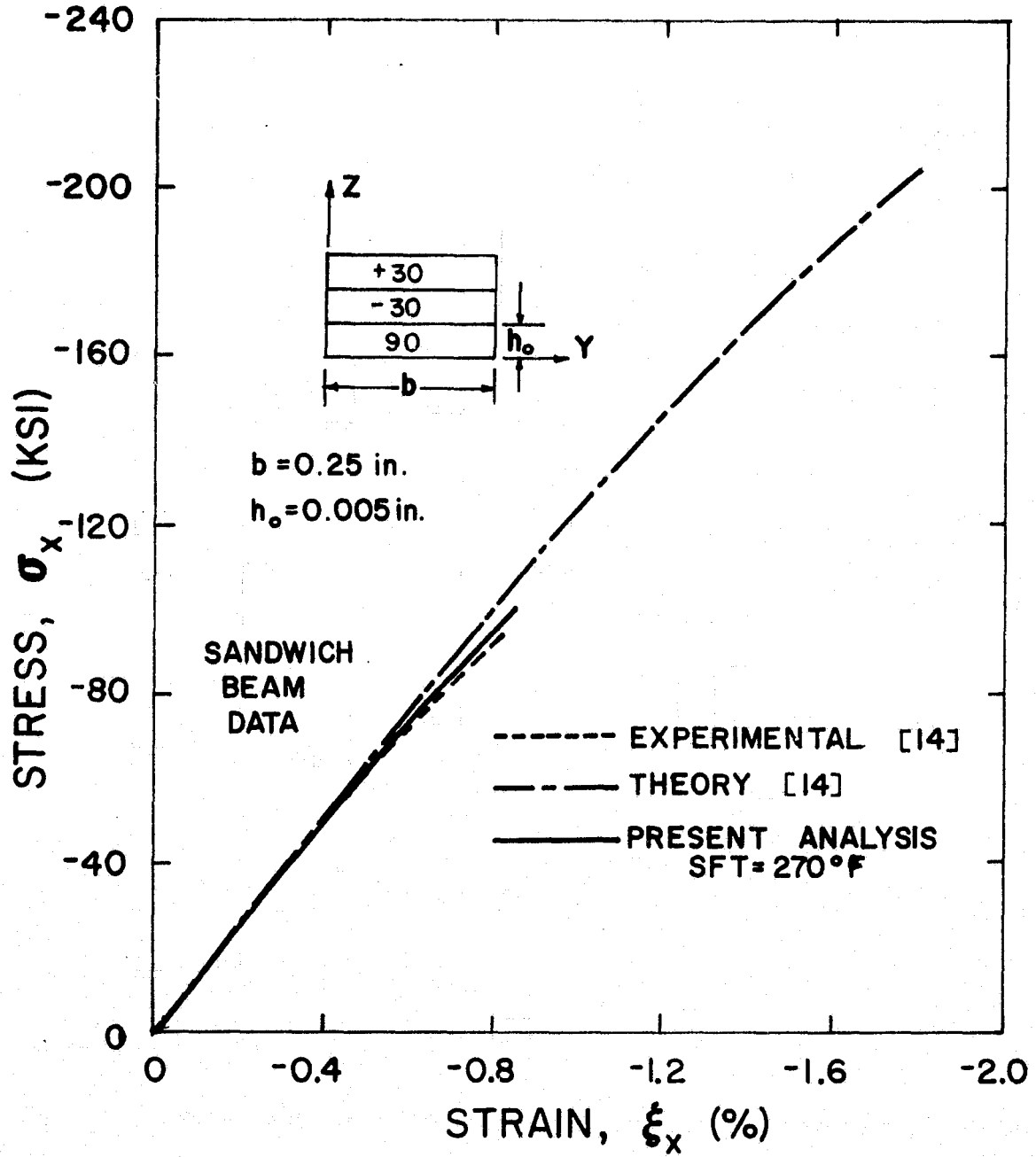
Figure 50. Compressive Stress-Strain Behavior of [+30/-30/90]$_s$ Boron/Epoxy Laminate

modes exhibited for these metal matrix laminates when compared to similar boron/epoxy laminates. Results of this investigation indicated that failure modes are material dependent.

6.5.1 $[(0/90)_2]_s$ Laminate

Tensile results for this laminate are shown in Figure 51. As indicated in the figure, the present analysis showed good agreement with experiment for the initial part of the curve. By noting Figure B-5 in Appendix B it can be seen that the tensile lamina stress-strain curve for 90 degree fiber orientation exhibits high non-linearity at 0.2% strain. The present analysis predicted an initial tensile ε_2 strain in the 90 layer of 0.1% which can account for the early knee exhibited by the experimental curve at 0.1%. It is believed that the results indicate that the high nonlinearity that would be present at 0.1% strain cannot be sufficiently accounted for using the present method of analysis even for relatively small load increments. It may also be possible that input data did not give a good approximation of the nonlinear behavior in the 90 degree direction. However, the results gave a fairly good representation of the stress-strain behavior.

The present analysis indicated that simultaneous failure occurred in all layers. The 90 degree layers exhibited ε_2 tensile failure whereas the 0 degree layers exhibited ε_1 tensile failure. The individual failure modes were identical to those sustained by the cross-ply boron/epoxy laminate. However, in the boron/epoxy laminate, the 90 degree layer began to fail much earlier than the 0 degree layer.
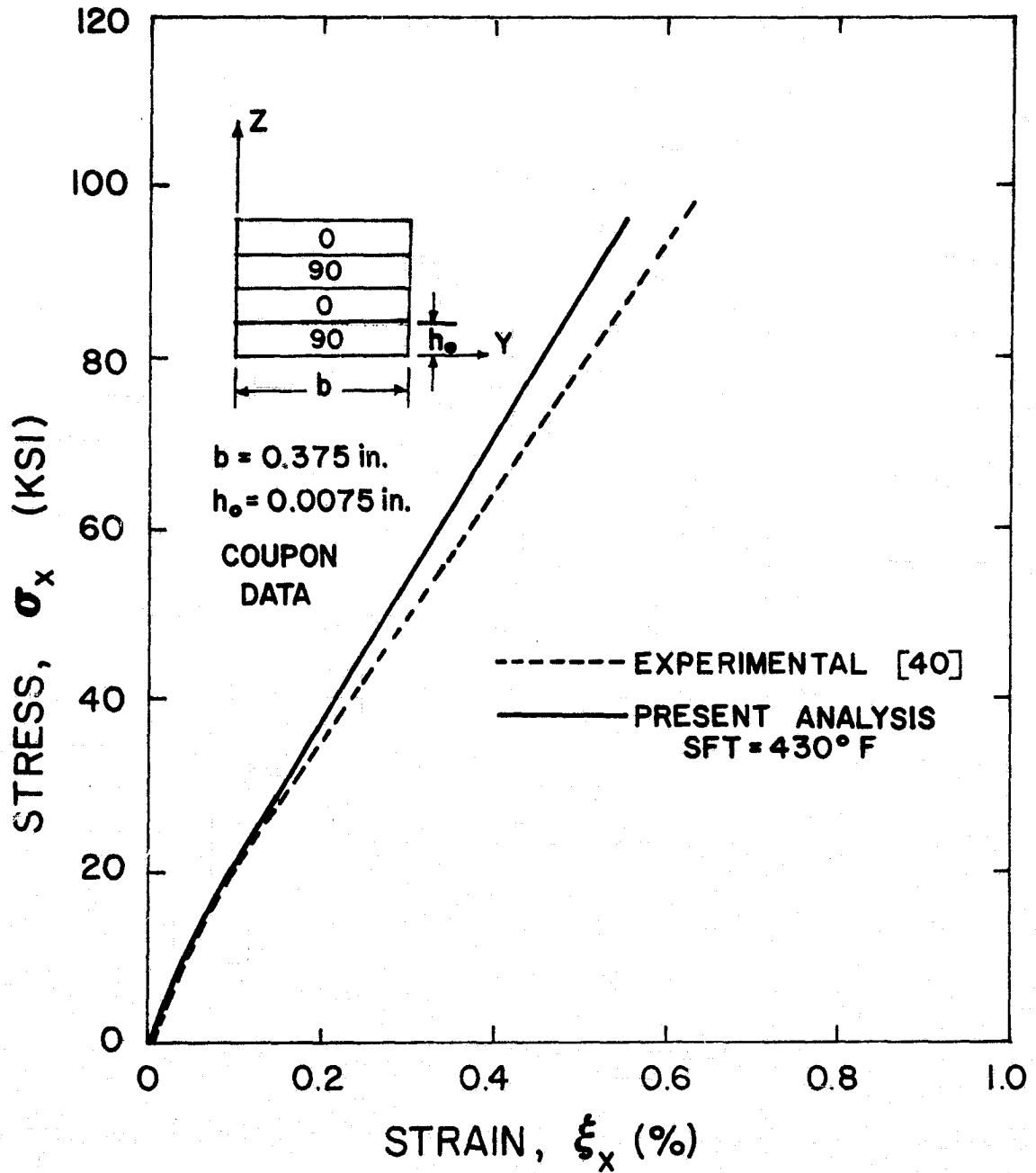
Figure 51. Tensile Stress-Strain Behavior of $[(0/90)_2]_s$ Borsic/ Aluminum Laminate

6.5.2 $[0/+45/-45]_S$ Laminate

Tensile results, Fig. 52, for this laminate exhibited agreement between experiment and the present analysis up to 0.2% strain. It is believed that the difference between the curves was a result of using tensile coupon shear data from Reference [41] due to the lack of such results in Reference [40] from which the experimental $[0/+45/-45]_S$ curve was taken.

The present analysis showed that the 0 degree layer would begin to sustain ε_1 tensile failure at an applied strain of 0.48% followed by ε_1 tensile failure in the 45 degree layers at an applied strain of 0.72%. Thus, the 45 degree layers can still support load even after the 0 degree layer begins to fail. This was not the case for the $[0_2/+45/-45]_S$ boron/epoxy laminate. It is interesting to note that for a relatively small stress-free temperature of 430°F (compared to 1000°F cure temperature) the 45 degree layers had attained an ε_1 tensile strain ratio of 0.75.

Figure 52. Tensile Stress-Strain Behavior of [0/+45/-45]$_s$ Borsic/ Aluminum Laminate
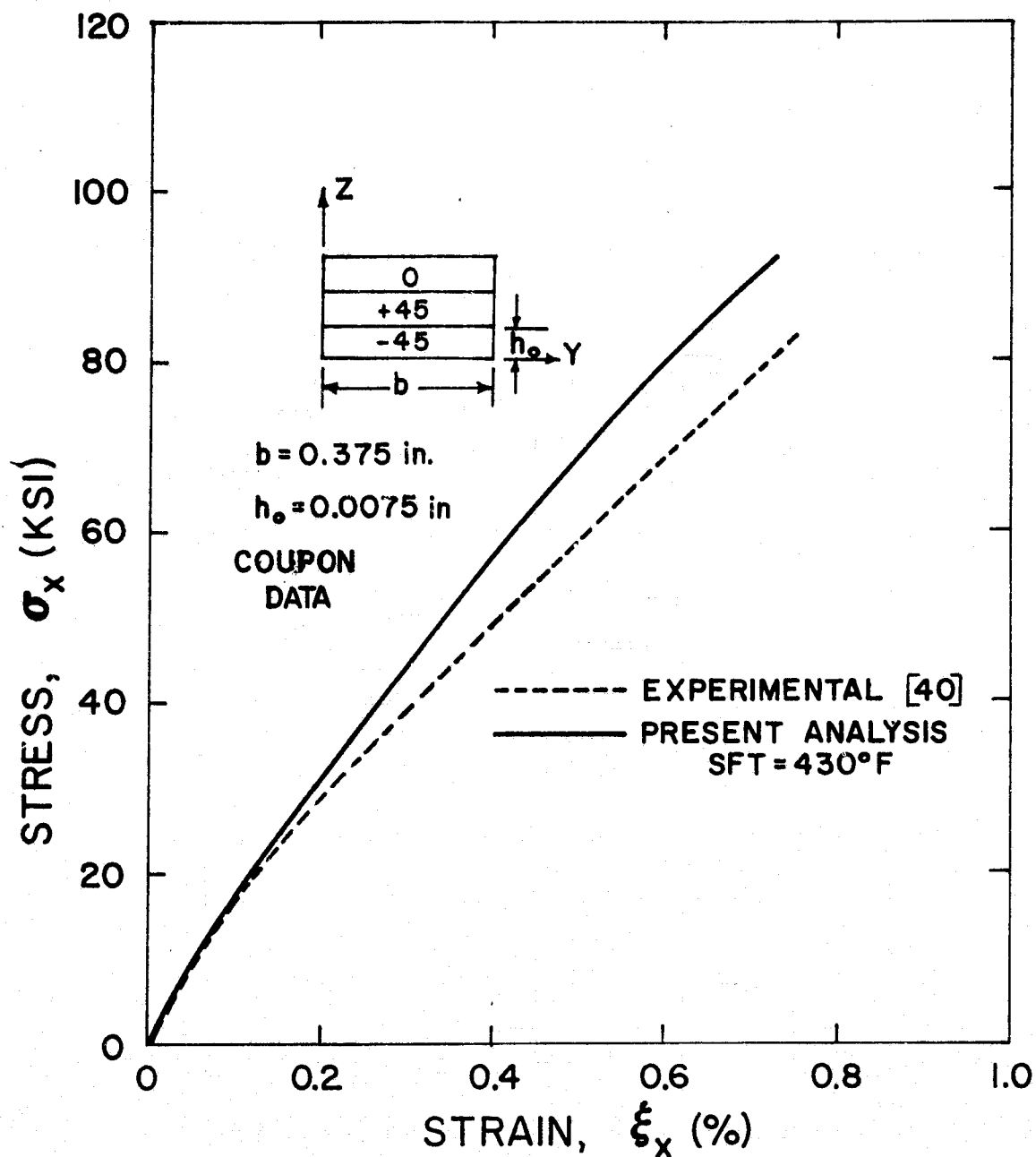
Chapter 7

SUMMARY AND CONCLUSIONS

The present investigation has been concerned with the nonlinear behavior of laminated fibrous composites including thermal effects, temperature dependent properties, and edge-effects. The results of the present study show that such considerations are important to the prediction of failure modes in composite laminates. The present study also shows that laminate failure is a function of the laminate configuration, material, and the type of loading.

In summary of the achievements of this study the following conclusions can be made.

1. Thermal effects influence the strength of laminates. The inclusion of thermal effects results in improved predictions for laminate stress-strain behavior. The thermal effect may be to either increase or decrease the range of strain for uniaxial loading.

2. Edge effects can cause total laminate failure. More accurate prediction of laminate strength can be obtained if edge-effects are considered.

3. Angle ply laminates fail as a result of in-plane strains exceeding maximum values. A material principal strain failure criteria adequately predicts failure of such laminates.

4. The mode of failure in angle-ply laminates under tensile loading is dependent on fiber orientation and matrix material. The mode of failure in angle-ply laminates under compressive loading is dependent on fiber orientation but essentially independent of matrix material.

5. The mode of failure for cross/ply laminates is matrix material dependent. For boron/epoxy laminates the 90 degree plies fail substantially below the ultimate strength whereas borsic/aluminum laminates exhibited simultaneous failure of 0 degree and 90 degree plies.

6. The mode of failure for boron/epoxy angle-plies in combination with 0 and/or 90 degree layers can be predicted according to specific failure criteria.

    a. The first ply theory adequately predicts failure for tensile loading of angle-plies in combination with 0 or 90 degree plies.

    b. The progressive failure theory adequately predicts failure for the tensile loading when both 0 and 90 degree plies are combined with angle-plies.

    c. The progressive failure theory adequately predicts failure for compressive loading of angle-plies combined with 0 degree plies.

    d. Failure of laminates consisting of angle-plies and 90 degree plies which are subjected to compressive loading is due to edge-effects.

7. The mode of failure for tensile loaded borsic/aluminum laminates containing 0 degree layers in combination with angle-plies can be adequately predicted using progressive failure.

8. For angle-ply laminates, the fiber orientation for the maximum interlaminar stresses due to mechanical loading is matrix material dependent whereas the maximum interlaminar stresses due to thermal loading are independent of the matrix materials. The interlaminar thermal stresses in angle-ply laminates are of opposite sign to the stresses due to mechanical loading.

9. The combined nonlinear thermal and mechanical analysis exhibits significant differences from the linear elastic predictions for interlaminar stresses. For cross-ply laminates the linear elastic solution (free of thermal effects) under-estimates the magnitude of the stresses whereas for angle-ply laminates the linear elastic solution (free of thermal effects) considerably over-estimates the stresses.

10. Ramberg-Osgood approximations and percent retention data are adequate means of representing material behavior.

The present investigation has also shown that future research is warrented in the following areas:

1. Experimental verification of laminate failure due to edge effects.

2. Determination of reliable sandwich beam and coupon data.

3. A more accurate representation of strain unloading.

4. A reliable determination of stress-free temperatures.

BIBLIOGRAPHY

1. C. B. Smith, "Some New Types of Orthotropic Plates Laminated of Orthotropic Material," J. Appl. Mech., Vol. 20, 1953, 286-288.

2. E. Reissner and Y. Stavsky, "Bending and Stretching of Certain Types of Heterogeneous Aeolotropic Elastic Plates," J. Appl. Mech., Vol. 28, 1961, 402-408.

3. J. E. Ashton, J. C. Halpin, and P. H. Petit, Primer on Composite Materials: Analysis, Technomic Pub. Co., Stamford, Conn., 1969.

4. J. E. Ashton and J. M. Whitney, Theory of Laminated Plates, Technomic Pub. Co., Stamford, Conn., 1970.

5. S. W. Tsai, "Structual Behavior of Composite Materials," NASA CR-71, July, 1964.

6. V. D. Azzi and S. W. Tsai, "Elastic Moduli of Laminated Anisotropic Composites," Exp. Mech., Vol. 5, 1965, 177-185.

7. V. D. Azzi and S. W. Tsai, "Anisotropic Strength of Composites," Exp. Mech., Vol. 5, 1965, 283-288.

8. R. Hill, The Mathematical Theory of Plasticity, Oxford University Press, 1950.

9. S. W. Tsai, "Strength Characteristics of Composite Materials," NASA CR-224, April, 1965.

10. O. Hoffman, "The Brittle Strength of Orthotropic Materials," J. Comp. Mat., Vol. 1, 1967, 200-207.

11. P. H. Petit and M. E. Waddoups, "A Method of Predicting the Non-linear Behavior of Laminated Composites," J. Comp. Mat., Vol. 3, 1969, 2-19.

12. S. W. Tsai and E. M. Wu, "A General Theory of Strength for Anisotropic Materials," J. Comp. Mat., Vol. 5, 1971, 58-80.

13. K. D. Chiu, "Ultimate Strengths of Laminated Composites," J. Comp. Mat., Vol. 3, 1969, 578-582.

14. B. E. Kaminski, G. H. Lemon, and E. L. McKague, "Development of Engineering Data for Advanced Composite Materials," AFML-TR-70-108, 1972.

15. Z. Hashin, D. Bagchi, and B. W. Rosen, "Non-linear Behavior of Fiber Composite Laminates," NASA CR, NAS1-11284, September, 1973.

16. W. Ramberg and W. B. Osgood, "Description of Stress-Strain Curves by Three Parameters," NASA TN 902, 1943.

17. R. S. Sandhu, "Ultimate Strength Analysis of Symmetric Laminates," Technical Report AFFDL-TR-73-137, February, 1974.

18. H. T. Hahn and S. W. Tsai, "On the Behavior of Composite Laminates After Initial Failures," J. Comp. Mat., Vol. 8, 1974, 288-305.

19. H. T. Hahn and N. J. Pagano, "Curing Stresses in Composite Laminates," J. Comp. Mat., Vol. 9, 1975, 91-106.

20. R. L. Foye, "Inelastic Micromechanics of Curings Stresses in Composites," Inelastic Behavior of Composite Materials, presented at the 1975 ASME Winter Annual Meeting, 1975.

21. N. J. Pagano and R. B. Pipes, "The Influence of Stacking Sequence on Laminate Strength," J. Comp. Mat., Vol. 5, 1971, 50-57.

22. R. B. Pipes and N. J. Pagano, "Interlaminar Stresses in Composite Laminates Under Uniform Axial Extension," J. Comp. Mat., Vol. 4, 1970, 538-548.

23. R. B. Pipes, B. E. Kaminski, and N. J. Pagano, "The Influence of the Free-edge Upon the Strength of Angle-ply Laminates," ASTM, STP-521, The Test Methods for High Modulus Fibers and Composites, 1972, 218-228.

24. R. B. Pipes, "Interlaminar Stresses in Composite Laminates," Technical Report AFML-TR-72-18, May, 1972.

25. G. Isakson and A. Levy, "Finite-Element Analysis of Interlaminar Shear in Fibrous Composites," J. Comp. Mat., Vol. 5, 1971, 273-276.

26. A. H. Puppo and H. A. Evensen, "Interlaminar Shear in Laminated Composites Under Generalized Plane Stress," J. Comp. Mat., Vol. 4, 1970, 204-220.

27. A. Levy, H. Armen, Jr., and J. Whiteside, "Elastic and Plastic Interlaminar Shear Deformation in Laminated Composites Under Generalized Plane Stress," Third Air Force Conference on Matrix Methods in Structural Mechanics, Wright-Patterson Air Force Base, Ohio, October, 1971.

28. C. T. Herakovich and E. W. Brooks, Jr., "Tensile Strength Behavior of Composite Reinforced Metals," Final Report, VPI&SU Report VPI-E-73-5, January, 1973.

29. R. L. Foye and D. J. Baker, "Design/Analysis Methods for Advanced Composite Structures," AFML-TR-70-299, Vol. 1, February, 1971.

30. E. F. Rybicki, "Approximate Three-Dimensional Solutions for Symmetric Laminates Under Inplane Loading," J. Comp. Mat., Vol. 5, July, 1971, 354-360.

31. C. T. Herakovich, "On Thermal Edge Effects in Composite Laminates," Int. J. Mech. Sci., (In Press).

32. N. J. Pagano, "On the Calculation of Interlaminar Normal Stress in Composite Laminate," J. Comp. Mat., Vol. 8, 1974, 65-81.

33. S. Tang and A. Levy, "A Boundary Layer Theory - Part II: Extension of Laminated Finite Strip," J. Comp. Mat., Vol. 9, 1975, 42-52.

34. P. W. Hsu, "Interlaminar Stresses in Composite Laminates--A Perturbation Analysis," Ph.D. Thesis, VPI&SU, January, 1976.

35. S. G. Lekhnitskii, Theory of Elasticity of an Anisotropic Elastic Body, Holden-Day, Inc., San Francisco, 1963.

36. R. B. Pipes and I. M. Daniel, "Moire Analysis of the Interlaminar Shear Edge Effect in Laminated Composites," J. Comp. Mat., Vol. 5, 1971, 225-259.

37. M. Renieri, "Rate and Time Dependent Behavior of Structural Adhesives," Ph.D. Thesis, VPI&SU, April, 1976.

38. S. Oken and R. R. June, "Analytical and Experimental Investigation of Aircraft Metal Structures Reinforced with Filamentary Composites, Phase I--Concept Development and Feasibility," NASA CR-1859, December, 1971.

39. S. W. Tsai and H. T. Hahn, "Failure Analysis of Composite Materials," Inelastic Behavior of Composite Laminates, presented at the 1975 ASME Winter Annual Meeting, 1975.

40. C. N. Viswanathan, "Tensile and Compressive Behavior of Borsic/ Aluminum Composite Laminates," Ph.D. Thesis, VPI&SU, June, 1975.

41. Advanced Composites Design Guide, AFML, Wright-Patterson Air Force Base, Ohio, CN-F33615-71-C-1362.

42. K. E. Hofer, Jr., N. Rao, and D. Larsen, "Development of Engineering Data on the Mechanical and Physical Propert'~ of Advanced Composite Materials," AFML-TR-72-205, Part II, February, 1974.

43. J. Suhara and J. Fukuda, "Automatic Mesh Generation for Finite Element Analysis," Ad. Comp. Meth. Struct. Mech. Design, UAH Press, Univ. of Alabama, Huntsville, Ala., 1972.

44. C. O. Frederick, Y. C. Wong, and F. W. Edge, "Two Dimensional Automatic Mesh Generation for Structural Analysis," Int. J. Numer. Meth. Eng., Vol. 2, 1970.

45. J. M. Boisserie, "Generation of Two- and Three-Dimensional Finite Elements," Int. J. Numer. Meth. Eng., Vol. 3, 1971, 327-347.

46. O. C. Zienkiewicz and D. V. Phillips, "An Automatic Mesh Generation Scheme for Plane and Curved Surfaces by 'Isoparametric' Co-ordinates," Int. J. Numer. Meth. Eng., Vol. 3, 1971, 519-528.

47. F. A. Akyuz, "Natural Coordinate Systems--An Automatic Input Data Generation Scheme for a Finite-Element Method," Nuc. Eng. and Design, Vol. 11, 1970.

48. B. K. Neale, "A Finite Element Mesh Generation Program for Arbitrary Two- and Three-Dimensional Structures," 2nd Int. Conf. Struc. Mech. in Reac. Tech., Vol. 5, M4/5, 1973.

49. F. A. Ambartsumyan, Theory of Anisotropic Plates, translated from Russian by T. Cheron and edited by J. E. Ashton, Technomic. Publishing Co., Stamford, Conn., 1969.

50. A. Mendelson, Plasticity: Theory and Application, MacMillian Co., New York, 1968.

51. L. M. Kachanov, Foundations of the Theory of Plasticity, North-Holland Pub. Co., London, 1971.

52. R. M. Christensen, Theory of Viscoelasticity--An Introduction, Academic Press, Inc., New York, 1971.

53. W. Flugge, Viscoelasticity, Blaisdell Pub. Co., Waltham, Mass., 1967.

54. O. C. Zienkiewicz, The Finite Element Method in Engineering Science, McGraw-Hill, London, 1971.

55. E. A. Thornton and K. H. Murray, Fundamentals of the Finite Element Method (Prepared course notes), Old Dominion University, Virginia.

56. L. R. Calcote, The Analysis of Laminated Composite Structures, Van Nostrand Reinhold Co., New York, 1969.

57. C. S. Desai and John F. Abel, Introduction to the Finite Element Method, Van Nostrand Reinhold Co., New York, 1972.

58. H. T. Hahn and S. W. Tsai, "Nonlinear Elastic Behavior of Uni-directional Composite Laminae," J. Comp. Mat., Vol. 7, 1973, 102-118.

59. H. T. Hahn, "Nonlinear Behavior of Laminated Composites," J. Comp. Mat., Vol. 7, 1973, 257-271.

60. R. L. Foye, "Theoretical Post-Yielding Behavior of Composite Laminates - Part I--Inelastic Micromechanics," J. Comp. Mat., Vol. 7, 1973, 48-61.

61. R. L. Foye, "Theoretical Post-Yielding Behavior of Composite Laminates - Part II--Inelastic Macromechanics," J. Comp. Mat., Vol. 7, 1973, 310-319.

62. R. C. Reuter, Jr., "Concise Property Transformation Relations for Anisotropic Lamina," J. Comp. Mat., Vol. 5, 1971, 270-272.

63. G. P. Sendeckyj, "Cross-Ply Laminates," J. Comp. Mat., Vol. 6, 1972, 160-163.

64. R. L. Sierakowski and I. K. Ebcioglu, "On Interlaminar Shear Stresses in Composites," J. Comp. Mat., Vol. 4, 1970, 144-149.

65. G. J. Dvorak, M. S. M. Rao, and J. Q. Tarn, "Yielding in Uni-directional Composites Under External Loads and Temperature Changes," J. Comp. Mat., Vol. 7, 1973, 194-216.

APPENDIX A

FINITE ELEMENT MESH GENERATION AND ELEMENTAL

STIFFNESS MATRIX

A.1 Mesh Generation

Sophisticated two- and three-dimensional mesh generation schemes have been developed for the finite element method [43-48]. The methods basically involve data generation of nodes so as to eliminate excessive input data. A mesh generator was devised for the present analysis which requires limited initial discretization by the investigator.

The principle of the mesh generator is that of subdividing initial triangular elements into four elements. The new elements are uniquely renumbered by assigning the center new element the number n + 1 where n = 0, 4, 8, 12, ..., and then, depending on the sequence of initial data, numbers the surrounding three elements n + 2, n + 3, n + 4, in a counterclockwise fashion. The subdivision mechanism can be utilized for any number of subdivisions depending on the dimensions available in the computer program. A plotting capability was incorporated into the program to allow immediate recognition of the orientation of the newly generated mesh. This was ideally accomplished by having the plotter write the numbers of the new elements in the center of each element, respectively.

The element nodes are also renumbered in a logical fashion and a corresponding plot of the elements with numbers at the nodes can

144

be obtained.

A.2 Elemental Stiffness Matrix

Equation A.1 is the elemental stiffness matrix for prescribed strain loading. Equation A.2 is the elemental stiffness for average force loading.

$$
\begin{bmatrix} \text{SEE MATRIX} \\ \text{ENCLOSED BY} \\ \text{DASHED PORTION} \\ \text{ON NEXT PAGE} \\ 9 \times 9 \end{bmatrix}_K
\begin{bmatrix} u_1 \\ u_2 \\ u_3 \\ v_1 \\ v_2 \\ v_3 \\ w_1 \\ w_2 \\ w_3 \end{bmatrix}
+ \xi_x
\begin{bmatrix} C_{16}a \\ C_{16}c \\ C_{16}e \\ C_{12}a \\ C_{12}c \\ C_{12}e \\ C_{13}b \\ C_{13}d \\ C_{13}g \end{bmatrix}_K
=
\begin{bmatrix} f_{1x} \\ f_{2x} \\ f_{3x} \\ f_{1y} \\ f_{2y} \\ f_{3y} \\ f_{1z} \\ f_{2z} \\ f_{3z} \end{bmatrix}_K
\qquad (A.1)
$$

$$\frac{1}{\bar{A}_K} \left[\text{SYMMETRIC matrix} \right] \{u\} - \{r\} = \{e\} \tag{A.2}$$

APPENDIX B

MATERIAL DATA AND RAMBERG-OSGOOD APPROXIMATIONS

This appendix presents a description of the stress-strain as well as the thermal data used in the present analysis. Ramberg-Osgood [16] approximations were used to represent nonlinear lamina stress-strain curves. The following is a description of the method used to obtain the Ramberg-Osgood coefficients.

Noting Fig. B-1 the curve is assumed to have the form

$$\varepsilon = \varepsilon_E + \varepsilon_I = \frac{\sigma}{E_e} + K\sigma^n \tag{B.1}$$

where ε_E and ε_I are the elastic and inelastic strains, respectively, E_e is the constant elastic modulus, and K and n are the Ramberg-Osgood coefficients. Appropriate components of stress and strain and modulus are used in Eq. (B.1) for normal or shear behavior. A log (ε_I) - log (σ) plot for an arbitrary number of data points above the elastic limit stress, σ^e, will yield results typified by Fig. B-2. The bilinearity shown may not be present.

A least squares fit is performed on each segment of the bilinear data and respective values of K and n are determined. The value of the stress at which the segments intersect, σ^*, can be determined from

$$K_1(\sigma^*)^{n_1} = K_2(\sigma^*)^{n_2} \tag{B.2}$$

or

$$\sigma^* = (K_1/K_2)^{(n_1 - n_2)} \tag{B.3}$$

147
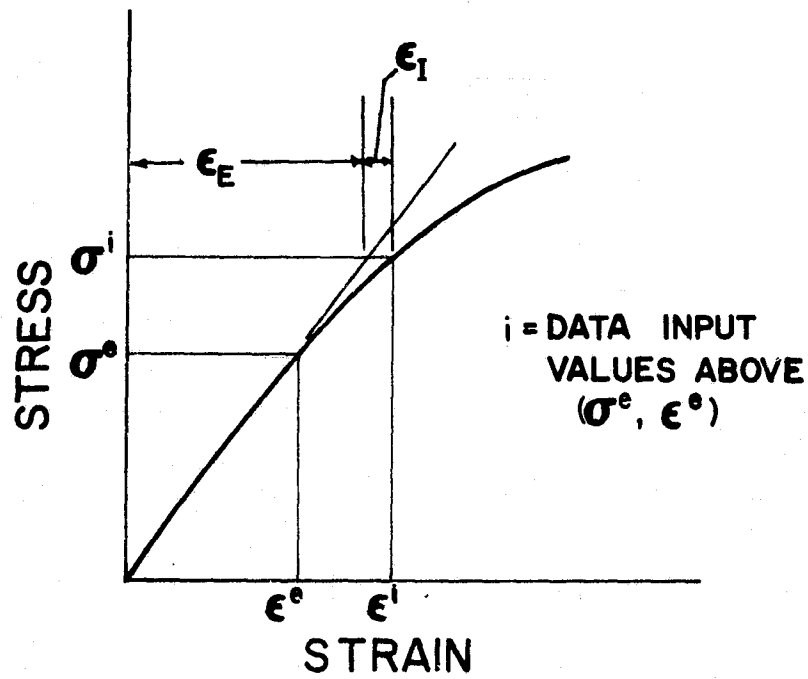
Figure B-1. Typical Nonlinear Stress-Strain Curve
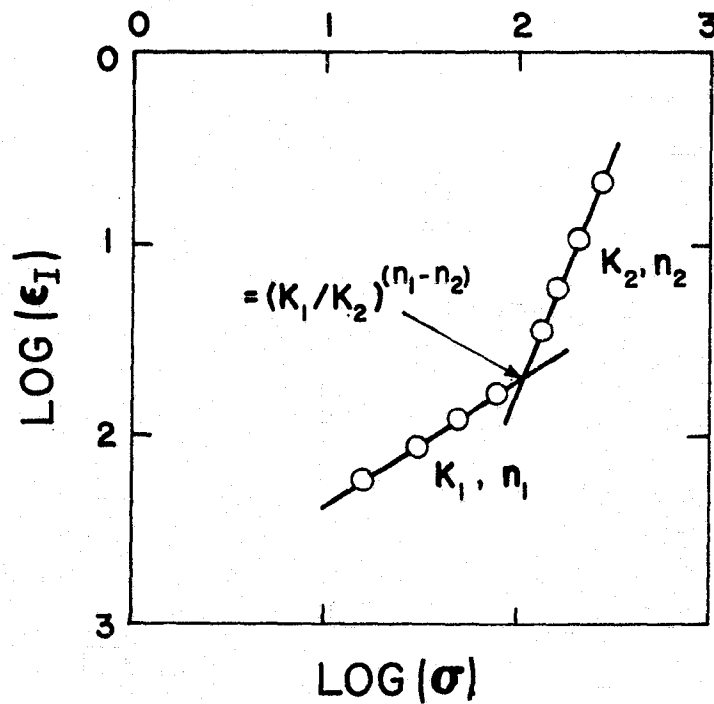
Figure B-2. Typical Log (ϵ_I) - Log (σ) Curve

Differentiating Eq. (B.1), the modulus, $\bar{E}$, for an arbitrary value of σ becomes

$$\bar{E} = \frac{d\sigma}{d\varepsilon} = \frac{E_e}{KE_e n\sigma^{n-1} + 1} \qquad (B.4)$$

For the general case of bilinearity, the value of $\bar{E}$ is determined from

$$\bar{E} = \frac{E_e}{K_1 E_e n_1 \sigma^{n_1-1} + 1} \qquad 0 \leq \sigma \leq \sigma^*$$

$$\bar{E} = \frac{E_e}{K_2 E_e n_2 \sigma^{n_2-1} + 1} \qquad \sigma > \sigma^* \tag{B.5}$$

Figures B-3 through B-8 contain the nonlinear stress-strain approximations for the boron/epoxy (NARMCO 5505), borsic/aluminum (AVCO - 5.6 mil fiber, 6061 aluminum), and graphite/epoxy (Hercules - High Strength) composite systems. Figures B-9 through B-11 contain the percent retention of room temperature properties curves for the three materials. Figure B-12 gives the coefficient of thermal expansion curves for each material. Table B-1 gives the pertinent information for all the stress-strain curves.

The mechanics of the method to determine the Ramberg-Osgood coefficients was incorporated into a computer program ROCO. Appendix C.1 contains a user's guide and program listing of ROCO.
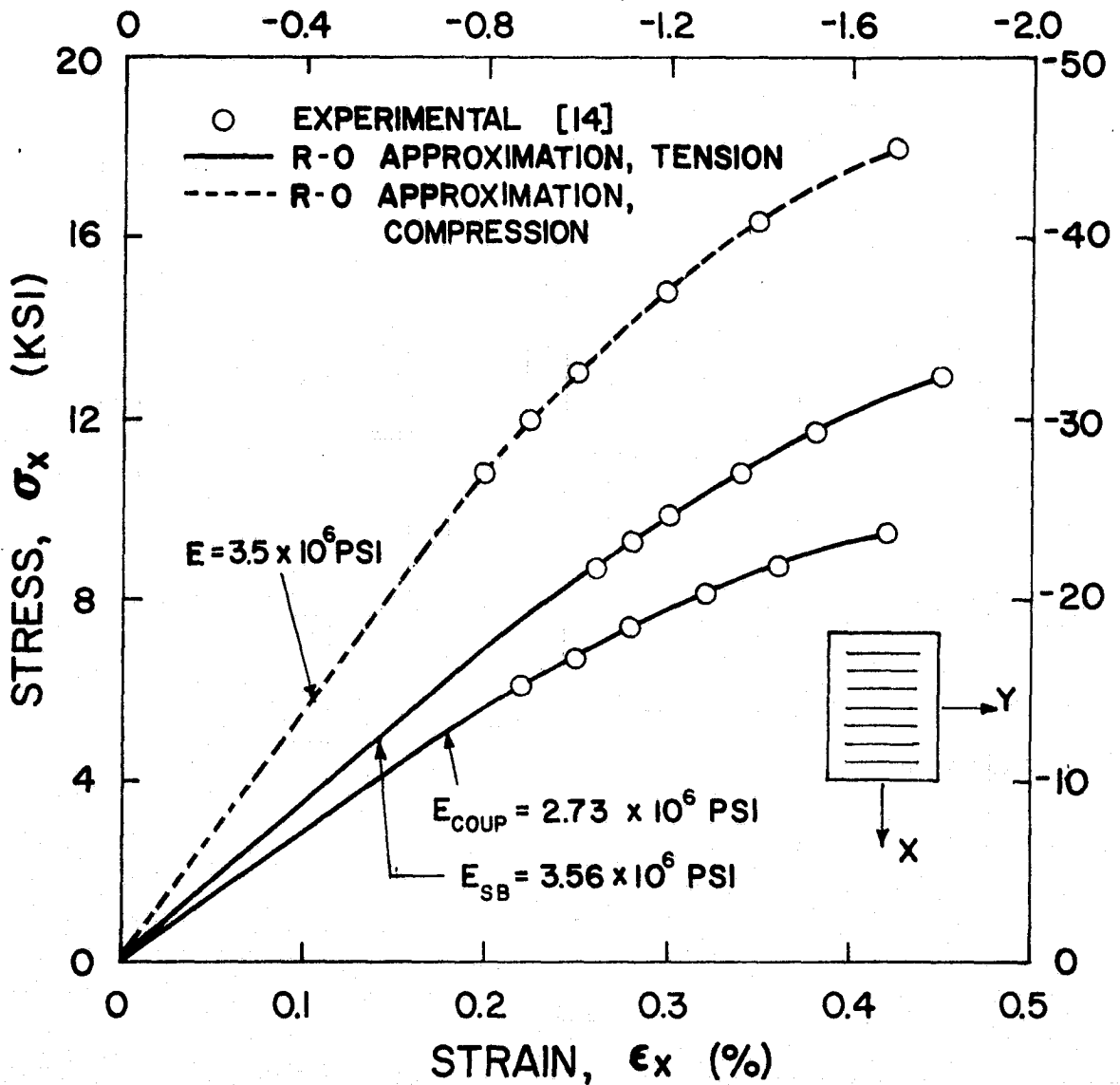
Figure B-3. Stress-Strain Curves of [90] Boron/Epoxy Laminates
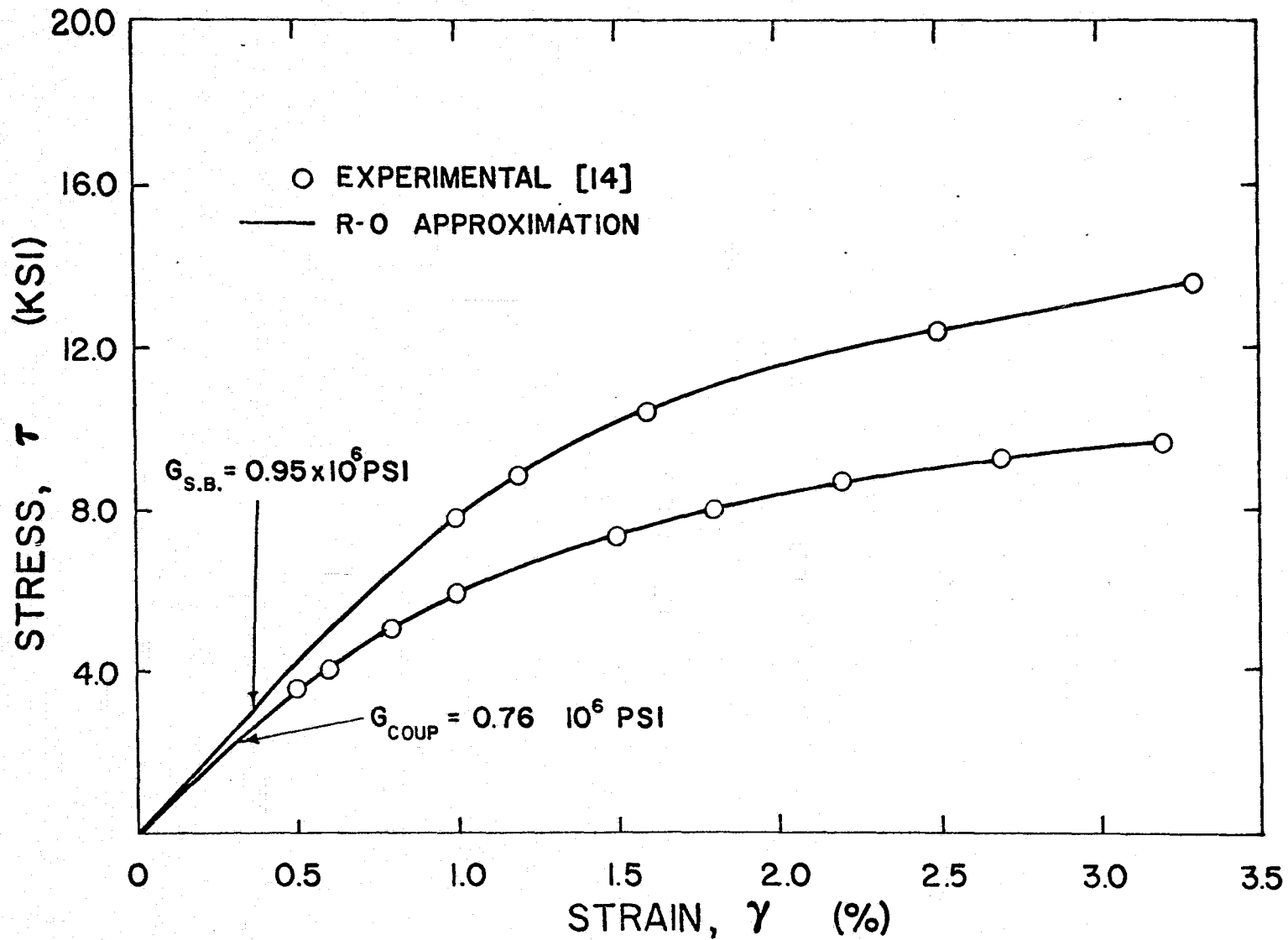
Figure B-4. Shear Stress Strain Curves of Boron/Epoxy
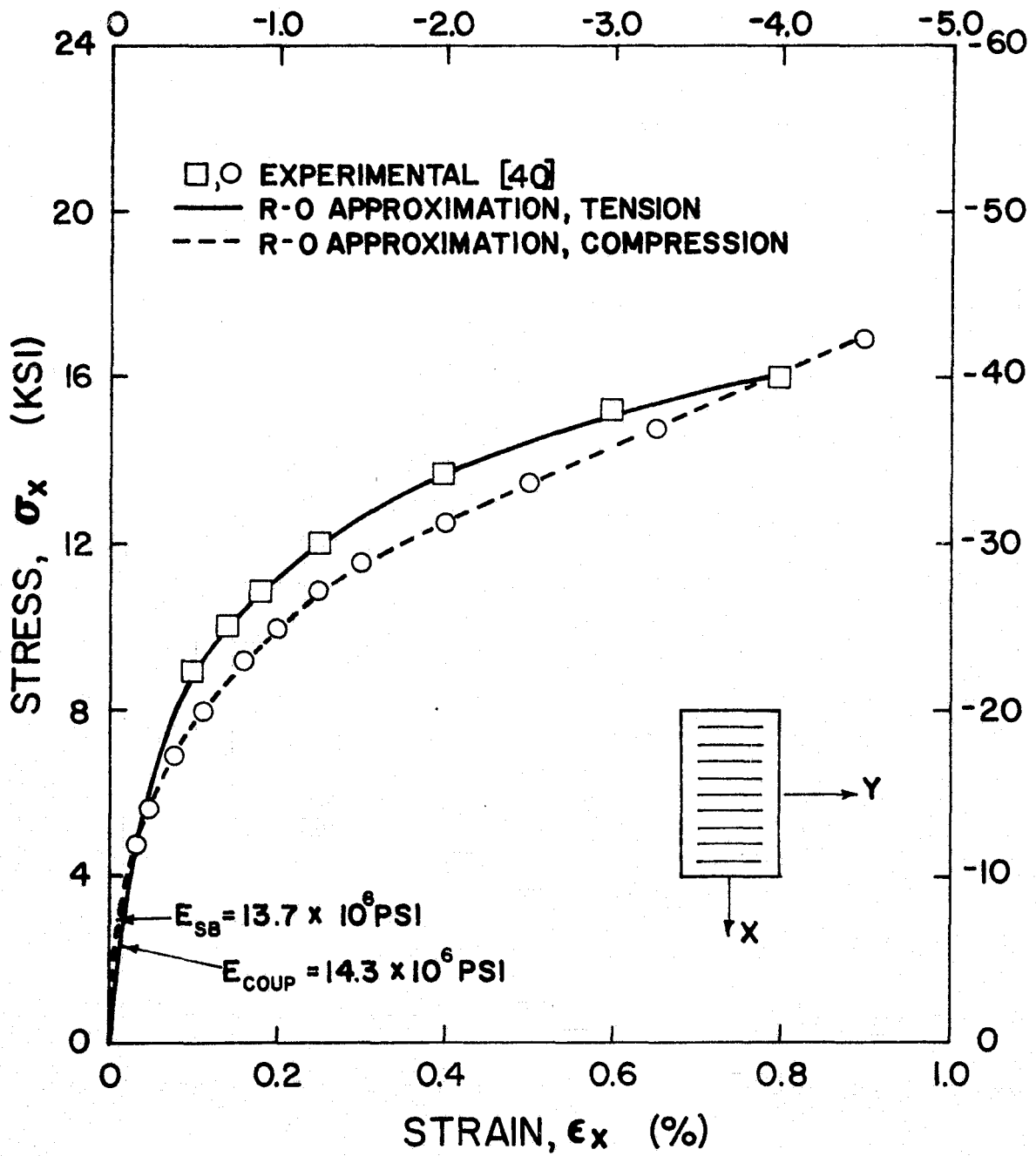
Figure B-5. Stress-Strain Curves of [90] Borsic/Aluminum Laminates
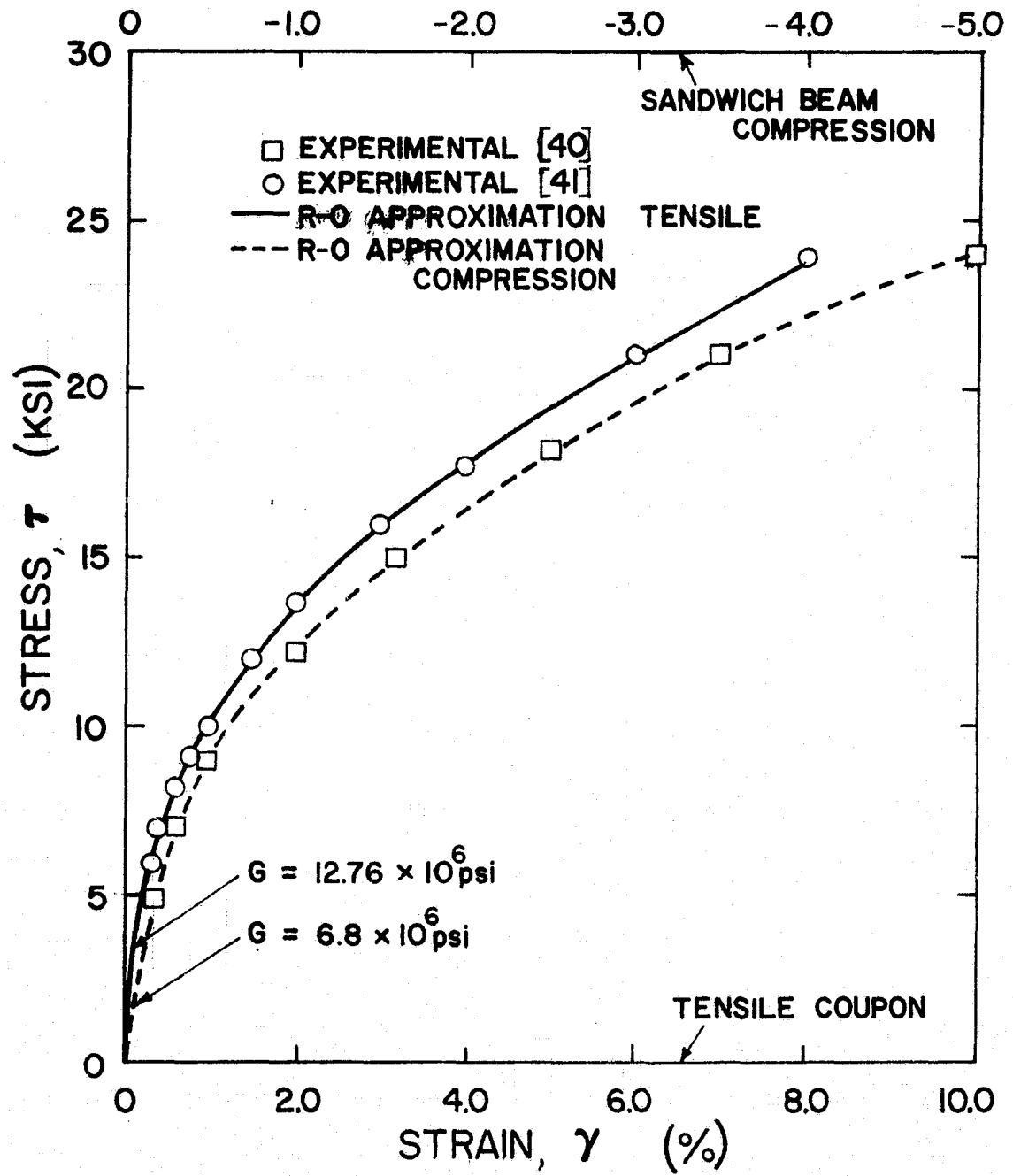
Figure B-6. Shear Stress-Strain Curves of Borsic/Aluminum
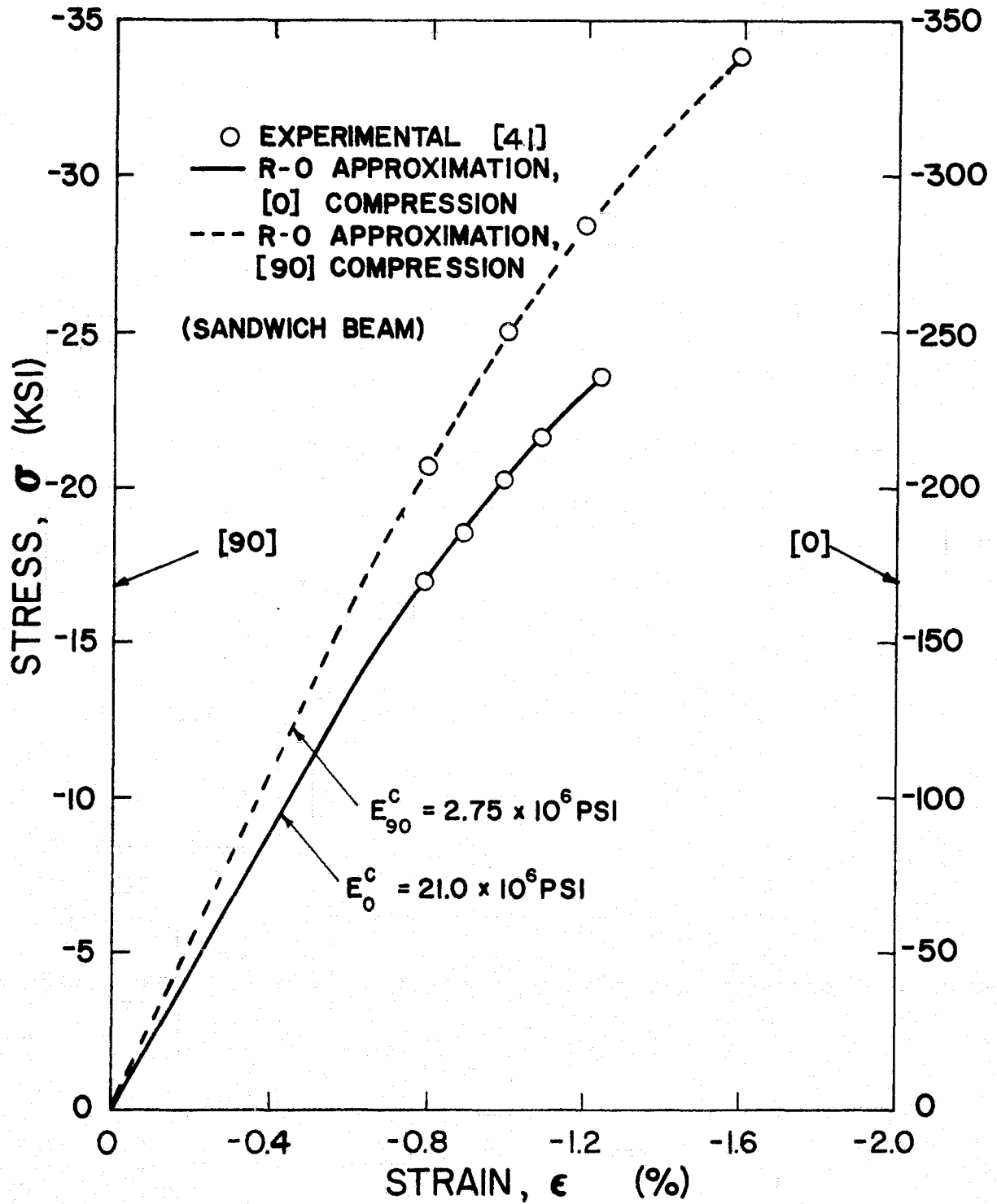
Figure B-7. Compressive Stress-Strain Curves of [0] and [90] Graphite/Epoxy Laminates
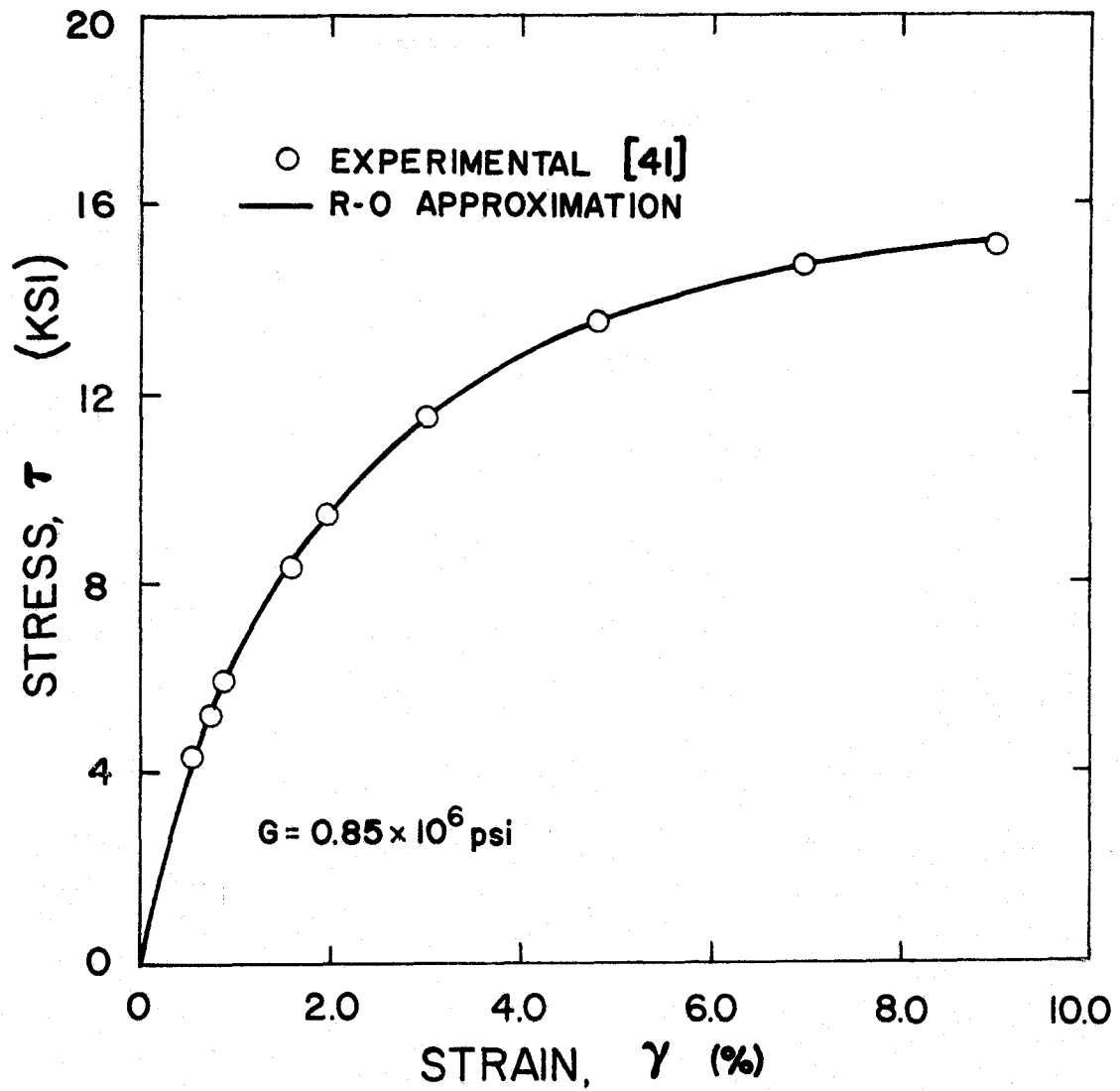
Figure B-8. Shear Stress-Strain Curve of Graphite/Epoxy
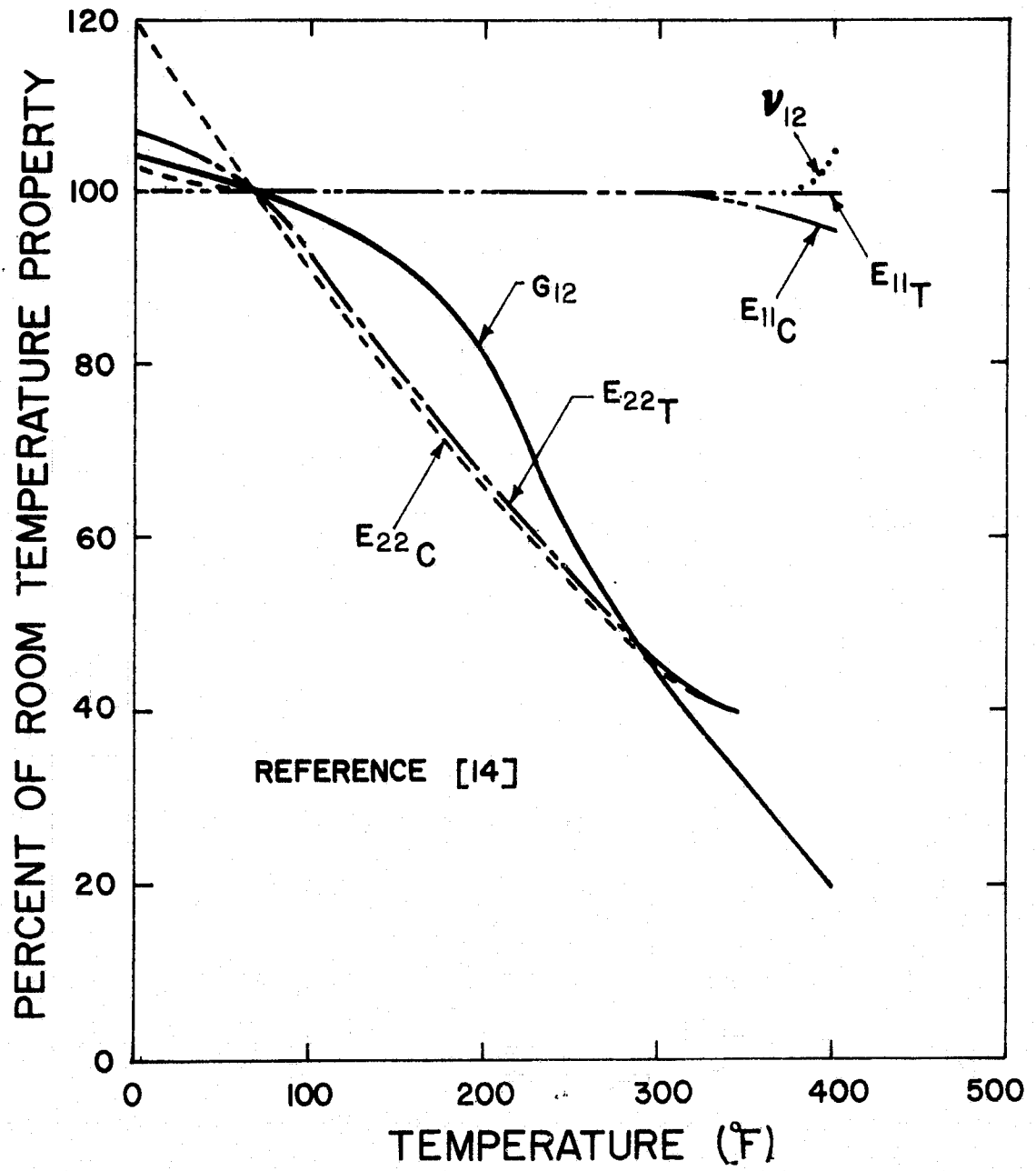
Figure B-9. Percent Retention Curves for Boron/Epoxy
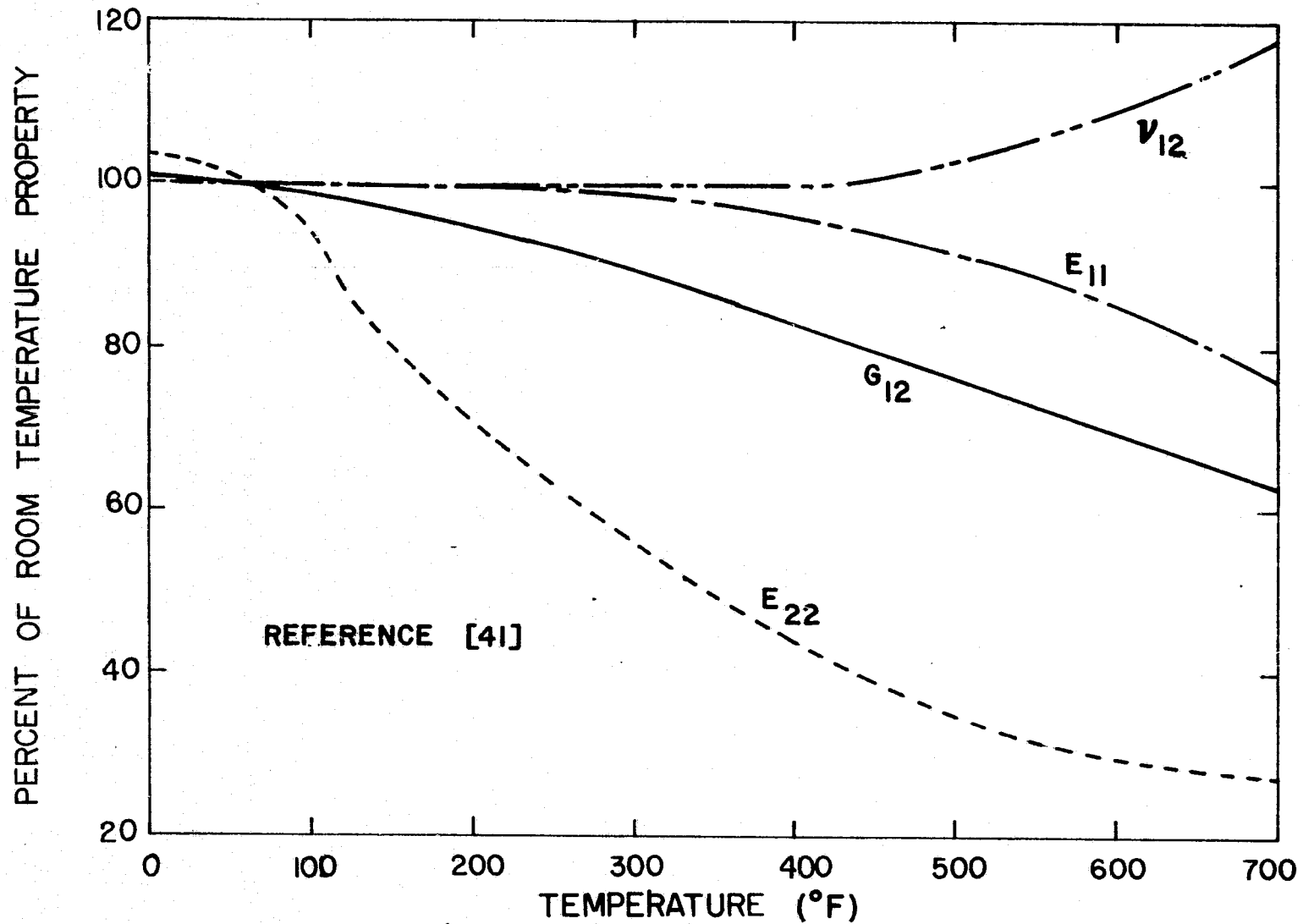
Figure B-10. Percent Retention Curves for Borsic/Aluminum

157
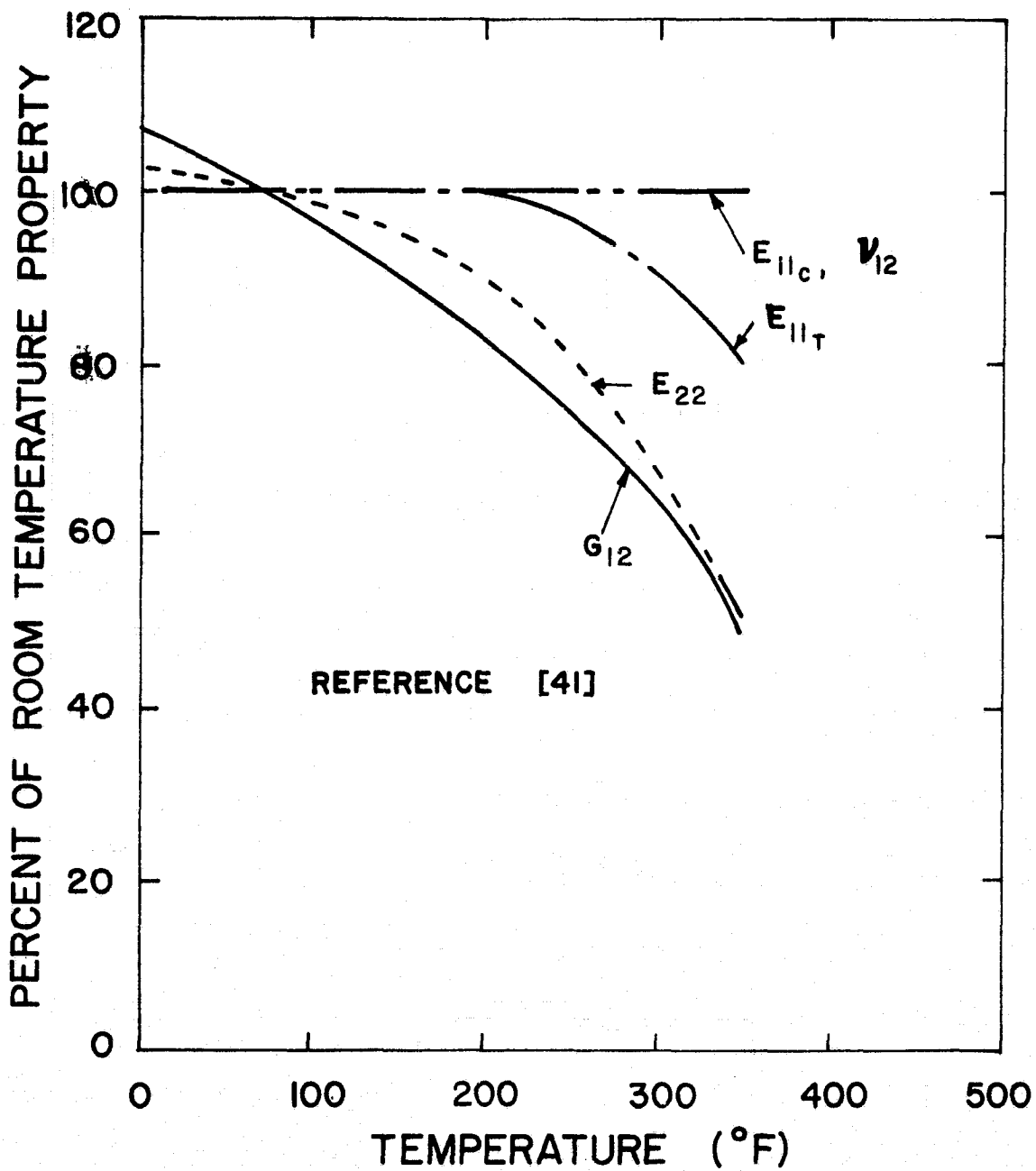
Figure B-11. Percent Retention Curves for Graphite/Epoxy
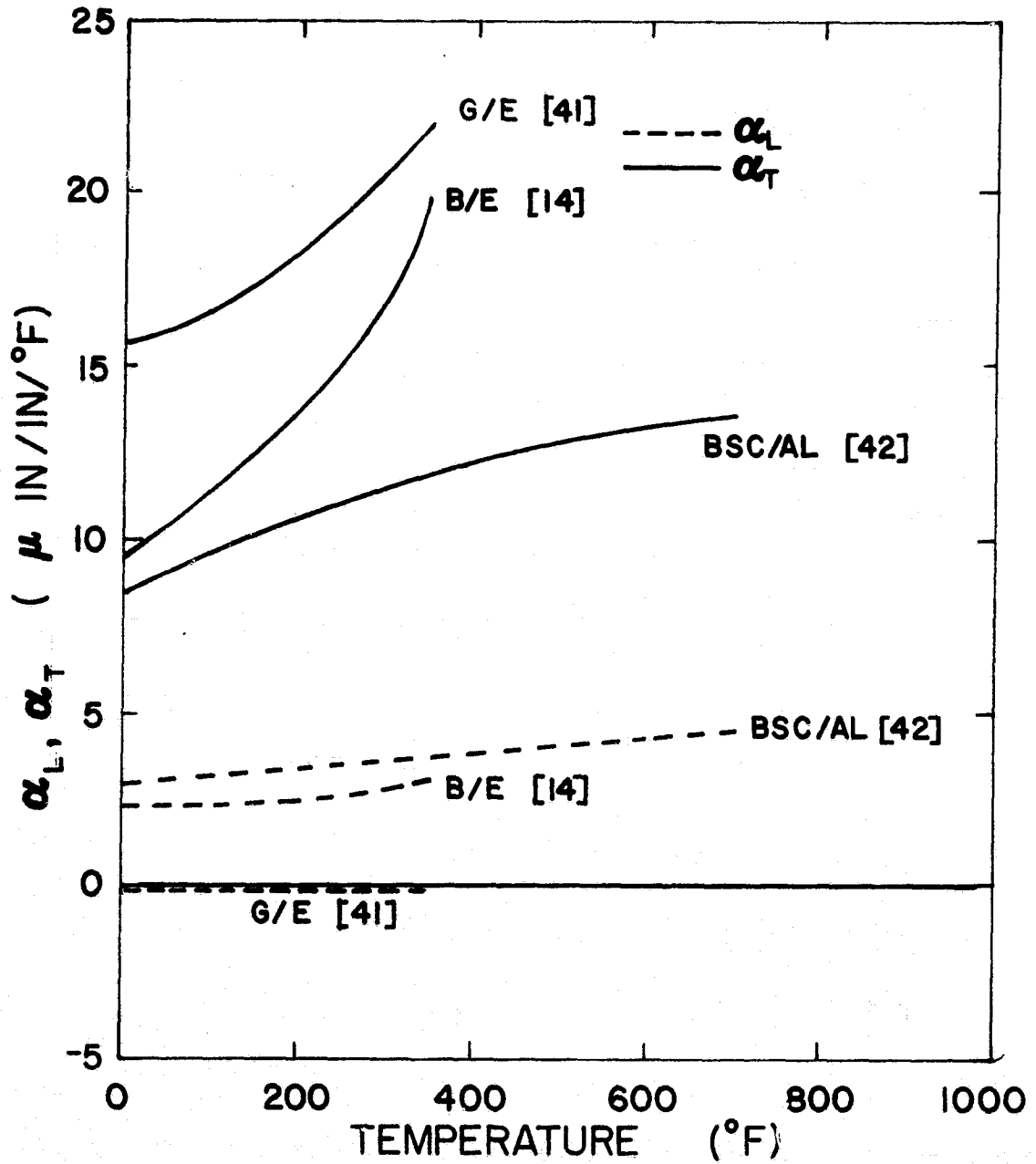
Figure B-12. Coefficient of Thermal Expansion Curves

Table B-1. MATERIAL PROPERTIES AND RAMBERG-OSGOOD COEFFICIENTS.

MATERIAL	CURVE	$E, G \times 10^{-6}$ (psi)	ν	σ^e, τ^e (ksi)	n_1	K_1	σ^* (ksi)	n_2	K_2	σ^u (ksi)	ε_A (%)
BORON/EPOXY	[0] Ten. Coupon	30.1	0.21 (ν_{12})							200.5	
	[0] Ten. S. B.	32.2	0.50 (ν_{12})							206.0	
	[0] Comp. S. B.	32.4	0.53 (ν_{12})							350.0	
	[90] Ten. Coupon	2.73	0.35 (ν_{23})	1.6	7.3050	5.5536×10^{-33}				9.6	0.25
	[90] Ten. S. B.	3.56	0.35 (ν_{23})	1.6	5.0683	1.1986×10^{-24}				13.5	0.25
	[90] Comp. S. B.	3.5	0.35 (ν_{23})	3.0	5.2589	1.3157×10^{-27}				45.0	1.2
	Shear Coupon	0.76		1.0	4.0251	1.4874×10^{-18}	7.7177	4.7175	3.0231×10^{-21}	9.5	1.5
	Shear S. B.	0.95		0.1	4.0165	4.2085×10^{-19}				13.5	1.5

Table B-1. (Continued)

MATERIAL	CURVE	E, G $\times 10^{-6}$ (psi)	ν	σ^e, τ^e (ksi)	n_1	K_1	σ^* (ksi)	n_2	K_2	σ^u (ksi)	ε_A (%)
BORSIC/ALUMINUM	[0] Ten. Coupon *	33.7	0.23 (ν_{12})							152.4	
	[0] Comp. S. B.	39.5	0.26 (ν_{12})							441.3	
	[90] Ten. Coupon *	14.3	0.30 (ν_{23})	0.4	4.8772	2.0865×10^{-23}				16.0	0.2
	[90] Comp. S. B.	13.4	0.30 (ν_{23})	0.1	3.1208	1.5974×10^{-16}				42.5	1.0
	Shear Coupon	12.76		0.125	2.4928	9.7084×10^{-13}				24.0	3.0
	Shear S. B.	6.8		0.125	2.4995	4.9584×10^{-13}				24.0	3.0
GRAPHITE/EPOXY	[0] Ten. Coupon *	21.0	0.21 (ν_{12})							200.0	
	[0] Comp. S. B.	21.0	0.21 (ν_{12})	89.0	12.593	3.3363×10^{-71}				235.0	1.2
	[90] Ten. Coupon *	2.1	0.21 (ν_{23})							8.8	
	[90] Comp. S. B.	2.75	0.21 (ν_{23})	1.0	4.2305	2.3833×10^{-22}				34.0	0.8
	Shear Coupon *	0.85		0.1	3.4110	2.7474×10^{-16}	12.595	5.3158	4.2540×10^{-24}	15.0	3.0

*Sandwich beam and tensile coupon data assumed equal due to lack of experimental data for sandwich beam.

APPENDIX C

COMPUTER PROGRAMS

C.1 ROCO

The following is the data input description for determining the Ramberg-Osgood coefficients K and n for a stress-strain curve. The program is used in two steps

Step 1 - Generate log (σ) versus log $(\varepsilon_I - \frac{\sigma}{E})$ curve.

Step 2 - After observing the curve generated in Step 1 a linear or bilinear fit is specified. The respective values of K and n and the stress intersect, if required, are then determined.

The general content of each individual card is as follows.

C.1.1 Input Data Description

Card 1 (20A4)

Column	Contents
1-80	Problem title card

Card 2 (4I12)

Column		Contents
1-12	NL	= Number of data points
13-24	INCR	= Number of points to divide maximum stress by for curve fit check
25-36	IPLOT	= If Plot

1 - Plot log (σ) versus log $(\varepsilon_I - \frac{\sigma}{E})$ curve only.

2 - Do not plot curve but calculate Ramberg-Osgood coefficients

37-48   NL1   = Number of data points to be used in first segment of bilinear fit. (If linear fit, NL1 = NL.)

<u>Card 3</u> (E12.5)

<u>Column</u>		<u>Contents</u>
1-12	E	= Elastic modulus

<u>Card 4</u> (2E12.5)

<u>Column</u>		<u>Contents</u>
1-12	STRA(I)	= Strain at data point I (in/in)
13-24	STRE(I)	= Stress at data point I (KSI)

Card 4 is repeated NL times.

END OF DATA

```
C************************************************************************
C*        RAMBERG - OSGOOD APPROXIMATION                                *
C************************************************************************
C
      REAL N,K,K1,K2
      DIMENSION VX(20),VY(20),SIG(500),SLOPE(500),ITITLE(20)
      DIMENSION X(50),Y(50),CHANGE(100)
      DIMENSION N(2),K(2)
      DIMENSION STRAIN(500)
      DIMENSION STRE(20),STRA(20)
      WRITE(6,40)
  999 READ(5,1,END=99) (ITITLE(I),I=1,20)
      WRITE(6,2) (ITITLE(I),I=1,20)
      READ(5,5) NL,INCR,IPLOT,NL1
      READ(5,6) E
      DO 400 I=1,NL
      READ(5,10) STRA(I),STRE(I)
      STRE(I) = STRE(I)*10.0**3
  400 CONTINUE
      WRITE(6,65)
      WRITE(6,70) (STRA(I),STRE(I),I=1,NL)
      WRITE(5,90)
      SUMX2 = 0.0
      SUMX = 0.0
      SUMY = 0.0
      SUMXY = 0.0
      DO 20 I=1,NL
      XE = ALOG10(STRE(I))
      YE = ALOG10(STRA(I)-STRE(I)/E)
    8 WRITE(6,70) XE,YE
      J = I
      X(J) = XE
      Y(J) = YE
   20 CONTINUE
      NN = NL
      IF(IPLOT.EQ.1) GO TO 300
      NSUM=NL1+1
      IF(NL1.EQ.NL) NSUM = NL
      DO 110 J=1,NSUM
      I=J
      SUMX = SUMX + X(I)
      SUMY = SUMY + Y(I)
      SUMX2 = SUMX2 + X(I)**2
      SUMXY = SUMXY + X(I)*Y(I)
  110 CONTINUE
      NK = NL1
      DET = SUMX2*NSUM- SUMX**2
      N(1) =(NSUM*SUMXY-SUMX*SUMY)/DET
      B = (-SUMX*SUMXY+SUMX2*SUMY)/DET
      K(1) = 10.0**B
      WRITE(6,75) E,K(1),N(1)
```

```
      IF(NK.EQ.NN) GO TO 350
      SUMX2 = 0.0
      SUMX = 0.0
      SUMY = 0.0
      SUMXY = 0.0
      NPLUS=NK-1
      DO 120 J=NPLUS,NN
      I=J
      SUMX = SUMX + X(I)
      SUMY = SUMY + Y(I)
      SUMX2 = SUMX2 + X(I)**2
      SUMXY = SUMXY + X(I)*Y(I)
120   CONTINJE
      NKK = NN-NPLUS+1
      DET = SUMX2*NKK - SUMX**2
      N(2) = (NKK*SUMXY-SUMX*SUMY)/DET
      B = (-SUMX*SUMXY+SUMX2*SUMY)/DET
      K(2) = 10.0**B
      WRITE(6,75) E,K(2),N(2)
      SPI = (K(2)/K(1))**(1.0/(N(1)-N(2)))
      WRITE(6,880) SPI
880   FORMAT(T10,'SPI =  ',E14.7)
350   SINC=STRE(NN)/INCR
      STOT = 0.0
      WRITE(6,50)
      IF(NK.LT.NN) GO TO 360
      DO 30 I=1,INCR
      STOT = STOT+SINC
      KK = 1
      STRAIN(I) = STOT/E + K(KK)*(STOT)**N(KK)
      SLOPE(I) = 1.0/E + K(KK)*N(KK)*(STOT)**(N(KK)-1)
      SLOPE(I) = 1.0/SLOPE(I)
210   WRITE(6,60) I,STOT,STRAIN(I),SLOPE(I)
30    CONTINUE
      GO TO 370
360   DO 35 I=1,INCR
      STOT = STOT+ SINC
      IF(STOT.LE.SPI) GO TO 230
      KK=2
      GO TO 240
230   KK=1
240   STRAIN(I) = STOT/E + K(KK)*(STOT)**N(KK)
      SLOPE(I) = 1.0/E + K(KK)*N(KK)*(STOT)**(N(KK)-1)
      SLOPE(I) = 1.0/SLOPE(I)
215   WRITE(6,60) I,STOT,STRAIN(I),SLOPE(I)
35    CONTINUE
370   IF(IPLOT.EQ.0) GO TO 380
300   CALL ABPLOT(NL,X,Y)
380   WRITE(6,40)
40    FORMAT(1H1)
50    FORMAT(//T10,'INCR',T20,'STRESS',T40,'STRAIN',T60,'SLOPE')
```

```
60    FORMAT(T10,I3,T25,E12.5,T45,E12.5,T65,E12.5)
 5    FORMAT(4I12)
 6    FORMAT(E12.5)
10    FORMAT(2E12.5)
 1    FORMAT(20A4)
 2    FORMAT(//T10,20A4)
65    FORMAT(//T10,'DATA',/T15,'STRAIN',T35,'STRESS'/)
70    FORMAT(T15,E12.5,T35,E12.5)
75    FORMAT(/T10,'E = ',E12.5,T40,'K= ',E12.5,T70,'N = ',E12.5)
90    FORMAT(////,T15,'LOG(STRESS)',T35,'LOG(P-STRAIN)',//)
      GO TO 999
99    STOP
      END
```

168

C.2 NONCOM

The following is the data input description for the nonlinear version of NONCOM for a laminate analysis. The program can be used for either elastic or nonlinear analyses of less than 100 elements. Data contained in the problem deck(s) will consist of integers and real numbers. All integers must be right adjusted in the proper card field. Real numbers should contain a decimal point in the proper position. The general content of each individual card is as follows.

C.2.1 Input Data Description

Cards 1-5 (20A4)

Column	Contents
1-80	Problem title cards (5 cards always)

Card 6 (12I6)

1-6	NPS	= Type of loading for the generalized plane strain analysis
		1 - Uniaxial strain loading
		2 - Thermal only or thermal followed by uniaxial loading
7-12	IKIND	= Type of boundary conditions
		2 - Symmetric boundary conditions for laminates
13-18	IFTYPE	= Type of force loading in-plane
		0 - For laminates

19-24	NPLUS	= Used in conjunction with NPS

1 - When NPS = 1 or when thermal only

2 - Thermal loading will be followed by uni-axial strain loading

3 - Thermal loading will be followed by uni-axial force loading

25-30	NE	= Number of original elements
31-36	NDS	= Number of original nodes
37-42	NSUB	= Number of element subdivisions
43-48	IPLOT	= Plots original and final element grids

0 - No plot

1 - Plot

>1 - Plot only

49-54	NDIFM	= Number of different materials
55-60	NANG	= Number of different angles
61-66	NINCR	= Number of increments for first type of loading
67-72	NINCRT	= Number of increments for second type of loading

Note: When one type of loading is considered the number of increments must go into NINCR.

Card 7 (5F12.6,I12)

Column		Contents
1-12	SMY	= Physical scale factor for Y coordinate values.

(1.0 if input coordinate values are actual size.)

13-24	SMZ	= Physical scale factor for Z coordinate values.

(1.0 if input coordinate values are actual size.)

25-36	YSL	= Size of grid plot in Y-direction (inches - must be < 10 inches)
37-48	ZSL	= Size of grid plot in Z-direction (inches - must be < 30 inches)
48-60	FMULT	= Scale multiplier if final grid is to be larger than original grid for clarity. (1.0 if YSL and ZSL remain fixed.)
61-72	NGRID	= Internal grid

                      0 - Finite element grid will be read in

                      1 - Analysis will use internally programmed grid

---

Note: If IPLOT > 1 skip to Card 23.

Card 8 (3E12.5)

Column		Contents
1-12	DSTX	= Increment for uniaxial strain loading (in/in)
13-24	FORCK	= Increment for uniaxial force loading (lbs)
25-36	DELT	= Increment for thermal loading (°F)

.The following cards are repeated NDIFM times--Cards 9-16.

K = material number 1, 2,...NDIFM

Card 9 (6E12.5)

Column		Contents
1-12	EK11(K,1)	= Longitudinal tension modulus (psi)
13-24	EK11(K,2)	= Longitudinal compression modulus (psi)

25-36	EK22(K,1)	= Transverse tension modulus (psi)
37-48	EK22(K,2)	= Transverse compression modulus (psi)
49-60	GK12(K)	= Shear modulus (psi)

Card 10 (6E12.5)

Column		Contents
1-12	SP1(K,1)	= Elastic limit stress for longitudinal tension (psi)
13-24	N1(1,K,1)	= Ramberg-Osgood coefficient n_1 for longitudinal tension
25-36	K1(1,K,1)	= Ramberg-Osgood coefficient K_1 for longitudinal tension
37-48	SPI1(K,1)	= Bilinear intersect stress σ^* for longitudinal tension (psi)
49-60	N1(2,K,1)	= Ramberg-Osgood coefficient n_2 for longitudinal tension
61-72	K2(2,K,1)	= Ramberg-Osgood coefficient K_2 for longitudinal tension

Card 11 (6E12.5)

Column		Contents
1-12	SP1(K,2)	=
13-24	N1(1,K,2)	=
25-36	K1(1,K,2)	=
37-48	SPI1(K,2)	=
49-60	N1(2,K,2)	=
61-72	K1(2,K,2)	=

Same as Card 10 but for longitudinal compression.

Card 12 (6E12.5)

Column			Contents
1-12	SP2(K,1)	=	
13-24	N2(1,K,1)	=	
25-36	K2(1,K,1)	=	Same as Card 10 but for transverse
37-48	SPI2(K,1)	=	tension.
49-60	N2(2,K,1)	=	
61-72	K2(2,K,1)	=	

Card 13 (6E12.5)

Column			Contents
1-12	SP2(K,2)	=	
13-24	N2(1,K,2)	=	
25-36	K2(1,K,2)	=	Same as Card 10 but for transverse
37-48	SPI2(K,2)	=	compression.
49-60	N2(2,K,2)	=	
61-72	K2(2,K,2)	=	

Card 14 (6E12.5)

Column			Contents
1-12	SP3(K)	=	
13-24	N3(1,K)	=	
25-36	K3(1,K)	=	Same as Card 10 but for in-plane shear
37-48	SPI3(K)	=	data.
49-60	N3(2,K)	=	
61-72	K3(2,K)	=	

<u>Card 15</u> (6E12.5)

Column		Contents
1-12	SL1(1,K)	= Ultimate stress for longitudinal tension (psi)
13-24	SL1(2,K)	= Ultimate stress for longitudinal compression (psi)
25-36	SL2(1,K)	= Ultimate stress for transverse tension (psi)
37-48	SL2(2,K)	= Ultimate stress for transverse compression (psi)
49-60	SL3(1,K)	= Ultimate stress for shear (psi)

<u>Card 16</u> (6E12.5)

Column		Contents
1-12	UK12(K,1)	= Poisson's ratio ν_{12} in tension
13-24	UK12(K,2)	= Poisson's ratio ν_{12} in compression
25-36	UK23(K,1)	= Poisson's ratio ν_{23} in tension
37-48	UK23(K,2)	= Poisson's ratio ν_{23} in compression

Note: If no thermal analysis is required skip to Card 23.

The following cards are repeated NDIFM times--Cards 17-22.

<u>Card 17</u> (6I12) Subroutine THINC

Column		Contents
1-12	NT1(K)	= Number of linear segmented points for longitudinal modulus percent retention curve
13-24	NT2(K)	= Number of linear segmented points for transverse modulus percent retention curve

25-36   NT3(K)   = Number of linear segmented points for shear

                                  modulus percent retention curve

37-48   NT4(K)   = Number of linear segmented points for longitudinal

                                  thermal coefficient curve

49-60   NT5(K)   = Number of linear segmented points for transverse

                                  thermal coefficient curve

<u>Card 18</u> (6F12.0) I = 1, NT1(K)

<u>Column</u>   —   <u>Contents</u>

 1-12   PERMR1(I,K) = Percent retention of longitudinal modulus at

                                  point I.

13-24   TEMP1(I,K) = Temperature in °F at point I

 etc.   Repeated NT1(K) times

<u>Card 19</u> I = 1, NT2(K) (PERMRZ(I,K), TEMPZ(I,K))

         Same as Card 18 but for transverse modulus

<u>Card 20</u> I = 1, NT3(K) (PERMR3(I,K), TEMP3(I,K))

         Same as Card 18 but for shear modulus

<u>Card 21</u> (3(E12.5, F12.0)) I = 1, NT4(K)

<u>Column</u>   <u>Contents</u>

 1-12   ALP1(I,K) = Longitudinal thermal coefficient at point I

                                  (in/in / °F)

13-24   TEMP4(I,K) = Temperature in °F at point I

 etc.   Repeated NT4(K) times

__Card 22__ I = 1, NT5(K) (ALP2(I,K), TEMP5(I,K))

Same as Card 21 but for the transverse thermal coefficient

__Card 23__ (6F12.6)

THE(K), K = 1, NANG (maximum of 20 angles)

Column		Contents
1-12	THE(1)	= Angle No = 1 (in degrees)
13-24	THE(2)	= Angle No = 2 (in degrees)

etc.

Note: If NGRID = 1 skip to Card 27

__Card 24__ (2(I12,2F12.0))

Two sets of nodal coordinates per card. At present INODE(I) must be in the order I = 1, NDS.

Column		Contents
1-12	INODE(I)	= I
13-24	YY(I)	= Y coordinate of node I (need not be actual physical size if it is to be scaled by SMY) (in)
25-36	ZZ(I)	= Z coordinate of node I (need not be actual physical size if it is to be scaled by SMZ) (in)
37-48	INODE(I+1)	= I + 1
49-60	YY(I+1)	= ⎫
61-72	ZZ(I+1)	= ⎬ Same requirements as for node I

Card 24 is repeated until INODE(NDS) is reached.

Card 25 (6(1X,3I2,2X,2I2))

Six sets of elemental information per card. Node numbers must be counter-clockwise. Elements must be in the order I = 1,NE.

Column	Contents
1	Blank
2-3	ND(I,1) = Node 1 of Element I
4-5	ND(I,2) = Node 2 of Element I
6-7	ND(I,3) = Node 3 of Element I
8	Blank
9-10	IMAT(I) = Material number of Element I
11-12	THETA(I) = Angle number of Element I
13	Blank
14-15	ND(I+1,1) = Node 1 of Element I + 1
16-17	ND(I+1,2) = Node 2 of Element I + 1
18-19	ND(I+1,3) = Node 3 of Element I + 1
20	Blank
21-22	IMAT(I+2) = Material number of Element I + 1
23-24	THETA(I+2) = Angle number of Element I + 1
etc.	Procedure is repeated until NE is reached.

Card 26 (I12, 3F12.6)

Column	Contents
1-12	NUMCP = Points on curved boundary (set to 0 for laminate studies)
13-24	R = Radius of curved boundary (set to 0.0)
25-36	A = Y coordinate of curved boundary (set to 0.0)

C·3

37-48   B   = Z coordinate of curved boundary (set to 0.0)

Note: If NGRID = 0, data ends here.

Card 27 (12I6) Subroutine GRID   I = 1, NDIFM

        Must be in order from layer at midplane.

Column		Contents
1-6	MAT(I)	= Layer material number
7-12	NANG(I)	= Layer angle number
etc.	Maximum of 5 layers of equal thickness	

END OF DATA

OR

NEW DATA DECK

A listing of the program NONCOM is available upon request from either author.